**T.R.**
**GEBZE TECHNICAL UNIVERSITY**
**GRADUATE SCHOOL OF NATURAL AND APPLIED SCIENCES**

# EVALUATION OF NOVEL ZINC, INDIUM AND SILICON PHTHALOCYANINES' ANTI-CANCER PROPERTIES

**BAŞAK ARU**
**A THESIS SUBMITTED FOR THE DEGREE OF**
**DOCTOR OF PHILOSOPHY**
**DEPARTMENT OF MOLECULAR BIOLOGY AND GENETICS**

**GEBZE**
**2021**

**T.R.**

**GEBZE TECHNICAL UNIVERSITY**

**GRADUATE SCHOOL OF NATURAL AND APPLIED SCIENCES**

# EVALUATION OF NOVEL ZINC, INDIUM AND SILICON PHTHALOCYANINES' ANTI-CANCER PROPERTIES

**BAŞAK ARU**

**A THESIS SUBMITTED FOR THE DEGREE OF**

**DOCTOR OF PHILOSOPHY**

**DEPARTMENT OF MOLECULAR BIOLOGY AND GENETICS**

THESIS SUPERVISOR

PROF. DR. AYŞE GÜL GÜREK

II. THESIS SUPERVISOR

PROF. DR. GÜLDEREN YANIKKAYA DEMİREL

**GEBZE**

**2021**

**T.C.**
**GEBZE TEKNİK ÜNİVERSİTESİ**
**FEN BİLİMLERİ ENSTİTÜSÜ**

# ÖZGÜN ÇİNKO, İNDİYUM VE SİLİSYUM FTALOSİYANİNLERİN ANTİ-KANSER ETKİNLİKLERİNİN DEĞERLENDİRİLMESİ

**BAŞAK ARU**

**DOKTORA TEZİ**

**MOLEKÜLER BİYOLOJİ VE GENETİK ANABİLİM DALI**

DANIŞMANI
PROF. DR. AYŞE GÜL GÜREK
II. DANIŞMANI
PROF. DR. GÜLDEREN YANIKKAYA DEMİREL

**GEBZE**

**2021**

| GEBZE TEKNİK ÜNİVERSİTESİ | YÜKSEK LİSANS JÜRİ ONAY FORMU |
|---|---|

GTÜ Fen Bilimleri Enstitüsü Yönetim Kurulu'nun 25/12/2020 tarih ve 2020/60 sayılı kararıyla oluşturulan jüri tarafından 18/01/2021 tarihinde tez savunma sınavı yapılan Başak Aru'nun tez çalışması Moleküler Biyoloji ve Genetik Anabilim Dalında DOKTORA tezi olarak kabul edilmiştir.

**JÜRİ**

ÜYE
(TEZ DANIŞMANI) : PROF. DR. AYŞE GÜL GÜREK

ÜYE : PROF. DR. TAMER YAĞCI

ÜYE : PROF. DR. DEVRİM ATİLLA

ÜYE : DOÇ. DR. MEHTAP KAÇAR

ÜYE : DOÇ. DR. GÜLŞAH GÜMRÜKÇÜ KÖSE

**ONAY**

Gebze Teknik Üniversitesi Fen Bilimleri Enstitüsü Yönetim Kurulu'nun
…..…/…..…/..…..… tarih ve ……/…….... sayılı kararı.

İMZA/MÜHÜR

# SUMMARY

Photodynamic therapy (PDT), which relies on the photosensitive molecules' local administration and activation via irradiation at a specific wavelength (600–800 nm) has been studied years for many diseases; it is especially promising in cancer therapy due to its specificity and sensitivity. Upon absorbing photons, photosensitizer transforms from its ground state to an excited singlet state that emits fluorescence while a portion of the excited singlet state molecules are transformed into the excited triplet state that forms free radicals or radical ions. Substitution of photosensitizer molecules with chemotherapy drugs enables not only to increase their solubility in aqueous media but also to combine chemotherapeutic action with PDT. Currently, combinatorial administration of histone deacetylase inhibitors (HDACi) and photosensitizer molecules are restricted while none of them involves a phthalocyanine derivative.

In this thesis project, we aimed to synthesize a HDACi (3-hydroxypyridine-2-thione) bearing silicon, zinc and indium phthalocyanine derivatives and investigate their anti-cancer mechanisms on two breast cancer (MCF-7, double positive and MDA-MB-231, triple negative) cell lines as well as a healthy (human endothelial cell line, HUVEC) cell lines in terms of the metal coordinated and substitution of the HDACi residues (axial, peripheral, non-peripheral). Our results revealed that all Pc-HDACi derivatives are localized to different regions of the cells (nucleus and nucleolus for SiPc-HDACi, cytoplasm/membrane or nucleus for ZnPc-HDACi derivatives according to the position of HDACi moieties, cytoplasm/membrane and mitochondria for InPc derivatives) and induced different programmed cell death pathways. Among all Pc-HDACi derivatives, SiPc-HDACi stands out as a promising alternative for PDT applications thanks to its' high singlet oxygen yield and effective HDAC inhibitory action.

**Key Words: Phthalocyanines, Histone Deacetylase Inhibitors, Programmed cell death pathways, Anti-cancer activity.**

# ÖZET

Işığa duyarlı moleküllerin bölgesel uygulamayı takiben belirli dalgaboyunda ışık ile uyarılması yöntemine dayalı bir tedavi yöntemi olan Fotodinamik Terapi (FDT), yüksek derecede özgüllük ve hassasiyeti sayesinde özellikle kanser tedavisi için umut vaadetmektedir. Bu yöntemde ışık maruziyeti sonucu fotonları absorbe eden ışığa duyarlı molekül, uyarılarak uygulama bölgesinde serbest radikaller ya da radikal iyonları meydana getirir. Işığa duyarlı moleküllerin çeşitli kemoterapötik ilaçlar ile sübstitüe edilmesi, bu moleküllerin sudaki düşük çözünürlüklerinin giderilmesine ek olarak kemoterapi ile FDT'yi kombine etmeye de olanak sağlar. Günümüzde ışığa duyarlı moleküller ile histon deasetilaz inhibitörlerinin kombine kullanımları oldukça sınırlı olup bu çalışmalardan hiçbirinde fotodinamik aktivite bir ftalosiyanin (Pc) türevi ile sağlanmamıştır.

Bu tez çalışmasında bir histon deasetilaz inhibitörü (HDACi), 3-hidroksipiridin-2-tiyon sübstitüe silikon, çinko ve indiyum ftalosiyanin türevleri sentezlenerek moleküllerin anti-kanser aktiviteleri; içerdikleri metal ve sahip oldukları histon deasetilaz inhibitörü konumu (aksiyel, periferal, non-periferal) bağlamında iki farklı meme kanseri (MCF-7, çift pozitif ve MDA-MB-231, üçlü negatif) ile bir sağlıklı (insan endotelyal hücre hattı, HUVEC) hücre hatları üzerinde incelenmek amaçlanmıştır. Elde edilen sonuçlar, tüm Pc-HDACi türevlerinin hücrelerin farklı bölgelerine lokalize olduğunu (SiPc-HDACi türevi için nükleus ve nükleolus, ZnPc-HDACi türevleri için HDACi rezidülerinin konumuna bağlı olarak sitoplazma/membran ya da nükleus, InPc-HDACi türevleri için sitoplazma/membran ve mitokondri) ve farklı hücre ölüm mekanizmalarını aktive ettiğini göstermiştir. Özellikle SiPc-HDACi, yüksek singlet oksijen verimi ve histon deasetilaz inhibitör etkinliği ile FDT uygulamaları için gelecek vaat eden bir alternatif olarak ön plana çıkmaktadır.

**Anahtar Kelimeler: Ftalosiyanin, Histon deasetilaz inhibitörü, Programlı hücre ölümü, Anti-kanser aktivite.**

# ACKNOWLEDGEMENTS

First, I would like to thank my thesis supervisor Prof. Dr. Ayşe Gül GÜREK for her support and guidance through this thesis project as well as Prof. Dr. Devrim ATİLLA, who designed, synthesized and characterized the phthalocyanine derivatives used in this study and Assoc. Prof. Elif ŞENKUYTU for performing photophysical experiments. I thank to my co-supervisor Prof. Dr. Gülderen YANIKKAYA DEMİREL, who has had an incredible effort on me during the seven years that I have been working in her laboratory.

I am grateful to my family for supporting and encouraging me through my life, and during my postgraduate education.

I thank to my labmates in Yeditepe University Hospital, Hüsniye DAĞDEVİREN, Ebru BAKTEMUR, Melis UĞUR and Ayşe YİĞİT and also PhD students of the Yeditepe University, Biotechnology programme, Nur EKİMCİ GÜRCAN and Utku ÖZBEY for their valuable help. I am grateful to Prof. Dr. Ömer Faruk BAYRAK, Head of the Yeditepe University, Medical Genetics Department for providing the cell lines and Dr. Öznur SUAKAR for her assistance in cell line authentication. I thank to ARU Elektronik and ICE LED Elektronik for constructing the irradiation device.

This study is funded by the Scientific and Technological Research Council of Turkey (TUBITAK) with the project number 118Z693 granted to Prof. Dr. Devrim ATİLLA.

# TABLE of CONTENTS

# LIST of ABBREVIATIONS and ACRONYMS

| Abbreviations and Acronyms | | Explanations |
|---|---|---|
| ° | : | Degree |
| μM | : | Micromolar |
| $^1O_2$ | : | Singlet oxygen |
| 3D | : | Three dimensional |
| 3-HPT | : | 3-hydroxypyridine-2-thione |
| 4SC202 | : | Domatinostat |
| 7-AAD | : | 7-aminoactinomycin D |
| ACKR | : | Atypical chemokine receptors |
| ADP | : | Adenosine 5′-diphosphate |
| ALA | : | Aminolaevulinic acid |
| AMD | : | Age related macular degeneration |
| AML | : | Acute myelogenous leukaemia |
| ANOVA | : | Analysis of Variance |
| APS | : | Ammonium persulfate |
| BBr3 | : | Boron tribromide |
| BCA | : | Bicinchoninic acid |
| Bcl-2 | : | B-cell lymphoma-2 |
| Bid | : | BH3 interacting-domain death agonist |
| BSA | : | Bovine serum albumin |
| C | : | Centigrade |
| $Ca^{2+}$ | : | Calcium |
| Casp | : | Caspase |
| CCL12 | : | Chemokine (C-C motif) ligand 21 |
| CCR7 | : | C-C chemokine receptor type 7 |
| CD | : | Cluster of Differentiation |
| Ce6 | : | Chlorin-6 |
| $CH_2Cl_2$ | : | Dichloromethane |
| cm | : | Centimetre |
| $CO_2$ | : | Carbon dioxide |

| | | |
|---|---|---|
| CXCL12 | : | C-X-C Motif Chemokine Ligand 12 (SDF-1) |
| CXCR4 | : | C-X-C Chemokine Receptor Type 4 |
| DAPI | : | 4′,6-diamidino-2-phenylindole |
| $dH_2O$ | : | Distilled water |
| DHR123 | : | Dihydrorhodamine 123 |
| DMEM | : | Dulbecco's Modified Eagle's Medium |
| DMSO | : | Dimethyl sulfoxide |
| DNA | : | Deoxyribonucleic acid |
| DPBS | : | Dulbecco's Phosphate Buffered Saline |
| ECM | : | Extracellular matrix |
| EDTA | : | Ethylenediaminetetraacetic acid |
| EMT | : | Epithelial-mesenchymal transition |
| eNOS | : | Endothelial nitric oxide synthase |
| ER | : | Endoplasmic reticulum |
| ERK | : | Extracellular-signal-regulated kinase |
| ERα | : | Oestrogen receptor alpha |
| EX-527 | : | Selisistat |
| FADD | : | Fas associated via death domain |
| FADH2 | : | Reduced flavin adenine dinucleotide |
| FBS | : | Fetal Bovine Serum |
| FMNH2 | : | Reduced 1,5-dihydro form of flavin mononucleotide |
| GAPDH | : | Glyceraldehyde 3-phosphate dehydrogenase |
| GPRC | : | G protein-coupled cell surface receptors |
| GSK-3β | : | Glycogen synthase kinase-3β |
| $H_2O_2$ | : | Hydrogen peroxide |
| HA | : | Hyaluronic acid |
| HAT | : | Histone acetyltransferase |
| HDAC | : | Histone deacetylase |
| HDACi | : | Histone deacetylase inhibitor |
| HER2 | : | Human epidermal growth factor receptor 2 |
| HLA | : | Human leukocyte antigens |
| HPD | : | Hematoporphyrin derivative |
| HPPH | : | 2-[1-Hexyloxyethyl]-2-devinyl pyropheophorbide-a |

| | | |
|---|---|---|
| HRP | : | Horseradish peroxidase |
| HSC | : | Heat shock cognate protein |
| $IC_{50}$ | : | Half maximal inhibitory concentration |
| ICC | : | Immunocytochemistry |
| IgG | : | Immunoglobulin G |
| IHC | : | Immunohistochemistry |
| In | : | Indium |
| ISH | : | In situ hybridization |
| IU | : | International unit |
| J | : | Joule |
| $K_2CO_3$ | : | Potassium carbonate |
| KAT | : | Lysine acetyltransferases |
| LAMP2A | : | Lysosomal-associated membrane protein 2A |
| LED | : | Light emitting diode |
| L | : | Litre |
| lncRNA | : | Long non-coding RNA |
| LuTex | : | Motexafin lutetium |
| MAM | : | Mitochondria-associated membrane |
| MAP1LC3 | : | Microtubule-associated protein 1 light chain 3 |
| MFI | : | Mean fluorescence intensity |
| miRNA | : | Micro RNA |
| mitROS | : | Mitochondrial ROS |
| MLKL | : | Mixed Lineage Kinase Domain-like |
| mmHG | : | Millimetre of mercury |
| mRNA | : | Messenger RNA |
| mTHPC | : | m-tetrahydroxyphenylchlorin (Foscan) |
| mW | : | Milliwatt |
| NaCl | : | Sodium Chloride |
| NADH | : | Reduced form of Nicotinamide adenine dinucleotide |
| NADPH | : | Nicotinamide adenine dinucleotide phosphate |
| NF-κB | : | Nuclear factor kappa B |
| NIR | : | Near infrared |
| NK cell | : | Natural killer cell |

| | | |
|---|---|---|
| nm | : | Nanometre |
| nM | : | Nanomolar |
| NPe6 | : | Mono-aspartyl chlorin e6 (MACE) |
| Pc | : | Phthalocyanine |
| Pc1 | : | Axial histone deacetylase inhibitor substituted silicon phthalocyanine |
| Pc2 | : | Non-peripheral histone deacetylase inhibitor substituted zinc phthalocyanine |
| Pc3 | : | Peripheral histone deacetylase inhibitor substituted zinc phthalocyanine |
| Pc4 | : | Non-peripheral histone deacetylase inhibitor substituted indium phthalocyanine |
| Pc5 | : | Peripheral histone deacetylase inhibitor substituted indium phthalocyanine |
| Pc-C1 | : | Tetrakis(4,7,10-trioxaundecan-1-sulfanyl) phthalocyaninato zinc |
| Pc-C2 | : | Octakis(4,7,10-trioxaundecan-1-sulfanyl) phthalocyaninato zinc |
| Pc-C3 | : | Polyoxo silicon phthalocyanine |
| Pc-HDACi | : | Phthalocyanine-histone deacetylase inhibitor derivative |
| $Pd(PPh_3)_4$ | : | Tetrakis(triphenylphosphine)palladium(0) |
| PDT | : | Photodynamic Therapy |
| PFC | : | Perfluorocarbon |
| PI | : | Propidium Iodide |
| PI3K | : | Phosphoinositide 3-kinase |
| $pO_2$ | : | Partial oxygen pressure |
| PR | : | Progesterone receptor |
| PS | : | Photosensitizer |
| PS | : | Phosphatidylserine |
| PTS | : | Singlet ground state |
| PVDF | : | Polyvinylidene fluoride |
| PVP-Ce6 | : | Polyvinylpyrrolidone - Chlorin e6 |
| RARγ | : | Retinoic acid receptor gamma |

| | | |
|---|---|---|
| RIP1 | : | Receptor Interacting Protein 1 |
| RIP3 | : | Receptor Interacting Protein 3 |
| RNA | : | Ribonucleic acid |
| ROS | : | Reactive oxygen species |
| s | : | Second |
| SAHA | : | Suberoylanilide hydroxamic acid (Vorinostat) |
| SDS | : | Sodium dodecyl sulphate |
| SDS-PAGE | : | Sodium dodecyl sulphate polyacrylamide gel electrophoresis |
| SHH | : | Sonic hedgehog |
| SIRT | : | Sirtuin |
| Si | : | Silicon |
| SnEt2 | : | Tin Ethyl Etiopurpurin |
| Src | : | SRC Proto-Oncogene, Non-Receptor Tyrosine Kinase |
| t-Bid | : | Truncated BH3 interacting-domain death agonist |
| TBS | : | Tris Buffered Saline |
| TBS-T | : | Tris Buffered Saline-Tween 20 |
| TEMED | : | N,N,N′,N′-Tetramethyl ethylenediamine |
| TGF-β | : | Transforming growth factor beta |
| THF | : | Tetrahydrofuran |
| TLR | : | Toll Like Receptor |
| TNBC | : | Triple negative breast cancer |
| TNFR | : | Tumour necrosis factor receptor |
| TNFR1 | : | Tumour necrosis factor receptor- 1 |
| TOOKAD | : | Padoporfin |
| TPE | : | Two-photon excitation |
| TRADD | : | Tumour necrosis factor receptor type 1-associated death domain |
| TRAF2 | : | Tumour necrosis factor receptor-associated factor 2 |
| TRAIL | : | Tumour necrosis factor -related apoptosis inducing ligand |
| Treg cell | : | T regulatory cell |
| TSA | : | Trichostatin A |
| TSP-1 | : | Thrombospondin-1 |
| ULK | : | UNC51 like kinase |

| | | |
|---|---|---|
| UPR | : | Unfolded protein response |
| VEGF | : | Vascular endothelial growth factor |
| VEGFR | : | Vascular endothelial growth factor receptor |
| VPA | : | Valproic acid |
| Wnt | : | Wingless |
| ZBG | : | Zinc-Binding Group |
| Zn | : | Zinc |

# LIST of FIGURES

# LIST of TABLES

# 1. INTRODUCTION

## 1.1. The Purpose, Contribution, and Content of Thesis

Photodynamic therapy (PDT), which relies on the photosensitive molecules' (PS) local administration and activation via irradiation at a specific wavelength (600–800 nm) has been studied years for many diseases; it is especially promising in cancer therapy due to its specificity and sensitivity. Upon absorbing photons, photosensitizer transforms from its ground state to an excited singlet state that emits fluorescence while a portion of the excited singlet state molecules are transformed into the excited triplet state that forms free radicals or radical ions. While unsubstituted Pcs have low solubility in water, various unsubstituted Pcs have low solubility in water which does not only overcome problems arising from hydrophobicity but also enables the researchers to combine chemotherapeutic approaches with photodynamic therapy successfully both *in vivo* and *in vitro*. Currently, studies combining PS and histone deacetylase inhibitors (HDACi) for cancer treatment are restricted, and none of the few previous studies involve a phthalocyanine (Pc) derivative for photodynamic activity.

In this thesis project, we aimed to develop HDACi (*3-hydroxypyridine-2-thione*, 3-HPT) bearing silicon, zinc and indium Pc derivatives, compounds with dual chemo- and photodynamic action, and investigate their mechanisms of action on two breast cancer cell lines (MCF-7, double positive and MDA-MB-231, triple negative) as well as a healthy (human endothelial cells, HUVEC) cell line. All compounds exerted cytotoxic activity in the cell lines abovementioned, while their localization and anti-cancer mechanisms differed according to the metal they contain and the position of HDACi moieties. The workflow of the study is given on Figure 1.1.

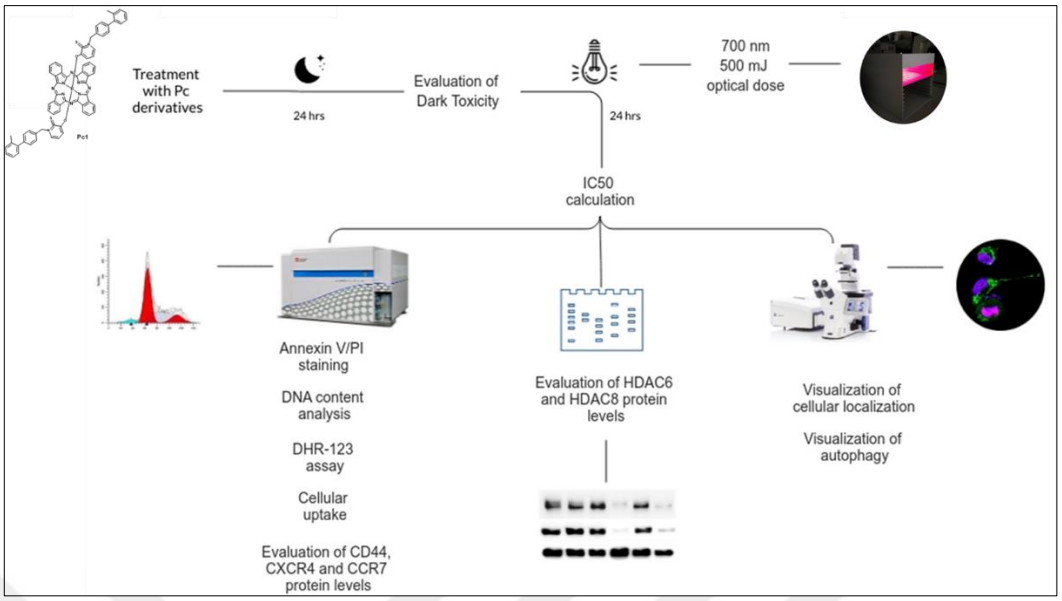


Figure 1.1: The workflow of the study. Cells were incubated with Pc-HDACi derivatives at 1-100μM concentrations for 24 hours under dark conditions to investigate dark toxicity of the compounds. For light toxicity, cells were irradiated with red light at 500 mJ optical dose and incubated for an additional 24 hours. $IC_{50}$ values of each compound for the respective cell line were calculated. Anti-cancer activity was investigated by evaluating given parameters: apoptosis, autophagy, necrosis, downregulation of respective HDACs, mitochondrial activity, DNA content, and various protein levels play role in cellular migration.

# 2. LITERATURE REVIEW

## 2.1. Photodynamic Therapy

Photodynamic therapy (PDT) involves the administration of a photosensitizer molecule (PS) locally or topically to a usually, but not always malignant lesion [1], [2]. The treatment procedure consists of three components: PS, light and oxygen which are all non-toxic individually [3]. After injecting the compound to the lesion, the area is irradiated with a light source at a certain wavelength to activate the PS which, in turn, activates programmed cell death pathways by generating toxic products [4], [5].

Due to several advantages over conventional cancer treatment options, PDT became an attractive option for cancer therapeutics [4], [6] - [8]. Its' local administration avoids systemic side effects as the photosensitive agent selectively accumulates in tumour and its surrounding tissues [8]. PDT can also be used on tumours that cannot be surgically resected. Unlike other invasive and systemic treatment options, PDT is repeatable and may offer long-term management [3].

PDT aims to destroy selectively malignant tissue via irradiating the photosensitizer by a light source at a wavelength matching its absorption maxima. Irradiation promotes chemical reactions that are induced by electron or energy transfer; as the result, reactive oxygen and nitrogen species are generated. Two reaction types are involved in reactive oxygen generation via PDT: Type I reactions involve electron or hydrogen transfer reactions directly from the photosensitizer and produce ions or involves electron/hydrogen extraction from a substrate to form free radicals. Type II reactions produce a highly reactive state of oxygen which is called singlet oxygen ($_1O^2$) [9]. Even though mainly $_1O^2$ plays role in the molecular action of PDT [10], both reactions occur simultaneously and the ratio between two reaction types depends on the nature of the PS [11], [12]. The cytotoxicity mechanism of PS upon irradiation is given in Figure 2.1.

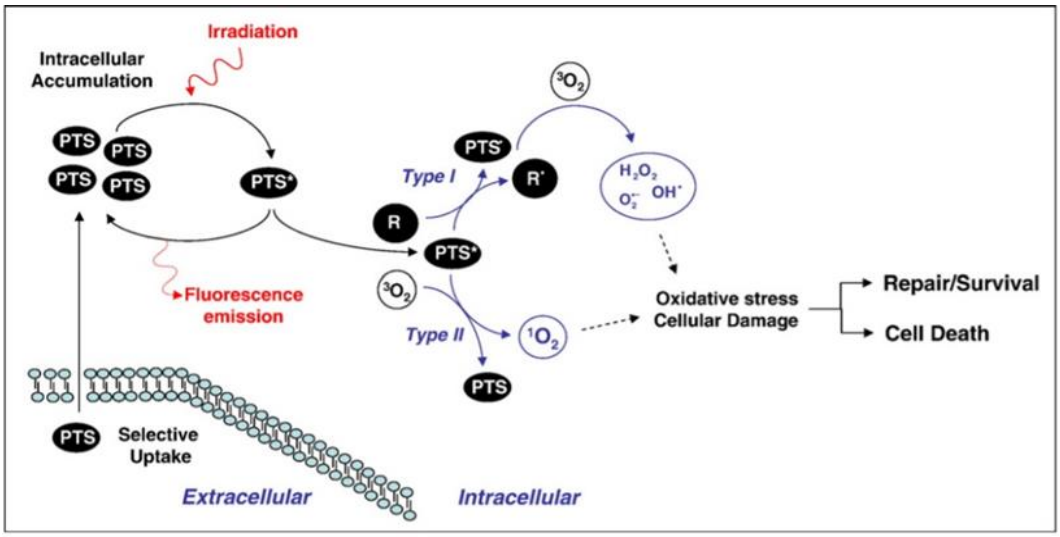


Figure 2.1: Action mechanism of PDT. Absorption of a photon causes excitation of the photosensitizer from its singlet ground state (PTS) to higher energy levels (PTS∗). Upon deactivation, singlet oxygen ($^1O_2$) causes formation of free radicals and reactive oxygen species that lead to cell death.

When compared to tetrapyrrolic porphyrins and chlorins, thanks to their high extinction coefficients and longer absorption wavelengths (due to additional benzene rings connected to each pyrrolic subunit that causes more electron delocalization) [13], [14], phthalocyanines (Pcs) are regarded as potent second-generation PS compounds in cancer treatment.

### 2.1.1. Photodynamic Therapy in Cancer Treatment

PDT contributes eradication or reduction of tumours via three distinct mechanisms. First, reactive oxygen species (ROS) generated upon treatment can directly kill tumour cells by activating a programmed cell death mechanism [4], [15]. Alternatively, PDT can impair tumour associated vascularization that leads to nutrient and oxygen deprivation, and PDT-induced stress signals enable immune system to recognise and destroy tumour cells [3], [16].

Role of each mechanism depends on the type and dose of PS administered, incubation duration of the target tissue with the PS, optical dose of irradiation and tumour oxygen levels [3], all three mechanisms are important for tumour regression [6], [17] and each of their importance on tumour eradication needs further research.

A hematoporphyrin derivative (HPD) (later named as Photofrin) was the first PS molecule clinically employed for cancer therapy and still considered the most widely

used one. Disadvantages of Photofrin include long term skin photosensitivity in addition to relatively low absorbance at 630 nm wavelength, which may be overcome by red-shifting the absorbance band [3]. Efforts for developing second generation PSs led to discovery of several different PS where the compounds clinically approved or under trial are presented in Table 2.1.

Table 2.1: Clinically applied photosensitizers, their structures, wavelengths and target cancer types.

| **Photosensitizer** | **Structure** | **Wavelength (nm)** | **Cancer Types** |
|---|---|---|---|
| Photofrin (HPD)* | porphyrin | 630 | lung, oesophagus, bile duct, bladder, brain, ovarian |
| ALA* | porphyrin precursor | 635 | skin, bladder, brain, oesophagus |
| ALA esters** | porphyrin precursor | 635 | skin, bladder |
| Foscan (mTHPC)** | Chlorine | 652 | head and neck, lung, brain, skin, bile duct |
| Verteporfin*** | Chlorine | 690 | ophthalmic, pancreatic, skin |
| HPPH**** | chlorin | 665 | head and neck, oesophagus, lung |
| Purlytin (SnEt2)**** | chlorin | 660 | skin, breast |
| Taloporfin, LS11, MACE, NPe6**** | chlorin | 660 | liver, colon, brain |
| Fotolon (PVP-Ce6), Radachlorin, Photodithazine**** | chlorin | 660 | nasopharyngeal, sarcoma, brain |
| Silicon phthalocyanine (PC4)**** | phthalocyanine | 675 | cutaneous T cell lymphoma |
| Padoporfin (TOOKAD)**** | bacteriochlorin | 762 | prostate |
| Motexafin lutetium (LuTex)**** | texaphyrin | 732 | breast |

*Clinically approved worldwide, ** Clinically approved in Europe, *** Clinically approved worldwide for Age Related Macular Degeneration (AMD), under clinical trial in the United Kingdom for cancer treatment, **** Under clinical trial. HPD: hematoporphyrin derivative, ALA: aminolevulanic acid, mTHPC: m-tetrahydroxyphenylchlorin, HPPH: 2-[1-Hexyloxyethyl]-2-devinyl pyropheophorbide-a, SnEt2: Tin Ethyl Etiopurpurin, NPe6: Mono-aspartyl chlorin e6 (MACE), PVP-Ce6: Polyvinylpyrrolidone- Chlorin e6 (1:1).

Different hypotheses were proposed for tumour selectivity and specificity of PS [18], including extensive vascularization of the tumour and absence of lymphatic drainage [19]. Different molecules, specific to tumour markers can also be linked to PSs for targeted anti-cancer therapy [20], which the latter may also overcome the low solubility of some PS molecules: introduction of functional groups, axially or peripherally to Pcs may alleviate their hydrophobicity while enabling them to target certain tumour specific proteins, enhancing their therapeutic specificity and selectivity [21]. This approach also applies to combining Pc derivatives with chemotherapeutic drugs to induce a synergistic effect [22] - [24].

### 2.1.2. Programmed Cell Death Pathways Induced by Photodynamic Therapy

Considering the halftime of the main toxic product generated by PDT, $_1O^2$ is very short, and its' damage is usually restricted to the area where the PS molecule localizes. This localization is likely to determine the mode of cell death in PDT [25]. Among PS abovementioned (see Table 2.1); Photofrin mainly targets lipid membranes while NPe6 localizes lysosomes, Verteporfin localizes to mitochondria while m-tetrahydroxyphenylchlorin (mTHPC) target both mitochondria and endoplasmic reticulum (ER); mitochondria are reported to be the main target of Pc4 [3]. Target organelles may differ between various cell types.

Generally, PS that target endoplasmic reticulum or mitochondria promote apoptosis by inducing oxidative stress while compounds localize to lysosomes or plasma membrane initiate necrosis [26]. PS localizing to mitochondria can induce transfer of $Ca^{2+}$ from the cytoplasm to mitochondria and initiate apoptosis in a non-nuclear manner. Increased intracellular $Ca^{2+}$ upon PDT also activates tumour suppressor p53 as p53-deficient cells were found to have impaired $Ca^{2+}$ response, thus resistant to PDT [27]. In addition to intracellular $Ca^{2+}$ increase, phospholipases $A_2$ and C [28] as well as ceramide generation [29] are involved in PDT-mediated apoptosis. Without caspase activity, the necroptotic pathway is occupied [30]. Moreover, $_1O^2$ originating from mitochondria upon PDT has also shown to induce necroptosis [31].

### 2.1.2.1. Apoptosis

Apoptosis which eliminates damaged cells that potentially disrupt healthy cells' function, is a genetically programmed cell death mechanism [32] - [34] that aims to protect organisms' integrity. A wide range of stimuli as a part of physiological processes or pathological conditions can induce apoptosis such as death receptor agonists triggering apoptosis in defective immune cells or elevated neurohormonal stimulation in patients with chronic heart failure inducing cell death in cardiac and skeletal muscle cell [35] - [37]. To date, two major pathways of apoptosis are defined: extrinsic and intrinsic [38], [39]. The extrinsic pathway is mediated via activation of *Tumour Necrosis Factor Receptors* (TNFR) superfamily which includes TNFR, Fas and *TNF-Related Apoptosis Inducing Ligand* (TRAIL). Ligand binding to these receptors activates initiator caspases that eventually induce an effector caspase, usually caspase 3. Cleavage of so-called death substrates via active caspase 3 leads to characteristic hallmarks of the apoptotic process: morphological and biochemical alterations such as DNA fragmentation, nuclear fragmentation, and membrane blebbing. Extrinsic pathway cross talks with the intrinsic apoptotic pathway as well as necrosis [39], [40].

The intrinsic pathway is initiated by hypoxia, cytosolic $Ca^{2+}$ imbalance, severe oxidative stress, unfolded protein response (UPR) and genetic damage [41], [42]. Even though stress-induced intrinsic pro-apoptotic cascade is well studied, it is not completely understood; as far as we know, stress causes activation and recruitment of pro-apoptotic Bcl-2 members like Bax or Bak to mitochondria that form pores which results in cytochrome c release [43] - [45]. Released cytochrome c from mitochondria forms apoptosome complex that cleaves initiator caspase 9 to activate executioner caspase 3. As a result, same type of apoptotic response observed in the extrinsic pathway occurs (Figure 2.2).

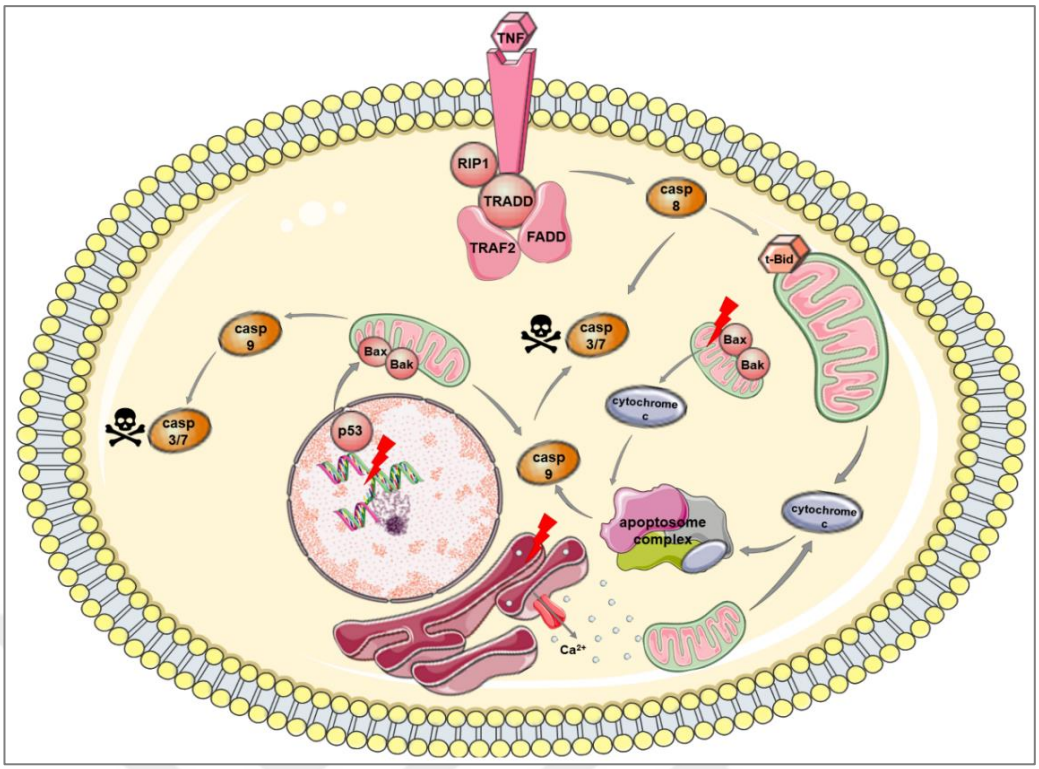


Figure 2.2: Overview of apoptosis. The extrinsic pathway is activated by the interaction between respective receptor-ligand pair that activates caspase 8 which either directly activates executioner caspases caspase 3 and/or caspase7, or processes Bid to form *truncated* Bid (t-Bid) that activates the intrinsic apoptotic pathway. Intrinsic pathway may be triggered due to the mitochondrial damage, DNA damage, or increased intracellular $Ca^{2+}$ concentration and initiated by the translocation of pro-apoptotic proteins to the mitochondrial membrane in the absence of anti-apoptotic signals. As a result, cytochrome c releases to the cytoplasm to form apoptosome complex. Apoptosome complex cleaves procaspase 9 to its active form that eventually activates executioner caspases caspase 3 and/or caspase7.

### 2.1.2.2. Necrosis

Necrosis has long been used to describe the death of tissue in an organism; however, after the term apoptosis defined in 1972 by Kerr, Wyllie and Currie utilizing morphological differences for discriminating two types of cell death, necrosis then has been used to define a distinct type of cell death [45] and refers a morphologically different form of cell death from apoptosis which was characterized by membrane swelling [46] - [48]. Nevertheless, stimuli that lead to necroptosis have received little attention as it was thought to be an unregulated, physical process [49], [50]. Today it is known that necrosis is controlled by various molecular mechanisms and occurs as a genetically encoded apoptosis-independent cell death. Several signalling elements of

regulated necrosis and apoptosis are shared and both cell death pathways are regulated by overlapping regulatory molecules [51], in example, inhibition of caspase 8 may shift the cell death mode from apoptosis towards necroptosis [52]. Necrosis is also associated with autophagy, mitochondrial dysregulation [53] and ER stress [54]. In addition to TNF receptor-1 (TNFR1) with TNF, ligand interaction with Fas [55] and Toll Like Receptors (TLRs) [56] are also able to initiate this pathway. In necrosis, upon activation, *Receptor Interacting Protein 1* (RIP1) interacts with *Receptor Interacting Protein 3* (RIP3) that phosphorylates *Mixed Lineage Kinase Domain-like* (MLKL) that translocates to the cellular membrane as well as mitochondria [57] and ER [54] to form pores. MLKL also interacts with ion channels to increase intracellular osmotic pressure [58]. DNA damage can also initiate necrosis in the presence of *Retinoic Acid Receptor gamma* (RARγ) [59] (Figure 2.3).

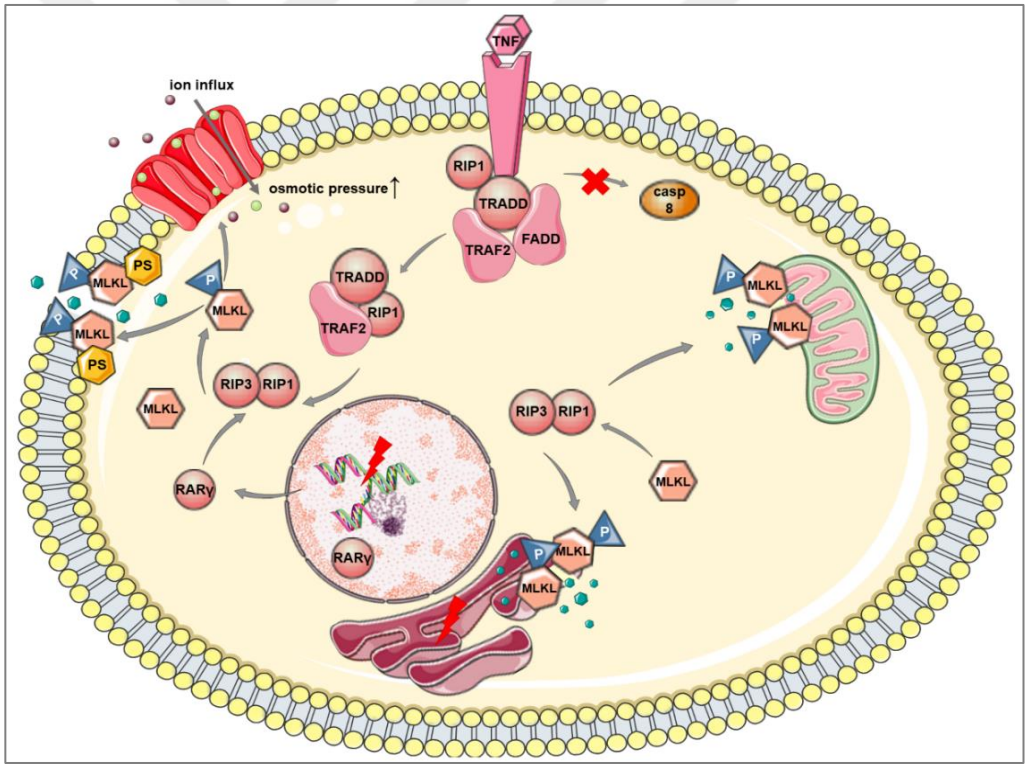


Figure 2.3: Overview of necrosis. In the absence of caspase 8 activity, ligand binding to TNFR results in the dissociation of TRADD-TRAF2-RIP1 complex to the cytoplasm. RIP1 interacts with RIP3 to phosphorylate MLKL that translocates cell membrane to form pores. Various studies indicate that MLKL can also form pores on ER or mitochondria. DNA damage can initiate necrotic response in the presence of RARγ activity.

### 2.1.2.3. Autophagy

Autophagy involves delivering old and/or damaged cytoplasmic components to lysosomes for degradation and mainly classified into three types: engulfment of cytoplasmic components by double membrane bound autophagosomes, macroautophagy [60]; direct engulfment of a substrate to be degraded by lysosomal proteases, microautophagy [61] and directing the target cargo to a lysosome by a pentapeptide motif, chaperone-mediated autophagy [62]. Autophagosome formation starts at the phagophore assembly site [63] and is characterized by the lipidation of microtubule-associated protein 1 light chain 3 (MAP1LC3; also known as LC3) via phosphatidylethanolamine [64].

Autophagy acts as a double-edged sword in the carcinogenesis process and its' exact role remains elusive. Induction of autophagy has tumour-suppressor potential, and disruption of this mechanism is shown to be related to increased cancer risk [65]. Autophagic cells secrete certain molecules that may recruit immune effector cells to the tumour site to induce immunogenic cell death [66]. On the other hand, it provides metabolic supply to malignant cells, enabling them to adjust stress conditions [67] and even may help tumour to cope with therapy-induced stress [68]. Various cancer therapies induce autophagy as a side effect [69], and pharmacological inhibition of this mechanism enhances the efficacy of the treatment while avoiding drug resistance [70] (Figure 2.4).

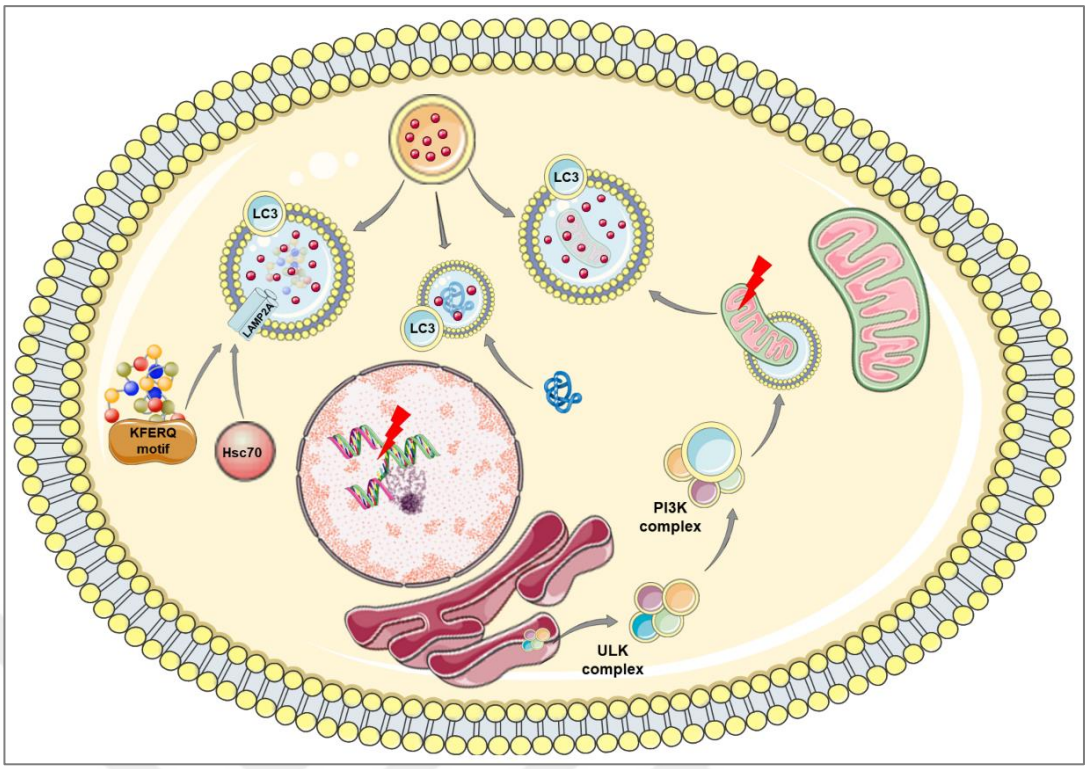


Figure 2.4: Overview of autophagy. Three distinct types of autophagy can be classified as macroautophagy (engulfment of the organelles by a vesicle), microautophagy (direct engulfment of cytosolic content) and chaperone mediated autophagy (engulfment of molecules labelled with a signalling peptide (KFERQ motif) that is recognised by cytosolic chaperone *heat shock cognate protein of 70 kDa* (hsc70) which promotes fusion of cargo and lysosome via lysosomal-associated membrane protein 2A (LAMP2A) receptor). Autophagy starts with the formation of the phagophore where UNC51 like kinase (ULK) complex forms a complex for initiating autophagosome formation. Then, activated ULK complex targets a class III PI3K complex which includes beclin 1. This complex promotes local phosphatidylinositol 3 phosphate production. At the expansion stage, ATG12–ATG5–ATG16 complex is recruited to the membrane of autophagosome where it facilitates microtubule-associated protein 1 light chain 3 (MAP1LC3; also known as LC3) lipidation with phosphatidylethanolamine.

## 2.2. Histone Structure and Nucleosomes

By interacting with certain proteins, long and fragile eukaryotic DNA is packed in the nucleus that form chromatin structure [71], [72]. After the initial studies regarding principles of chromatin organization indicating DNA is packed around the histones to form nucleosome structures, questions regarding how this “packaging” enables DNA replication have raised since this organization represents a physical barrier for the replication, repair and transcription processes [73]. Further studies

revealed that the formation of chromatin structure relies on the associations between DNA and nucleosomal histones, neighbour nucleosomes and non-histone proteins, mainly involving interactions with core histones' N-terminal tails reaching out from the compact nucleosomal core particle.

The first level of chromatin organization is the nucleosome core particle which consists of two copies of histones H2A, H2B, H3 and H4 that form an octameric structure where 146-147 bp of DNA packs around it [71]. Linker DNA connects nucleosomes to form nucleosomal arrays. The DNA sequence, the amino acid sequence of the histone and post-translational modifications play role in each nucleosomes' "primary structure" [74]. Next, packed nucleosomes are arranged as a two-start helical model that forms 30-nm fibre and is mediated by the internucleosomal interactions between core histones [71]. Further fibre-fibre interactions result in higher compaction which can be observed in condensed chromosomes [75]. Chromatin formation is schematized in Figure 2.5.

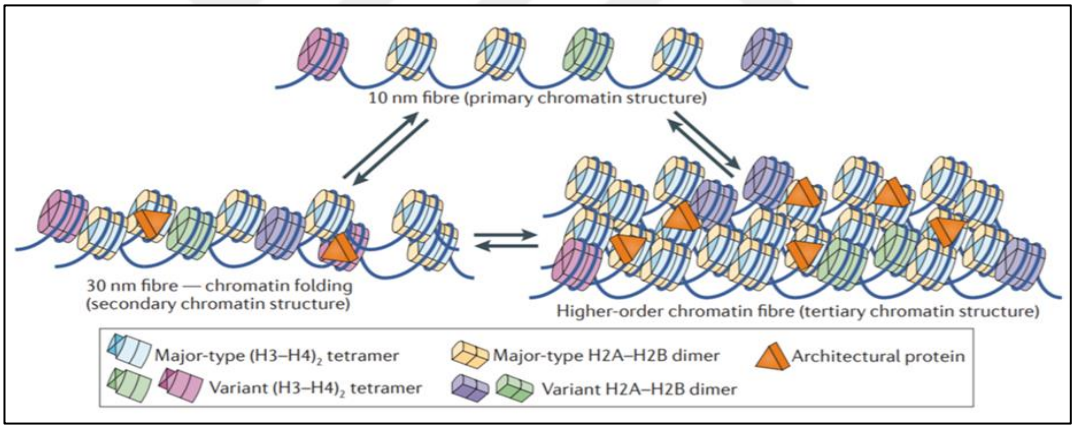


Figure 2.5: Structures of chromatin. Primary structure consists of nucleosomes with major histones or various histone variants. Histone variants and post-translational modifications may play role in nucleosome dynamics and structure. Protein sequence, the effect of chromatin-remodelling enzymes and DNA binding may have impact on the spacing between nucleosomes. Neighbouring nucleosome interactions result in secondary chromatin structure, the folded chromatin fibres which can be observed in the lower left panel. Interactions between fibres are affected by the primary structure. Various proteins stabilize secondary and tertiary structures (*architectural proteins*, orange triangles). Major type histone tetramer and dimer are shown in light blue and yellow, respectively whereas variant tetramers and dimers are shown in green and pink or purple and green, respectively. Double arrows represent transitions between different states which may be regulated via post-translational modifications, architectural proteins, chromatin-remodelling factors and changing histone variants.

## 2.3. Histone Deacetylases

The addition of an acyl group from an acyl-CoA donor to the lysine residue is termed acylation, and acylation involves acetylation [72]. N-termini of the core histones contain conserved and positive charged lysine residues that have affinity to negatively charged DNA. Acylation of lysine residues conceals the positive charge, reducing its affinity for chromatin and leaving the DNA uncovered. In other words, acetylation of the lysine residues of the histones enables gene expression whereas deacetylation leads to chromatin condensation and results in transcriptional gene silencing [76]. The number of the lysine residues in each N-termini correlates with the strength of the mechanism: lysines account for the 27%, 33%, 22% and 20% of the N-terminal tail of histones H2A, H2B, H3 and H4, respectively. It should be noted that lysines are also available for ubiquitination and methylation, suggesting a competition between post translational modifications [72].

As reported in the early 1960s, histone lysine acetylation was the first histone acylation identified [77], followed by the discovery of an enzyme that removes the acetyl groups from histones in 1969 [78]. Further studies focused on the connection between histone acetylation, altered chromatin structure and transcription, implying acetylation of the lysine residues mediate various transcriptional regulations in yeast and fruit flies [79]. Yet, the main link regarding transcription and histone acetylation has revealed with the discovery of *Tetrahymena* Histone Acetyltransferase A (HAT-A) that is related with the Gcn5 in yeast and acetylase histones [80]; and a mammalian histone deacetylase which is an ortholog of yeast Rpd3 and removes acetyl groups [81]. Later, studies have identified various members of both histone acetyltransferase (HAT) and histone deacetylase (HDAC) enzyme families. In fact, recent studies imply that some HDACs may also deacetylate nonhistone proteins which should be taken into consideration when aiming to unravel the function of the enzyme [82]. Moreover, HDACs can interact with the nuclear receptor, or interact with various transcription factors to regulate gene expression [83].

HDACs form multiprotein complexes that interact with DNA binding factors including various epigenetic modification-related genes, transcription factors and nuclear receptors to target specific genomic regions [76]. An example is the interaction between HDACs and methylated DNA mediated by methyl-binding proteins that

engage a multiprotein complex containing HDAC to the methylated gene promoter in order to repress transcription. HDACs can also interact with methyl transferases.

To our knowledge, the human HDAC family consists of 18 members and divides into four classes: class I Rpd-3-like proteins (HDAC1, HDAC2, HDAC3 and HDAC8); class II Hda-1-like proteins (HDAC4, HDAC5, HDAC6, HDAC7, HDAC9 and HDAC10); class III Sir2-like proteins (SIRT1-7) and class IV protein (HDAC11) [82].

### 2.3.1. Histone Deacetylase Families and Classes

HDACs belong to the histone deacetylase family or Sir2 regulator family. Conventional categorization of HDACs relies on the sequence similarities: Class I proteins have similar sequences with the yeast Rpd3 protein whereas Class II proteins share similarities between yeast Hda1 protein while Class III proteins have sequence similarities with yeast Sir2 protein. Class IV protein HDAC shares similarities with both Class I and Class II HDACs. As also indicated by the structural studies; the significant homology between human Class I and Class II HDACs and different species' HDAC homologs suggest a common mechanism for acetylated substrates' metal-dependent hydrolysis while Class III HDACs use NAD+ to deacetylate acetyl-lysine residues [82].

#### 2.3.1.1. Class I Histone Deacetylases

The first human histone deacetylase purified and characterized was HDAC1 [81]. This discovery was followed by the identification of HDAC2 as a negative regulator of transcription [84]. Both HDAC3 and HDAC8 were discovered during investigations of the GeneBank to identify proteins with similar sequences to other HDACs [85], [86]. Deacetylase domains of Class I HDACs share a 45–94% sequence identity [82]. While Class I HDAC members initially thought to be located to the nucleus, various studies suggest they also localize to the cytoplasm or certain organelles and exert certain extranuclear functions.

### 2.3.1.2. Class II Histone Deacetylases

Both HDAC4, HDAC5 and HDAC6 were identified during GeneBank searches in an effort to discover human HDACs with similar sequences to yeast Hda1 [87]. While these proteins resemble Class I human HDACs in terms of their catalytic domains, they also have other sequences that have no similarities with the Class I enzymes. HDAC4, HDAC5, and HDAC6 have lower *in vitro* HDAC activity at a lower level compared to their Class I counterparts. In addition, HDAC6 bears two deacetylase catalytic domains that function independently as a unique feature. HDAC7 was first isolated in 2000 and contains three repressor domains in which two of them have independent autonomous repressor activity whereas the third has deacetylase repressor function [88]. HDAC9 was discovered by a homology database search [89]. Altogether, Class IIa HDACs consist of HDAC4, 5, 7, and 9 which share a 48–57% similarity. HDAC10 was discovered to share the highest similarity with HDAC6, both possessing a unique second catalytic domain [90]. Thus, HDAC6 and HDAC10 make up the Class IIb. Both Class IIa and Class IIb HDACs show cytoplasmic in addition to nuclear localization, indicating cytoplasmic functional activity [82]. Conserved deacetylase domains of Class II HDACs share a 23%–81% sequence identity.

### 2.3.1.3. Class III Histone Deacetylases (Sirtuins)

Studies using *S. cerevisiae* Sir2 sequence as a probe enabled the identification of human sirtuin proteins SIRT1, SIRT2, SIRT3, SIRT4 and SIRT5 [91]. SIRT6 and SIRT7 were identified in a similar manner by using the SIRT4 as the probe. All sirtuins share 22%–50% similarities according to their amino acid sequences and 27–88% similarities when their conserved catalytic domains are compared [82]. Sirtuins possess mono-ADP-ribosyltransferase activity in addition to histone deacetylase, in addition, SIRT5 has shown to have lysine desuccinylase and demalonylase activities *in vitro* [92].

### 2.3.1.4. Class IV Histone Deacetylases (HDAC11)

HDAC11, the only member of the Class IV HDAC shares homology with both Class I and II HDACs and first discovered by Gao et al. [93]. HDAC11 is the least studied member among the classical HDAC family and is only known to regulate interleukin 10 expression as well as the protein stability of CDT1 [82].

## 2.3.2. Histone Deacetylase Inhibitors in Cancer

Chromatin is a long-known target for cancer treatment [94]. With the emergence of genome sequencing technology, various mutations have detected within the chromatin regulating genes, contributing to malignancy. In the beginning of the 2000s, DNA methylation, especially repressing tumour promoting genes via promoter hypermethylation was the most extensively studied epigenetic modification in cancer [95]. Further studies, however, provided more knowledge on histone modifications in cancer progression.

Histone acetylation controls approximately 2–10% of total gene expression [96]. Essentially, deacetylation results in chromatin condensation and subsequently downregulation of the respective gene while acetylation by histone acetyl transferases (HAT) unwinds the DNA and upregulate gene expression [97]. HDACs also present at active transcription sites to reset chromatin acetylation [98], or for certain complexes, to recognize acetylated lysine residues [99].

Acetylation affects the activity of various other non-histone proteins; examples include DNA repair enzymes, DNA-binding transcriptional factors and nuclear receptors, signalling mediators, proteins regulating transcription and remodelling [100]. This also explains why HDAC inhibition does not always result in transcriptional upregulation once the chromatin is loosened. Histone acetylation/deacetylation imbalance can alter gene expression profiles, thus may alter certain signalling pathways, change proteasomal degradation, alter protein kinase C activity and control other epigenetic alterations. Previous studies reported that HDAC inhibitors (HDACi) may increase the acetylation/deacetylation ratio and may provide beneficial effects for cancer management [100]. Five different HDACi classes include hydroxamic acids (hydroxamates), aliphatic acids; benzamides; cyclic tetrapeptides;

and sirtuin inhibitors. HDACi can target either certain HDACs (isoform specific HDACi) or all HDACs (pan HDACi). Table 2.2 demonstrates selected HDACi, their target HDACs and clinical status. Many other HDACis are under preclinical investigation.

Table 2.2: Overview of certain HDACis, their targets and clinical status.

| Class | HDAC inhibitor | Target Class | Clinical Status |
|---|---|---|---|
| hydroxamic acids | Trichostatin A (TSA) | pan | preclinical |
| | SAHA* | pan | approved for cutaneous T-cell lymphoma |
| | Belinostat | pan | approved for peripheral T-cell lymphoma |
| | Panabiostat | pan | approved for multiple myeloma |
| | Givinostat | pan | phase II clinical trials—relapsed leukaemia and multiple myeloma |
| | Resminostat | pan | phase I and II clinical trials—hepatocellular carcinoma |
| | Abexinostat | pan | phase II clinical trial—B-cell lymphoma |
| | Quisinostat | pan | phase I clinical trial—multiple myeloma |
| | Rocilinostat | II | phase I clinical trial—multiple myeloma |
| | Practinostat | I, II and IV | phase II clinical trial—prostate cancer |
| | CHR-3996 | I | phase I clinical trial—advanced/metastatic solid tumours refractory to standard therapy |
| short chain fatty acids | Valproic acid (VPA) | I, IIa | approved for epilepsy, bipolar disorders and migraine, phase II clinical trials—several studies |
| | Butyric acid | I, II | phase II clinical trials—several studies |
| | Phenylbutyric acid | I, II | phase I clinical trials—several studies |
| benzamides | Entinostat | I | phase II clinical trials—breast cancer, Hodgkin´s lymphoma, non-small cell lung cancer, phase III clinical trial—hormone receptor positive breast cancer |
| | Tacedinaline | I | phase III clinical trial—non-small cell lung cancer and pancreatic cancer |
| | 4SC202** | I | phase I clinical trial—advanced haematological malignancies |
| | Mocetinostat | I, IV | phase II clinical trials—Hodgkin´s lymphoma |
| cyclic tetrapeptides | Romidepsin | I | approved for cutaneous T-cell lymphoma |
| sirtuin inhibitors | Nicotinamide | all class III | phase III clinical trial—laryngeal cancer |
| | Sirtinol | SIRT 1 and 2 | Preclinical |
| | Cambinol | SIRT 1 and 2 | Preclinical |
| | EX-527*** | SIRT 1 and 2 | cancer preclinical, phase I and II clinical trials—Huntington disease, glaucoma |

* Suberoylanilide hydroxamic acid (Vorinostat), **Domatinostat, *** Selisistat.

### 2.3.3. Anti-Cancer Mechanism of Histone Deacetylase Inhibitors

HDACi can induce cell cycle arrest, differentiation, and programmed cell death mechanisms [100]. As many hallmarks of cancer are influenced by epigenetic alterations; Dawson and Kouzarides have suggested that HDACs may be crucial for cancer survival and growth, hence cancer cells would be relatively susceptible to HDACi treatment compared to healthy cells [101]. Anti-cancer properties of HDACis depend on various parameters such as the drug itself and type of cancer [102].

#### 2.3.3.1. Activating Programmed Cell Death Pathways

In addition to downregulating cyclin A and cyclin D expressions, HDAC1 inhibition enables tumour suppressor protein p53 to promote cell cycle arrest via increasing cyclin dependent kinase inhibitor p21 activity which, in turn, blocks interactions between cyclins and cyclin dependent kinases (CDKs), eventually leading to cell cycle arrest [100]. Romidepsin administration along with genetic HDAC1 ablation can also induce autophagy [103]. HDACis' role on autophagy is controversial; a study suggests that administration of autophagy inhibitors potentiate HDACis' anti-cancer efficacy [104] while another one indicates that an autophagy blocker is able to prevent Vorinostat (SAHA)-induced cytotoxicity [105]. Likewise, Vorinostat was proven to exert anti-cancer effects via autophagy in endometrial stromal sarcoma cells as well as in a glioblastoma multiforme murine model [106], [107]. In another study, p53-initiated apoptotic pathway was reported to be the preliminary target of Vorinostat, and the absence of this protein activates autophagy [108].

HDACis also modulate certain protein kinases' activities to regulate growth, differentiation and cell death. One example is ERK, which is induced by HDACis yet the exact mechanism remains unclear [109], [110]. Certain studies suggest HDACis may induce the expression of anti-apoptotic and growth-promoting proteins to support tumour cell growth [109]. Valproic acid (VPA) activates *wingless* (Wnt) pathway, which plays important role in many cancers via phosphorylation of glycogen synthase kinase-3β (GSK-3β) [111], [112]. Wnt pathway is proven to be aberrantly expressed in many cancers, and proven to play role in cancer stem cell development [100].

### 2.3.3.2. Regulating non-coding RNA

HDACi can regulate non-coding RNA expressions to promote different miRNAs expressions, and proven to induce apoptosis in thyroid cancer cells [113] and cellular senescence [114]. In addition to regulating various transcriptional and post-transcriptional events, Long non-coding RNAs (lncRNAs) make up the micro RNA (miRNA) precursors and exert epigenetic effects by recruiting histone modifying complexes to target loci according to the histone marks [114], [115]. Overexpression of intergenic lncRNAs is linked with cancer [116]. While alterations in lncRNA expression levels might provide insight into HDACis anti-cancer properties, further studies regarding non-coding RNAs are required to elucidate the mechanism.

### 2.3.3.3. Regulating the Immune System

Tumour antigens epigenetically silenced disable immune recognition of the malignant cells by the immune system [117]. By altering epigenetic modifications, HDACi may upregulate expression of human leukocyte antigens (HLA) and make the tumour "visible" by the immune system [118], [119]. *In vivo* studies indicate that HDACi may increase immunogenicity and promote T cell activation that eventually contributes to survival [120], [121]. Inhibition of different HDACs may have distinct effects on immune cells as Class II HDAC inhibition enhances T regulatory cells (Tregs) activity where Class I HDAC inhibition promotes Natural Killer (NK) cells and CD8+ T cells' functions [122].

### 2.3.3.4. Modulation of Angiogenesis

HDACi can downregulate many genes that involve in angiogenesis process including vascular endothelial growth factor (VEGF), vascular endothelial growth factor receptor (VEGFR), and endothelial nitric oxide synthase (eNOS) while increasing anti-angiogenic factors such as Transforming growth factor β (TGFβ) and Thrombospondin-1 (TSP-1) [123] - [126]. In addition, HDACi treatment induces hyperacetylation and subsequent degradation of pro-angiogenic modulator *hypoxia inducible factor 1 alpha* (HIF-1α) [127]. Yet, the anti-angiogenic effect of HDACis

may remain controversial as HDACi treatment also increase expressions of certain matrix metalloproteinases (MMPs), and remodelling of the extracellular matrix (ECM) is an important contributor to angiogenesis [128].

### 2.3.4. HDACi Treatment in Solid Tumours

HDACi treatments are mainly approved for haematological malignancies [94], [129]. The examples include Vorinostat, Belinostat, Panobinstat and Romidepsin for cutaneous T-cell lymphoma, peripheral T-cell lymphoma, multiple myeloma and cutaneous T-cell lymphoma, respectively [100], [129]. Due to high HDACi expression observed in certain solid tumours, (such as high HDAC6 expression in breast cancer or HDAC2 in colorectal, cervical and gastric cancers) [100], the success of HDACi in haematological cancers introduced them into clinical trials for targeting solid tumours. However, the results were not as it was anticipated: HDACi treatment in solid tumours remained ineffective while leading to toxic side effects [130]. Patients suffering from certain solid tumours such as colorectal, non-small cell lung, thyroid and refractory breast cancers and received Vorinostat did not show partial or complete response, yet the drug-induced side effects were very common [131], [132]. Even an *in vitro* study involving Vorinostat revealed that treatment triple negative breast cancer (TNBC) with this particular pan-HDACi is able to promote motility via promoting epithelial-mesenchymal transition (EMT) and may contribute to metastasis [133]. Trials involving patients receiving Romidepsin as a monotherapy for solid tumours indicated similar results in terms of ineffectiveness and toxicity [134], [135]. Only positive outcome reported was the clinical disease stabilization ability of HDACis abovementioned for certain patients.

Frankly, results obtained from combinations of chemotherapeutic drugs with HDACis were not in line with monotherapy results. In an animal inflammatory breast cancer (IBC) model, combinatorial administration of Romidepsin and Paclitaxel was found efficient for eliminating both primary and metastatic tumours [136]. An *in vitro* study revealed Vorinostat can sensitize oral squamous cell carcinoma cell lines to low doses of cisplatin [137]. It should be noted that these results may not entirely represent an absolute success since clinical trials showed relatively less striking results: In a phase I clinical study, patients administered Belinostat in combination with

Carboplatin (cyclobutane-1,1-dicarboxylate-O,O′) and/or paclitaxel. Six patients showed clinical stabilization while two of them had partial responses, and one had complete response among 23 patients [138].

Halsall et al. suggested that HDACi treatment downregulates lysine acetyltransferases (KATs), which also target acetylated promoters and eventually counteracts with HDACi activity [139]. Authors proposed a hypothetical model, where both acetylated and non-acetylated isoforms of a certain protein promote different gene sets. HDACi leads to a sharp increase in acetylated isoform of the target protein that results in downregulation of KAT complex. As a regulatory mechanism, transcription of KAT complex components increases to shift upregulated genes from one set to another set [129]. This phenomenon may be explained with evolutionary mechanisms: various HDACis are readily present in the nature and secreted by organisms to survive in a competitive environment [129]. Epigenetic control mechanisms are unique to *Eukaryota*, and likely to be the targets of competing *Prokaryota*. Thus, eukaryotic organisms are expected to have resistance against environmental HDACis as a survival mechanism, which may also be the underlying cause of HDACi treatments' ineffectiveness against solid tumours. The mechanism is schematized in Figure 2.6.

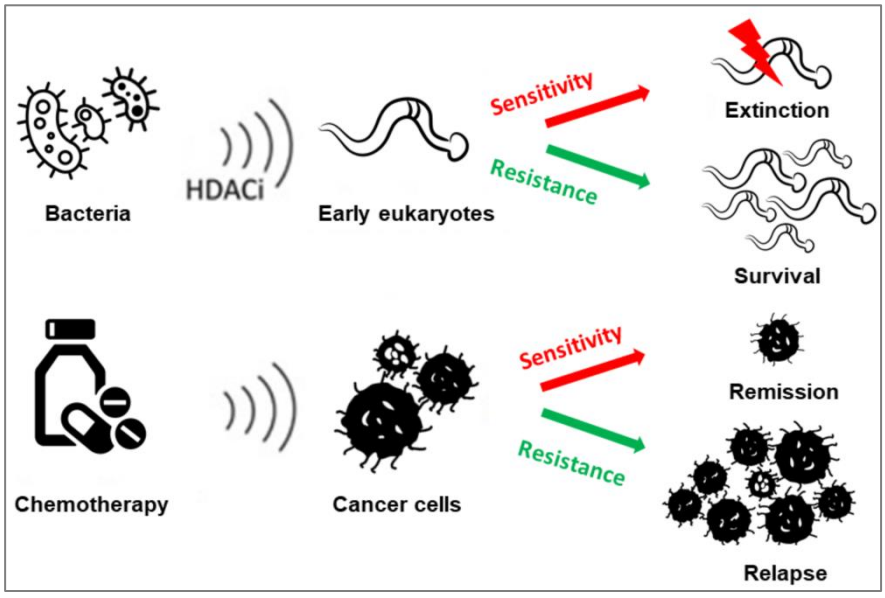


Figure 2.6: Suggested evolutionary mechanism behind tumour cells' HDACi resistance. Early eukaryotes developed a resistance mechanism to deal with the hyperacetylation caused by bacterial HDACi. Cancer cells conserving this mechanism may lead to HDACi resistance.

## 2.4. Breast Cancer

Being the most common malignancy among women, every year 1.5 million patients are being diagnosed with breast cancer (which accounts for 25% of all women diagnosed with cancer), and it is estimated that 12% of all women will be diagnosed with breast cancer during their lifetimes [140], [141]. Survival rates differ between countries: the estimated 5-year survival rate is ~ 80% in developed countries whereas it remains below 40% in developing countries [140]. Breast cancer is the most common oncological malignancy in Turkey as each year, 10.000 women are diagnosed with the disease while its ratios in different regions are reported as 20/100.000 for eastern regions and 40-50/100.000 for western regions [142]. The higher ratios in western regions of the country may be attributed to the effect of modern lifestyle on breast cancer development, or the accessibility of the women living in relatively developed parts of the country to healthcare services.

Due to its heterogenic nature as well as variable morphological and biological features, different clinical approaches are adopted for the treatment of the disease [143]. Breast cancer classification provides structural data to clinicians and facilitates successful treatment by aiming to answer two questions: type and degree of the tumour and stage of the tumour. Type and degrees of breast tumours rely on histological subtypes and stages which are determined by the World Health Organization (WHO). Breast tumours' stages are correlated with the size of the tumour, node invasion and metastasis. Routine investigation of breast cancer involves expression levels of oestrogen receptor alpha (ERα), progesterone receptor (PR) human epidermal growth factor receptor 2 (HER2) [143]. Evaluations of these three prognostic markers form the basis for breast cancer assessment by providing predictive information by guiding the physician to adopt hormone-based and/or anti-HER2-based therapy.

Expression of nuclear sex steroids ER and PR plays role in the proliferation of both healthy and neoplastic mammary epithelia and observed in 75% of all breast cancers. Both markers are assessed by immunohistochemistry (IHC) and directly correlate with the success of the hormone therapy [144]. Generally double positivity of the hormone receptors is observed as positivity of just one receptor is rather rare, and indicates relative aggressive nature and resistance to hormone-based therapies in comparison with double positive tumours [145], [146]. HER2 overexpression is

observed in approximately 15% in breast cancer and assessed by IHC and in situ hybridization (ISH). HER2 overexpression is related to aggressive clinical behaviour as well as poor prognosis, and HER2 is a predictive marker for the success of anti-HER2 based therapies [147]. Tumours that account for 10-15% of all breast cancer cases do not express the markers abovementioned are classified as "triple negative breast cancer" (TNBC). TNBC diagnosis is associated with poor prognosis and the patients can't benefit from hormone based or anti-HER2 therapies. Traditionally, breast cancer subtypes determined by the expressions of ER, PR, HER2, and Ki-67 markers with IHC are given below [143]:

- Luminal A-like (ER+, PR≥20%, HER2−, Ki67<20%)
- Luminal B-like (ER+, PR<20% and/or HER2+ and/or Ki67≥20%)
- HER2-overexpression (ER−, PR−, HER2+)
- Basal-like (triple negative: ER−, PR−, HER2−)

Current approaches also involve molecular profiling of breast cancer subtypes. Examples include Oncotype Dx assay (21-gene signature) and the Mammaprint assay (70-gene signature), both clinically approved and provide insight to the course of the disease as well as guiding the therapy [148].

### 2.4.1. Metastasis in Breast Cancer and the Role of Chemokine Receptors

The development of screening methods that allow the diagnosis of breast cancer at early stages led to a dramatic decrease in breast cancer related deaths [149]. On the other hand, the disease is nearly incurable for patients that are diagnosed with metastases. Even 30% of patients diagnosed at early stages eventually develop metastatic lesions, months or sometimes years later [150]. Metastases are considered as the main cause of cancer related deaths [148].

Small chemoattractive cytokines; chemokines are the largest family of cytokines that are classified into four according to the position of first to cysteine residues: the CC-chemokines, the CXC-chemokines, C-chemokines and $CX_3C$-chemokines [151]. Chemokine system consists of approximately 50 endogenous chemokine ligands and 20 chemokine receptors that regulate many cellular functions [152] including primary

and secondary adaptive cellular and humoral immune responses [151] as well as tumour proliferation, metastasis and invasion [153]. Chemokine receptors consist of seven transmembrane spanning domains that belong to G protein-coupled cell surface receptors (GPCRs) [154]. Chemokines also bind atypical chemokine receptors (ACKR) [155] or glycosaminoglycans [156]. Chemokine-ACKR interaction does not induce conventional chemokine receptor signalling pathways but maintains tissue chemokine gradient [157].

C-X-C chemokine receptor type 4 (CXCR4) binding to its ligand CXC chemokine stromal-derived-factor-1 (SDF-1, or CXCL12) regulates many physiological processes including immune cell homeostasis and homing hematopoietic cells within the bone marrow. It also initiates signalling cascades that lead to increased cell survival, proliferation and migration [152]. Various cancer cells express CXCR4 that are able to metastasize to distant sites expressing CXCL12. CXCL12- CXCR4 binding induces signalling pathways that result in chemotaxis, cell survival, proliferation and increased intracellular calcium. CXCR4 expressed by tumour cells also promotes vascular endothelial growth factor (VEGF) production by tumour cells to promote vascularization. Another study also proposed that CXCL12 can stimulate vasculogenesis in the absence of VEGF in vitro by promoting migration bone-marrow-derived pericytes to close association with endothelial cells, inducing remodelling of the vascular endothelium into a larger and functional structure [158].

Blocking the interaction between CXCR4 and its ligand CXCL12 has shown to reduce metastasis significantly including breast cancer *in vivo* [159]. Moreover, CXCR4 inhibitors are currently used in clinical trials and have shown promising results in haematological malignancies as various phase III clinical trials are still ongoing. By 2018, two clinical treatments evaluating CXCR4 inhibitors with standard chemotherapy were reported. These trials were performed on advanced small cell lung carcinoma and metastatic renal cell carcinoma. Even this approach is considered safe, it did not show any clinical efficiency, raising questions regarding other tumour promoting pathways that may be compensating when CXCR4 is lacking [160]. The role of CXCR4 on breast cancer can be summarized as given below [161]:

- CXCR4 to CXCL12 binding recruits endothelial progenitors to tumour sites to promote angiogenesis

- CXCR4 induces typical signalling pathways that promote cell proliferation: various effectors of CXCR4 include PI3K/AKT, Src/ERK1-2, NF-κB, and STAT3 which all known to contribute to primary breast cancer growth. CXCR4 also affect other stem cell-related pathways such as Notch, Wnt, and SHH that play role in breast cancer proliferation.
- CXCR4-CXCL12 interaction recruits immune cells to tumour site to promote tumour growth.
- Recent studies indicate that CXCR4 signalling also regulates hormone dependent breast cancer proliferation; oestrogen E2 promotes CXCR4 transcription via binding to CXCR4 promoter. On the contrary, even though it increases MCF-7 cells' growth; oestrogen inhibits CXCR7, which is another receptor for CXCL12 to decrease cancer growth rate.
- In metastatic breast cancer, CXCR4 promotes metastasis to organs expressing high level of CXCL12 including lung, bone and liver.

CD44 transmembrane glycoproteins belong to cell adhesion molecules; they involve in the regulation of many physiological and pathological processes including cancer [162]. CD44 also acts as a hyaluronan (HA) receptor, which is a major component of ECM [163]. In a study published in 2013; authors draw attention to a regulatory interaction between CXCR4, HA and CD44 on both tumour and endothelial cells: high molecular HA has shown to increase activation of CXCR4 by CXCL12 whereas small HA oligosaccharide blocks the pathway. Altogether, HA is proven to modulate CXCR4-CXCL12 signalling via CD44 [164]. Moreover, it is shown that CD44 to HER2 binding initiates signalling cascade to induce expression of CXCR4 in gastric cancer [165].

CC-chemokine receptor 7 (CCR7) is another chemokine receptor, known to play role in tumour formation, metastasis and invasion. CCR7 is also involved in EMT in breast cancer. In clinical studies, high CCR7 expression is linked with poor prognosis and short survival rate, indicating its involvement in breast cancer development and recurrence [166]. CCR7 over-expression has been shown to correlate with deeper lymphatic invasion and larger primary tumours. Clinical studies reveal that metastatic tumour formation is inhibited via diminishing CCL21 expression in secondary lymphoid organs, reducing CCR7-expressing tumour cells' chemotaxis [167].

CXCR4 or CCR7 increases chemotaxis and invasiveness in breast cancer by regulates actin polymerization and pseudopodia formation [168]. Besides, functional expressions of CXCL4 and CCR7 simultaneously initiate signalling pathways that promote metastasis by inhibiting detachment-induced cell death (anoikis) both *in vitro* and *in vivo* [169].

In the light of the information given above, in this thesis project, we aimed to investigate:

- Anti-cancer efficacy of the HDACi substituted Pc derivatives.
- Differential effects of various Pc derivatives bearing Si, Zn or In as the core metal.
- Differential effects of non-peripheral and peripheral HDACi substitutions.

For this purpose, we investigated anti-cancer efficacy of five different Pc-HDACi derivatives on breast cancer cell lines MCF-7, MDA-MB-231 and a healthy cell line, HUVEC. Parameters evaluated in this context included cellular localization, cell viability and apoptosis rates, DNA content, mitochondrial activity, protein levels of HDAC6 and HDAC8 (two targets of the HDACi moiety, 3-HPT), protein levels of three components that play role in migration and invasion, chemokine receptors CXCR4 and CCR7, and CD44.

# 3. MATERIALS AND METHODS

## 3.1. Construction of the LED Array

The irradiation device was constructed according to the study published by Pieslinger et al. [170] to enable irradiating multiple assay sets at a time. Light emitting diodes (LEDs) with 700 nm peak and 660 nm dominant wavelengths were purchased from Foryard Optoelectronics. LED array was constructed by soldering 432 hi-red LEDs to an aluminium printed circuit cardboard (15 × 24 cm) in parallel. Current permitted for each LED is 20 mA. After soldering, the array was placed to the ceiling of a 16 × 26 cm aluminium case. Grooves for placing a shelf to hold plates were added to the case; enabling to adjust the distance between the plate bottom and diode tips from 4 to 14 cm. A board, divided to 2 × 2 cm squares was used for holding plates as well as determining optical dose. This study was conducted at a 6 cm distance, which is proven to provide ideal illumination in previous studies, and further characterization studies were performed according to the mentioned distance [170]. Placing LEDs to the ceiling of the array instead of the bottom would allow the researcher to irradiate 3D cultures on agarose moulds or conventional petri dishes coated with different materials that prevent attachment [171]. Materials which cells are placed on may diffract the light and decrease the irradiation efficacy in such cultures whereas the light would not face an obstacle if LEDs are placed above cells.

### 3.1.1. Determination of Irradiation Homogeneity and Calculating Optical Dose

Power and homogeneity of illumination were measured with an optical powermeter (Ophir Photonics, Israel). The board was placed to adjust the distance between the diode tips and plate bottom to 6 cm. Power of light exposure on each square was measured individually in milliwatts (mW) and converted to joule/s with the formula *1 mW = 0.001J/s* to calculate the energy of light, measured on each square. The area showing most homogeneous irradiation pattern was measured as 180 $cm^2$ (Figure 3.1) and found to be sufficient for irradiating two 96 well plates at the same time. Since total optical dose was determined as 500 mJ according to a previous study

published by Atilla et al. [172] time required for delivering 500 mJ on the area mentioned above was calculated as 34 minutes.

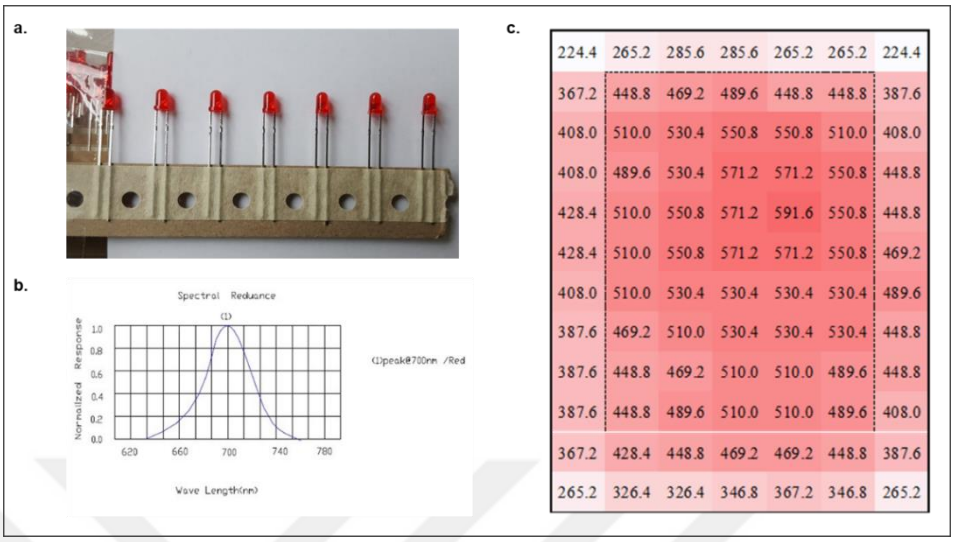


Figure 3.1: Construction of the LED array. a. LEDs before soldering to the aluminium cardboard. b. Peak wavelengths of the LEDs. c. Illumination power of LED irradiation device in millijoules on each 2×2 squares. Area indicated with dashed line was used for irradiating plates. Borders of the board was not used due to low illumination power.

### 3.1.2. Determination of Media Warming

Wells of a 96 well plate was filled with 100 µl of Dulbecco's phosphate buffered saline (DPBS) at room temperature and placed in irradiation device, Plate was exposed to light for 34 minutes; after, the temperature of the liquid in random 10 wells were measured with a liquid-in-glass laboratory thermometer to ensure that irradiation do not heat medium over 37ºC. Measurements were performed in a dark room; the ambient temperature was set to 22ºC and humidity was recorded as 35%. Temperature after irradiation was measured 29ºC, revealing operating irradiation device for indicated time period do not over-heat cultured cells.

## 3.2. Compounds Used in This Study

The HDACi used in this study, 3 hydroxypyridine-2-thione (3-HPT) (1d) is a Zinc-Binding Group (ZBG) HDACi that inhibits HDAC6 and HDAC8 with an $IC_{50}$ of 681 nM and 3675 nM, respectively [173]. 3-HPT was synthesized according to the

literature by Prof. Dr. Devrim Atilla, Prof. Dr. Ayşe Gül Gürek and Aysel Günay; the synthetic pathway is given in Figure 3.2.

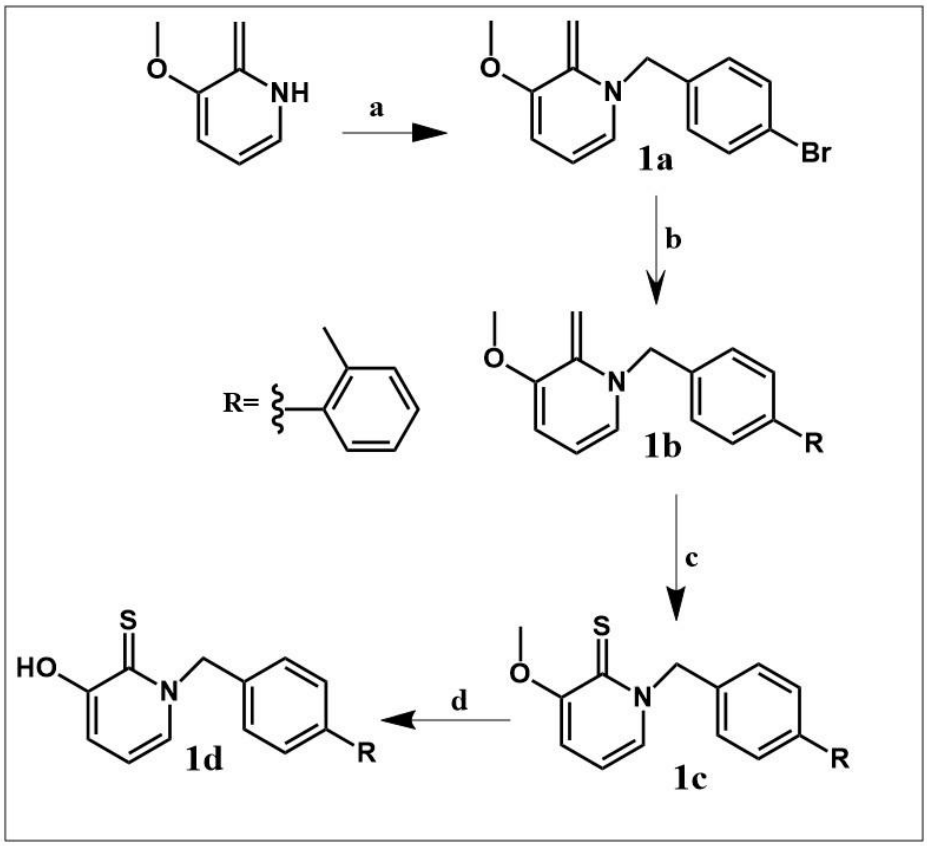


Figure 3.2: Synthetic pathway of 3-HPT. 1-(4-bromobenzyl)-3-metoxyprydine-2-one was synthesized (1a) from 3-methoxypryridine-2-one and 4-bromobenzyl bromide in presence of potassium carbonate and tetrahydrofuran (THF). 1-(2-methyl-(1,1'-biphenylmethyl)-3-metooxypyridine-2-one (1b) was obtained by the reaction of 1a with (4-(dimethylamino)fenyl)boronic acid, $Pd(PPh_3)_4$, $K_2CO_3$ in presence of toluen:ethanol:water followed at reflux temperature. 1b was heated with Lawesson reagent to obtain 3-methoxypyridine-2-thione (1c). HDAC inhibitor 1-(2-methyl-(1,1'-biphenylmethyl)-3-hidroxypyridine-2-thione (1d) was synthesized from reaction between 1c, $BBr_3$ and $CH_2Cl_2$.

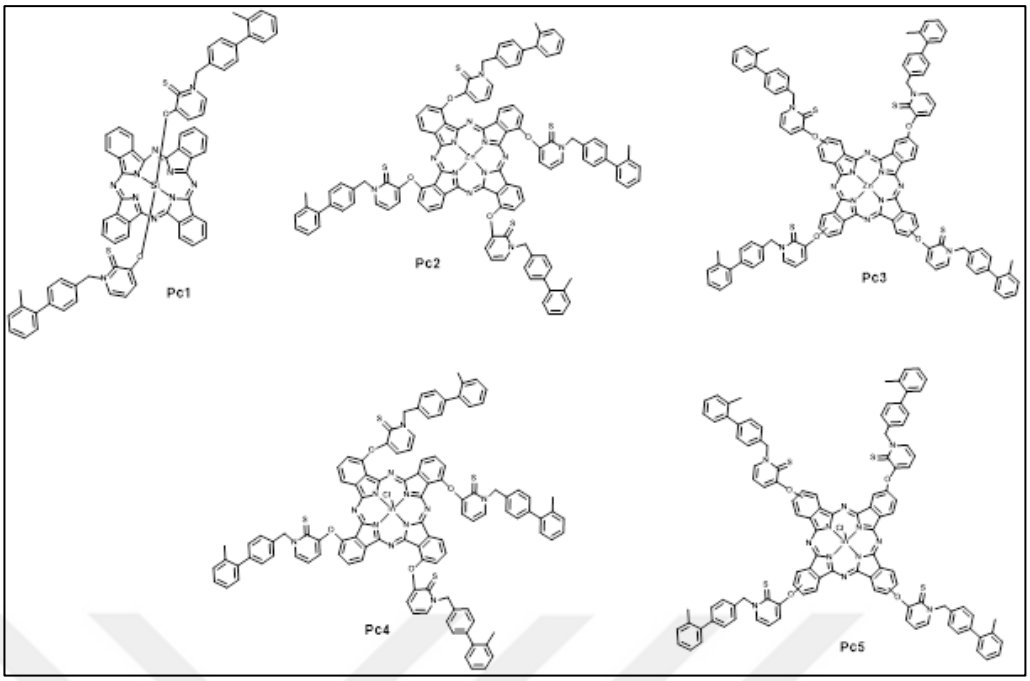


Figure 3.3: Chemical formulas of the compounds used in this study. Axial HDACi substituted SiPc, Pc1, non-peripheral HDACi substituted ZnPc, Pc2, peripheral HDACi substituted ZnPc, Pc3, non-peripheral HDACi substituted InPc, Pc4, and peripheral HDACi substituted InPc, Pc5.

The silicon phthalocyanine derivative (Pc1) contains axially substituted two 3-HPT residues while the zinc phthalocyanine derivatives (Pc2) contains non-peripherally substituted four 3-HPT residues and (Pc3) contains peripherally substituted four 3-HPT residues. Among indium phthalocyanine derivatives, (Pc4) contains non-peripherally substituted four 3-HPT residues whereas (Pc5) contains peripherally substituted four 3-HPT residues.

## 3.3. Cell Culture Conditions

MCF-7 and MDA-MB-231 cells were cultured in high glucose (4.5 g/L) Dulbecco's Modified Eagle's Medium (DMEM), while DMEM/F12 was used for culturing HUVECs; both supplemented with 10% fetal bovine serum (FBS) and antibiotic solution (100 IU penicillin and 0.1 mg streptomycin). Trypsin-EDTA solution (w/ phenol red, 0.25%) was used for detaching cells. HUVECs used in this study were between $8^{th}$ and $10^{th}$ passages whereas MCF-7 cells were at $24^{th}$ and MDA-MB-231 cells were $34^{th}$ passages.

For evaluating compounds' cytotoxic properties under dark and light conditions, cells were seeded as 5.000 cells per well into 96-well test plates as triplicates and incubated overnight in 5% $CO_2$ containing cell culture incubator with humid environment for attachment. All compounds were dissolved in dimethyl sulfoxide (DMSO) and diluted in culture medium in order to prepare 1, 5, 25, 50 and 100 μM solutions. The final concentration of DMSO did not exceed 0.1%, which is considered as safe in terms of cytotoxicity. Untreated cells were used as control.

For flow cytometric analyses and Western Blotting, 500.000 cells were seeded into 60 mm tissue culture dishes as triplicates; for confocal microscopy, cells were seeded on Millicell® EZ Slides (Merck Millipore, USA) as 20.000 cell per well and incubated overnight for attachment. Cells were treated with respective $IC_{50}$ doses 24 hours later cells were irradiated as indicated above. After an additional 24 hours, cells were detached with Trypsin-EDTA. For flow cytometric analyses, cells were washed twice with DPBS containing 0.1% sodium azide as a preservative. For Western Blotting, protein extraction was performed.

## 3.4. Determining Cytotoxicity Under Dark and Light Conditions

Dose interval (1-100μM) was determined according to a study published by Atilla et al. [172]. For evaluating compounds' cytotoxicity under dark conditions, viability was measured after incubating cells with compounds for 24 hours. For evaluating light toxicity and determining $IC_{50}$ doses of each compound, cells were irradiated by red light at 5mA for 34 minutes to obtain 500mJ optical dose [172] after 24 hours of incubation at dark. Viability was measured after an additional 24 hours. Tetrakis(4,7,10-trioxaundecan-1-sulfanyl)phthalocyaninato zinc (Pc-C1), Octakis(4,7,10-trioxaundecan-1-sulfanyl)phthalocyaninato zinc (Pc-C2) [172] and Polyoxo-SiPc (Pc-C3) [174], [175], were used as positive controls in this study, applied, irradiated and analysed in the same manner.

Alamar Blue assay was used for assessing viability (Sigma Aldrich, USA) which relies on the reduction in response to metabolic activity as non-oxidized resazurin (blue) forms pink resorufin [176]. Unlike other tetrazolium salts, Alamar Blue does not interfere with the activity of the respiratory chain. Since redox potentials of other commonly used tetrazolium salts are more negative than electron accepting

components of the electron transport chain, reduction of these tetrazolium salts require energy. On the other hand, the reduction potential of Alamar Blue is more positive than FMNH2, FADH2, NADH, NADPH, cytochromes and it is reduced via energy expenditure. This indicates that Alamar Blue does not have any cytotoxic effect itself on cells unlike other tetrazolium salts [176]. At the end of incubation periods, assay reactive was added to each well (final reagent:medium ratio was 1:10 as indicated in kit datasheet) and plates were further incubated for 4 hours in cell culture incubator. Absorbance was measured at 570 nm and 600 nm with a spectrophotometer (Epoch, BioTek Instruments). Viability percentages were calculated according to the equation given in the Appendix B.

## 3.5. Measurement of Cellular Uptake by Flow Cytometry

Both Si, Zn and In Pcs used in this study were shown to have fluorescence emission spectra around 700 nm when excited with a fluorescence spectrometer at 650 nm wavelength (data kindly provided by Prof. Dr. Devrim Atilla). For measuring cellular drug uptake, we measured each compounds' fluorescence percentages at their respective emission maxima (channel 6 for Pc1, channel 7 for Pc2, Pc3, Pc4 and Pc5) by flow cytometry. Cells incubated with compounds at their respective $IC_{50}$ values for 24 hours were detached, washed twice with DPBS, then suspended in DPBS containing 0.1% sodium azide and analysed with CytoFLEX flow cytometry system. Data was evaluated with CytExpert software. These data indicate the total fluorescence positivity ratio of the compound on cells upon treatment and do not reflect if the compound is internalized or membrane attached.

## 3.6. Annexin V/Propidium Iodide Staining

Apoptosis, necrosis and viability were evaluated with Annexin V/Propidium Iodide staining, which is considered as the gold standard for apoptosis detection [177]. Annexin V binds to phosphatidylserine (PS) residues which mainly located in the inner leaflet of the cellular membrane. PS residues translocate to the outer leaflet of the cellular membrane upon induction of apoptosis, enabling Annexin V to bind and label early apoptotic cells. Annexin V can also enter cells with compromised membranes

and binds PS located at the inner leaflet, labelling cells during the last apoptotic stages. Propidium iodide (PI) which is a cell impermeable DNA intercalating agent that is used for discriminating apoptotic cells from living and necrotic cells [178].

In this study, detached cells were washed twice and then suspended in Annexin V Binding Buffer (BioVision Inc.), followed by staining with Annexin V-FITC reagent (1µl/1×$10^5$ cells) (Biovision Inc.) and Propidium Iodide (0.25µg/1×$10^5$ cells) (Thermo Fisher Scientific) by incubating cells on ice for 15 minutes. Analyses were immediately performed on Beckman Coulter CytoFLEX flow cytometry system. CytExpert software was used for evaluating data.

## 3.7. DNA Content Analysis

DNA content analysis relies on the difference DNA amount cells have through cell division stages $G_{0/1}$ pre-replicative cells), S (dividing cells) and $G_2$+ M (post replicative plus mitotic cells) [179]. Cells with fragmented DNA can also be identified and this fraction is named as "sub-$G_1$" population. Most common DNA fluorochromes used in DNA content analysis are 4′,6-diamidino-2-phenylindole (DAPI), propidium iodide (PI), and 7-aminoactinomycin D (7-AAD). RNase A treatment is required prior to staining with fluorochromes that bind to both DNA and RNA such as PI [179]. In this study, Coulter DNA Prep Reagents Kit (Beckman Coulter) was used. Detached cells were fixed and permeabilized via suspending in LPR, followed by staining with DNA PREP stain. Cells were incubated at room temperature for 40 minutes (duration was validated and optimized) and kept at 4°C until analysis. Samples were read with Navios EX flow cytometry system (Beckman Coulter). Analyses were performed on ModFit Software (Version 5).

## 3.8. Evaluation of Protein Expression by Western Blotting

### 3.8.1. Preparation of Protein Lysates

Protein extraction buffer (for composition please see Table 3.1) was prepared at 2-fold concentration, filtered through a 0.4 micron filter and stored at 4 °C. One protease inhibitor tablet (Roche cOmplete™, Mini, EDTA-free Protease Inhibitor

Cocktail) was dissolved in molecular grade distilled water to prepare a 2-fold concentrate protease inhibitor cocktail and aliquoted to avoid freeze-thaw cycles. Prior to protein extraction, equal volumes of protein extraction buffer and protease inhibitor cocktail solution was mixed to obtain the working buffer. Working buffer of protein extraction buffer was immediately used and not subjected to freeze-thaw cycles.

Table 3.1: Composition of the protein extraction buffer.

| Component | Final amount in 2X buffer |
|---|---|
| Triton X-100, 100% | 1 mL |
| NP-40 substitute, 10% in molecular grade water | 5 mL |
| Sodium Chloride | 4.38 g |
| Sodium Dodecyl Sulphate (SDS) | 0.1 g |
| 100 mM Tris base solution, pH:7.4 | 5 mL |
| Glycerol, 87% | 11.5 mL |
| Molecular grade water | up to 50 mL |

After detachment, cells were washed with DPBS twice and placed on ice. 150 µL protein extraction buffer was added on each tube. Cells were suspended with pipetting and incubated on ice for 40 minutes for cell lysis. Lysates were transferred into sterile Eppendorf tubes chilled on ice and centrifuged at 15000g for 25 minutes at 4 °C. Supernatants were collected into new sterile Eppendorf tubes and stored at -80° C. Protein concentrations were determined by Pierce bicinchoninic acid (BCA) assay Kit (Thermo Fisher Scientific).

## 3.8.2. Western Blotting

Anti-HDAC6 (Cat. No. 7558, Cell Signaling Technologies) and anti-HDAC8 (Cat. No. 685502, BioLegend Inc.) primary antibodies were prepared at 1:1000 dilutions, anti-GAPDH antibody (M00227-1, Boster Bioscience) was prepared at 1:5000 dilution and anti-β Actin antibody (4970, Cell Signaling Technologies) was prepared at 1:2000 dilution in Tris buffered saline-Tween 20 solution (TBS-T) with 3% *Blocker*™ BSA (Cat. No. 37520, Thermo Fisher Scientific). 30 µg denaturated protein samples were separated on 10% bis-acrylamide gels by running gels at 80 V for 3.5 hours at room temperature. Proteins were transferred to 0.45 µm PVDF membranes (Cat. No. IPVH00010, Merck Millipore) at 300 mA for 1 h by wet transfer.

Transfer efficiency was controlled by staining the gel with Coomassie Blue staining. Membranes were blocked by incubating with 5% skimmed milk powder in TBS-T at room temperature for one hour. Proteins were labelled by incubating membranes with primary antibody solutions overnight at 4 °C on shaker platform, followed by probing with either HRP-conjugated anti-rabbit or anti-mouse IgG secondary antibodies (7074 and 7076, respectively, both from Cell Signaling Technologies) at room temperature for 1 h. Images were acquired on a Vilber Fusion Pulse imaging system.

Table 3.2: Compositions of the solutions used for SDS-PAGE.

| | |
|---|---|
| Ammonium persulfate (APS), 10% | 1g APS in 10 mL $dH_20$<br>*Aliquoted in 1 mL Eppendorf tubes and stored at -20ºC* |
| SDS, 10% | 5g APS in 50 mL $dH_20$<br>*Stored at room temperature* |
| 1.5 M Tris solution (for separating gel) | 18.2g Tris-base in 100 mL $dH_20$, pH:8.8<br>*Stored at 4ºC* |
| 0.5 M Tris solution (for stacking gel) | 6.06g Tris-base in 100 mL dH20, pH:6.8<br>*Stored at 4ºC* |

Table 3.3: Compositions of the SDS-PAGE gels.

| Stacking Gel (2 gels) | Acrylamide concentration, 4% |
|---|---|
| $dH_2O$ | 3 mL |
| 0.5 M Tris solution | 1.25 mL |
| SDS, 10% | 50 µL |
| 30% Acrylamide/Bis Solution, 29:1 | 670 µL |
| APS, 10% | 80 µL |
| TEMED | 10 µL |
| **Separating Gel (2 gels)** | **Acrylamide concentration, 10%** |
| $dH_20$ | 3.8 mL |
| 1.5 M Tris solution | 2.6 mL |
| SDS, 10% | 100 µL |
| 30% Acrylamide/Bis Solution, 29:1 | 3.4 mL |
| APS, 10% | 100 µL |
| TEMED | 10 µL |

Table 3.4: Compositions of the solutions used for Western Blotting.

| | |
|---|---|
| Running buffer stock solution (10X) | 144g glycine, 30.2g Tris-Base, 10g SDS, $dH_2O$ (up to 1 L), pH:8.3<br>*1 part of running buffer stock solution was mixed with 9 parts of $dH_20$ to obtain working solution* |
| Transfer buffer stock solution (10X) | 144 g glycine, 30.2g Tris-Base, $dH_2O$ (up to 1 L), pH:8.5<br>*1 part of transfer buffer stock solution was mixed with 7 parts of $dH_2O$ and 2 parts of methanol to obtain working solution* |
| Coomassie staining solution | 500 mL $dH_2O$ 100 mL glacial acetic acid, 400 mL methanol, 1g Coomassie R250 |
| Tris buffered saline (TBS) stock solution (10X) | 24g Tris-HCl, 5.6g Tris-base, 88g NaCl, dH2O (up to 1 L), pH:7.6<br>*1 part of TBS stock solution was mixed with 9 parts of $dH_2O$ to obtain working solution* |

## 3.9. Confocal Microscopy Studies

All Pcs' cellular localization as well as their ability to induce autophagy were visualized by confocal microscopy. Cells seeded on 8-well microscopy slides were treated with respective $IC_{50}$ doses of the compounds and incubated 24 hours before irradiation. Irradiated cells were fixed by incubating cells with glutaraldehyde solution at 4°C for 15 minutes. 0.1 M glycine solution was applied to quench residual aldehydes for one hour at room temperature, followed by permeabilization with 0.25% Triton X-100 in PBS at room temperature for an hour. Cells were incubated with TBS containing *Blocker*™ BSA for an hour at room temperature prior to antibody incubation. Slides were washed trice between each step. Table 3.5 summarizes compositions of solutions used in immunocytochemistry procedures.

For labelling mitochondria, cells were stained with an Alexa Fluor 488 conjugated anti-mitochondria antibody (Clone 113-1, Merck Millipore) at 1:500 dilution by incubating overnight. For imaging autophagosome formation, slides were incubated overnight with LC3A/B antibody (Cell Signaling Technologies, polyclonal) at 1:200 dilution, followed by incubating with an Alexa Fluor® 488 conjugated donkey anti-rabbit secondary antibody (Abcam, polyclonal) at 1:100 dilution for an hour at room temperature. Antibody solutions were prepared in TBS containing 3% *Blocker*™ BSA. Slides were mounted with Dianova Immunoselect Antifading Mounting

Medium with DAPI and visualized via confocal microscope. Photos were taken by Zeiss Zen Black software (black edition).

Table 3.5: Compositions of the solutions used for ICC.

| | |
|---|---|
| Fixation | Glutaraldehyde solution for microscopy, diluted to 2.5% in DPBS, pH:7.4 |
| Quenching | 0.1 M glycine in DPBS |
| Permeabilization | Triton X-100 (0.25%) and *Blocker*™ BSA (1%) in DPBS, final sodium azide concentration 0.1% |
| Blocking | *Blocker*™ BSA (3%) in DPBS, final sodium azide concentration 0.1% |
| Antibody preparation | *Blocker*™ BSA (3%) in DPBS, final sodium azide concentration 0.1% |
| Washing | DPBS, final sodium azide concentration 0.1% |

## 3.10. Evaluation of Mitochondrial Activity

Mitochondrial activity was measured by Dihydrorhodamine 123 (DHR123), a non-fluorescent substance which gains its fluorescent properties under oxidizing conditions and shown to identify cells with disrupted mitochondrial respiratory chain function [180]. DHR123 is excited at 488 nm, and its emission is detected with peak intensity at 525 nm [181]. In this study, $2.5\times10^5$ cells were incubated with 5 µM DHR123 at room temperature for 25 minutes and immediately analyzed by Beckman Coulter CytoFLEX system. Analyses were performed on CytExpert software.

## 3.11. Evaluation of Protein Expression by Flow Cytometry

For measuring protein levels, $2.5\times10^5$ cells were washed twice with DPBS and suspended in 100 µL DPBS containing 0.1% sodium azide. Cells were labelled with Anti-CD44 PE, anti-CXCR4 PerCP/Cy5.5 and anti-CCR7 PE/Cy7 antibodies (all purchased from BioLegend Inc.) by incubating at room temperature for 20 minutes under dark. Each antibody was used as 5 µL per test, according to the manufacturer's instructions. Cells were washed twice, resuspended in PBS and analyzed on CytoFLEX flow cytometry system. Data analysis was performed on CytExpert software.

## 3.12. Statistical Analyses

GraphPad Prism Software (Version 8) was used for statistical analysis. Two-way analysis of variance (ANOVA) followed by Tukey's multiple comparison test was used for comparing treatment efficiency between cell lines, while effects of the treatment within the cell lines compared to respective controls were compared by using two-way ANOVA followed by Sidak's multiple comparison test in Annexin V/PI staining, Western Blotting and DHR123 assay. Two-way ANOVA followed by Bonferroni's multiple comparisons test was performed to investigate the significant differences in DNA content analysis. When comparing CD44, CXCR4 and CCR7 protein levels after treatment, comparisons between treatment and control groups were done with two-way ANOVA followed by Sidak's multiple comparison test while differences in the per cent changes in CD44, CXCR4 and CCR7 positive populations after treatment compared to their respective control groups between the cell lines were analysed by one-way ANOVA followed by Tukey's multiple comparison test. P values lower than 0.05 was considered as statistically significant.

# 4. RESULTS

## 4.1. Determination of Dark and Light Toxicity

None of the compounds tested showed toxicity after incubation for 24 hours under dark conditions, even at high concentrations ($p>0.05$) (Figures 4.1-4.3). In terms of phototoxicity, $IC_{50}$ values for Pc1 were calculated as 42.0, 9.2 and 37.3 μM for HUVECs, MCF-7 and MDA-MB-231 cells, respectively.

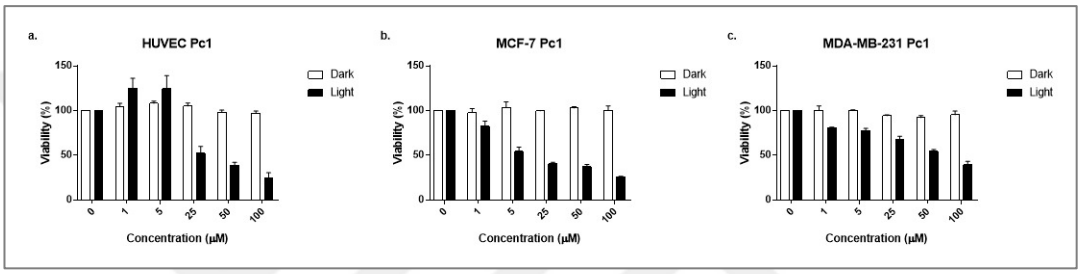


Figure 4.1: Bar graphics indicating cytotoxic properties of Pc1. Measurements were performed after incubating cells with the compound for 24 hours under dark conditions, the irradiating cells and further incubating for an additional 24 hours. Pc1 did not influence viability on a. HUVECs, b. MCF-7 and c. MDA-MB-231 cell lines while decreasing viability upon irradiation in a dose dependent manner. Each test was done as triplicates.

When considering Zn-Pcs; $IC_{50}$ values of Pc2 on HUVECs, MCF-7 and MDA-MB-231 were reported as 72.1, 65 and 63; whereas calculated as 24.9, 16.8 and 24, respectively for Pc3. $IC_{50}$ values for InPcs were calculated as: 84.3, 67.4 and 56.5 for Pc4; 80.7, 56.4 and 48.4 for Pc5 on HUVECs, MCF-7 and MDA-MB-231 cells, respectively.

$IC_{50}$ values for Tetrakis (4,7,10-trioxaundecan-1-sulfanyl) phthalocyaninato zinc (Pc-C1), Octakis(4,7,10-trioxaundecan-1-sulfanyl) phthalocyaninato zinc (Pc-C2) and Polyoxo-SiPc (Pc-C3) are given in the Table 4.1. Molecular structures of control Pcs are given in Figure B1.1. Dose-dependent viability graphics are given in Figure B1.2.

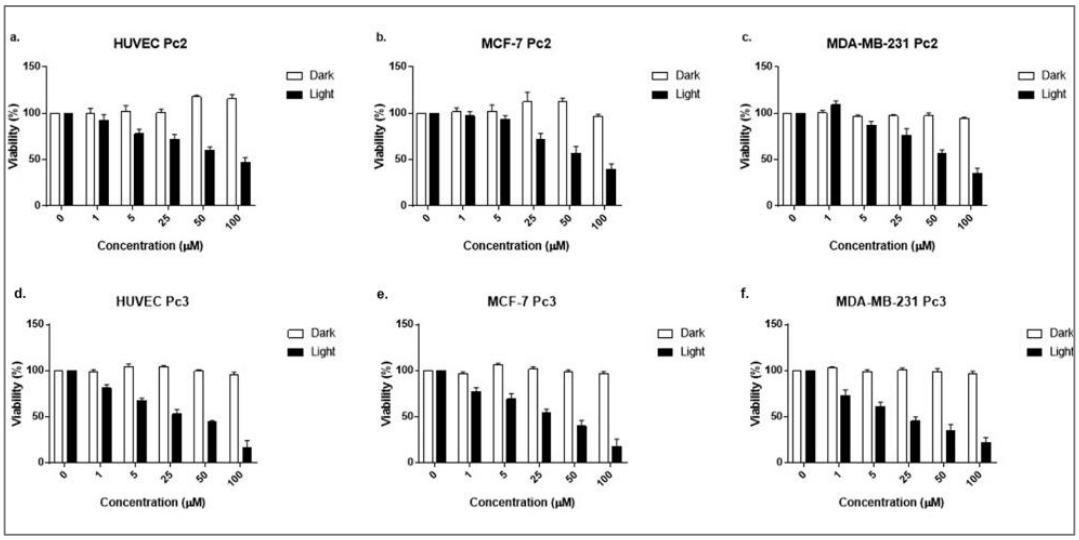


Figure 4.2: Bar graphics indicating cytotoxic properties of ZnPc-HDACi derivatives Pc2 and Pc3. Measurements were performed after incubating cells with compounds for 24 hours under dark conditions, and after irradiating cells and further incubating for an additional 24 hours. Both Pc2 (a-c) (non-peripheral) and Pc3 (peripheral) (d-f) did not influence viability on HUVECs, MCF-7 and MDA-MB-231 cell lines while decreasing viability upon irradiation in a dose dependent manner. Each test was done as triplicates.

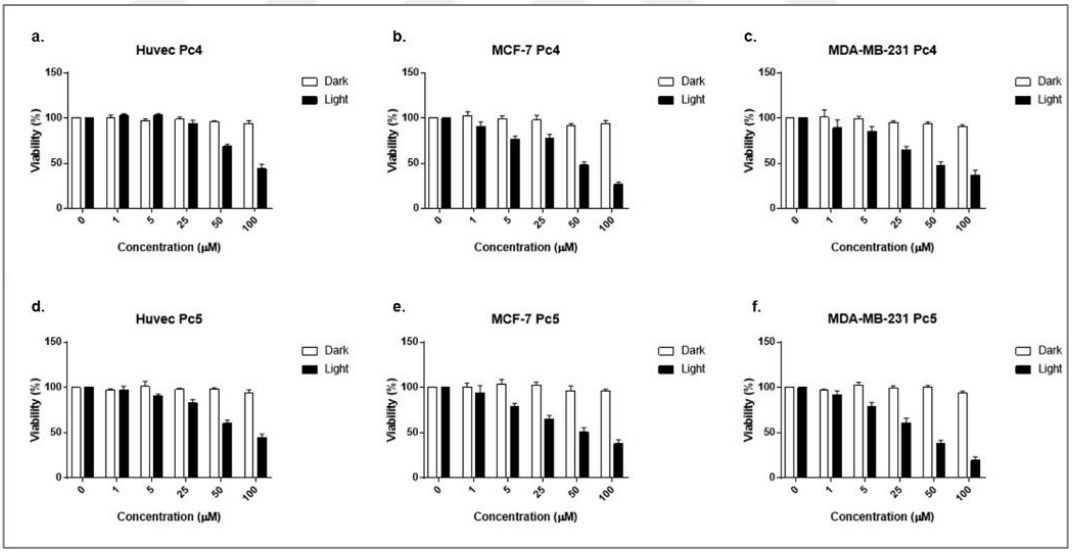


Figure 4.3: Bar graphics indicating cytotoxic properties of InPc-HDACi derivatives Pc4 and Pc5. Measurements were performed after incubating cells with compounds for 24 hours under dark conditions, and after irradiating cells and further incubating for an additional 24 hours. Both Pc4 (a-c) (non-peripheral) and Pc5 (peripheral) (d-f) did not influence viability on HUVECs, MCF-7 and MDA-MB-231 cell lines while decreasing viability upon irradiation in a dose dependent manner. Each test was done as triplicates.

Table 4.1: $IC_{50}$ values of different Si and Zn Pcs that do not contain HDACi residues used as positive controls.

| | $IC_{50}$ (μM) | | |
|---|---|---|---|
| | HUVEC | MCF-7 | MDA-MB-231 |
| Pc-C1 | 89.5 | 63.5 | 82.4 |
| Pc-C2 | - | - | - |
| Pc-C3 | 45.6 | 69.1 | 89.3 |

## 4.2. Anti-Cancer Properties of Silicon Phthalocyanine Derivative (Pc1)

### 4.2.1. Measurement of Cellular Uptake by Flow Cytometry

Fluorescence positivity rate of Pc1 on HUVECs was significantly lower compared to MCF-7 and MDA-MB-231 cells ($p<0.0001$). Similarly, Pc1 positivity on TNBC cell line MDA-MB-231 was higher compared to its double positive counterpart, MCF-7 ($p<0.05$). Altogether, these data may indicate that Pc1 have a selectivity towards malignant cells, not only by exerting cytotoxic effects in higher concentrations (42.0 vs. 9.2 and 37.3 μM) but also not interacting with the non-malignant cells (Figure 4.4).

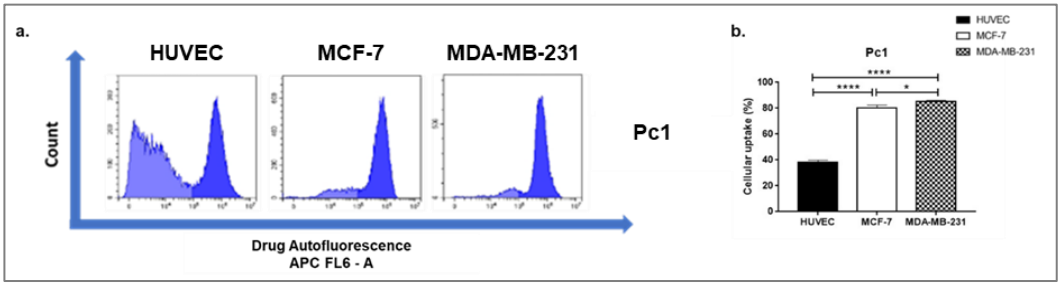


Figure 4.4: Determination of Pc1 intensity on each cell line after treatment with respective $IC_{50}$ doses. a. Representative histograms indicating Pc1's fluorescence intensity on each cell line. Fluorescence emission maximum was detected at 6$^{th}$ channel. b. Bar graphics indicating fluorescence positivity for Pc1. Compounds emission maxima was detected on 6$^{th}$ channel. Significance was considered as $p<0.05$. * denotes significance between cell lines. $^{*}p<0.05$ $^{****}p<0.0001$.

### 4.2.2. Annexin V/Propidium Iodide Staining

Pc1 treatment increased early apoptosis on all cell lines ($p<0.0001$) with a relatively lower efficiency on HUVECs compared to MCF-7 ($p<0.0001$) and MDA-MB-231 cells ($p<0.0001$) (Figure 4.5). MCF7 has a notably higher early apoptosis rates compared to MDA-MB-231 cells ($p<0.0006$) (Figure 4.5.c) while late apoptosis rates was significantly higher in MDA-MB-231 cells ($p<0.0001$) (Figure 4.5.e). Pc1 treatment did not change necrosis levels between cell lines (Figure 4.5.d). Altogether, these data indicate that Pc1 does not initiate necrotic pathway and induces apoptosis more efficiently in TNBC cell line MDA-MB-231 compared to its double positive counterpart as well as healthy cells when administered in each cell lines' respective $IC_{50}$ value.

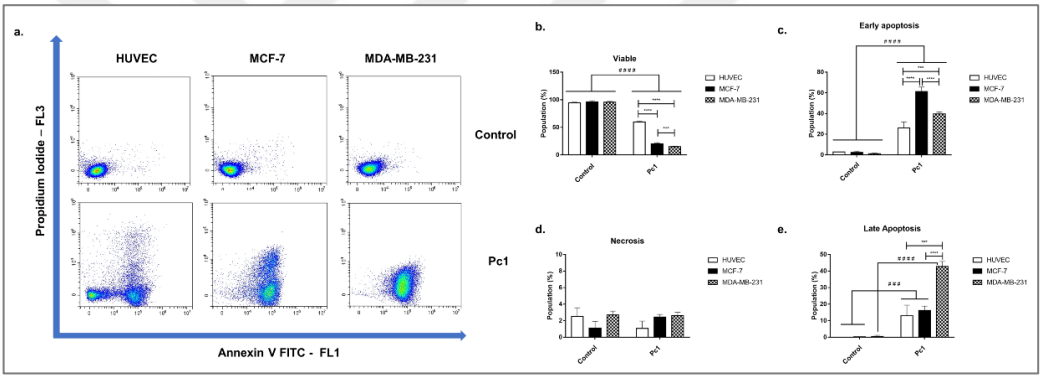


Figure 4.5: Pc1 promotes apoptosis without altering necrosis significantly when cells were treated with respective $IC_{50}$ values determined according to Alamar Blue Assay. a. Representative flow cytometry quadrants. b. Pc1 treatment significantly decreased viability in all cell lines, with a greater effect on cancer cells compared to healthy cell line. c. Treatment significantly increased early apoptosis in all cell lines. d. Pc1 was found ineffective in initiating necrosis pathway. e. Pc1 significantly increased apoptotic population in all cell lines after treatment. Significance was considered as $p<0.05$. * denotes significance between cell lines upon treatment whereas # denotes significance between treatment and control groups.

### 4.2.3. DNA Content Analysis

Pc1 treatment increased $SubG_1$ ($p<0.0001$), S ($p<0.001$) and $G_2$/M phases ($p<0.0001$), while significantly decreasing $G_1$ phase ($p<0.0001$) in HUVECs, suggesting $G_2$/M arrest. In MCF-7 and MDA-MB-231 cells, cell cycle arrest at $G_2$/M

phase was accompanied by a significant increase in $SubG_1$ ($p<0.0001$) and a significant decrease in $G_0/G_1$ and S phases ($p<0.0001$ and $p<0.01$ for MCF-7 and MDA-MB-231, respectively) (Figure 4.6).

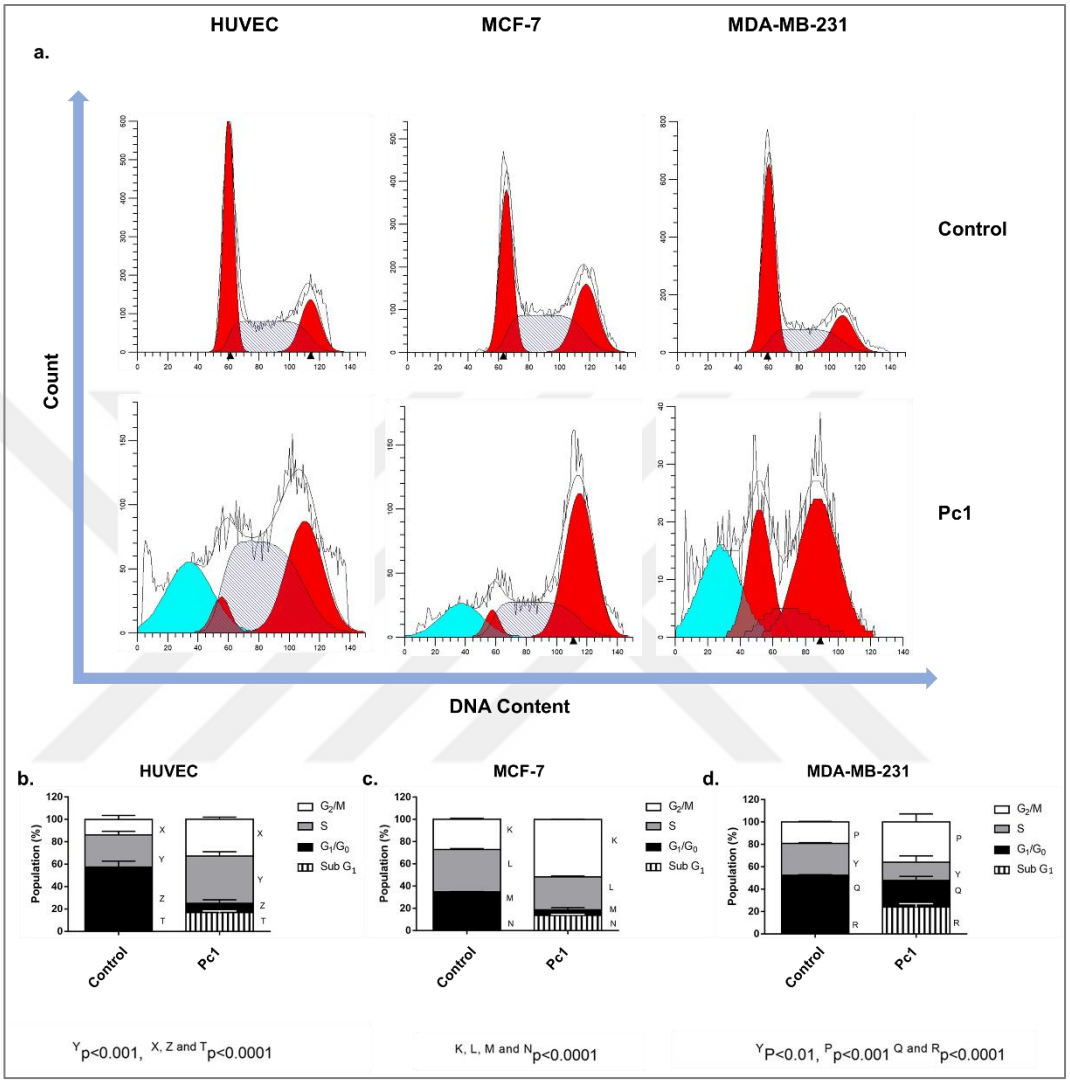


Figure 4.6: Pc1 leads to accumulation at $G_2/M$ phase. a. Representative flow cytometry histograms. b. Treatment decreased $G_0/G_1$ phase in HUVECs while increasing both S, $G_2/M$ and $SubG_1$ phases. c. Pc1 increased $G_2/M$ and $SubG_1$ phases while decreasing both $G_0/G_1$ and S phases. d. Similar to MCF-7 cells, an increase in $G_2/M$ and $SubG_1$ phases that was accompanied by a decrease in $G_0/G_1$ and S phases was observed in MDA-MB-231 cells. A p value lower than 0.05 was considered as statistically significant.

### 4.2.4. Evaluation of HDAC6 and HDAC8 levels by Western Blotting

Pc1 treatment decreased both HDAC6 ($p<0.0001$ for HUVECs and MDA-MB-231 cells while $p<0.01$ for MCF-7 cells) and HDAC8 ($p<0.001$ for HUVECs and MDA-MB-231 cells while $p<0.05$ for MCF-7 cells) protein levels in all cell lines (Figure 4.7). Comparisons between cell lines upon treatment revealed no difference in terms of HDAC8 levels between cell lines while HDAC6 levels were found significantly higher in MCF7 cells ($p<0.01$).

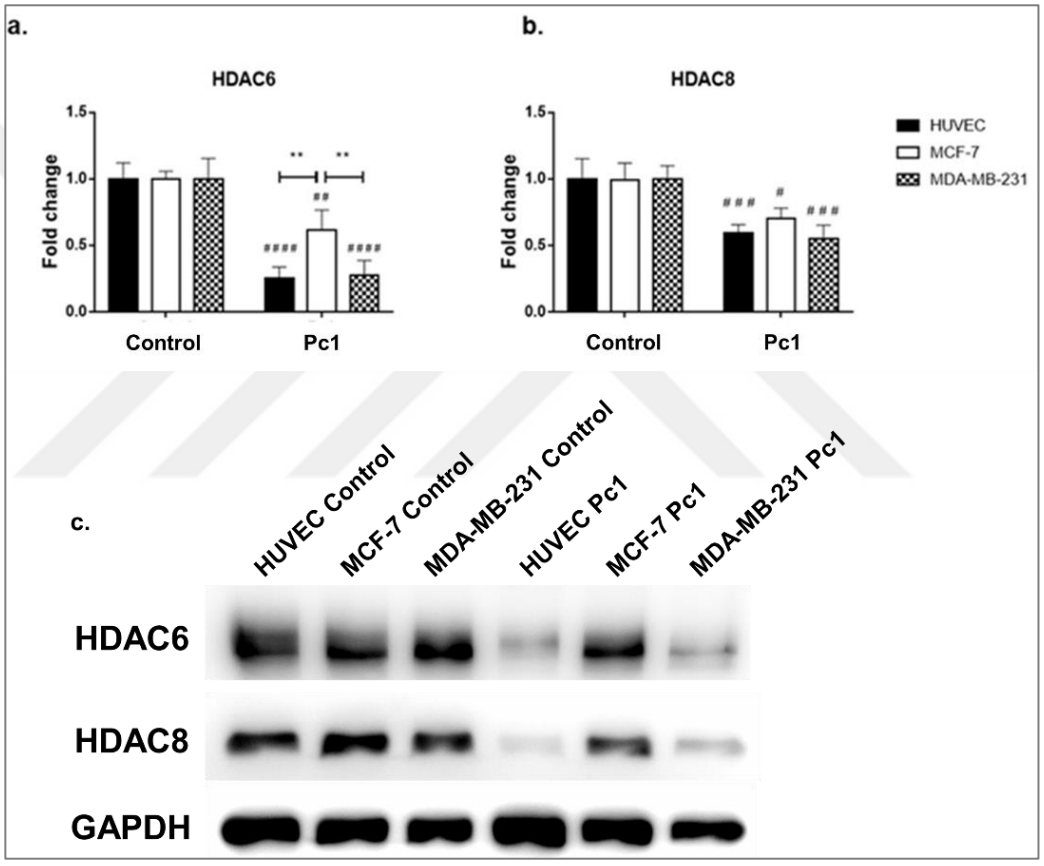


Figure 4.7: Pc1 significantly decreases both HDAC6 and HDAC8 levels in all cell lines. a. Comparisons between treatment groups revealed that MCF-7 cells have significantly higher HDAC6 levels compared to other two cell lines after treatment. b. The decrease in HDAC8 levels on HUVECs and MDA-MB-231 cells were higher compared to MCF-7 cells, yet no significant difference between cell lines after treatment was observed. c. Representative immunoblot images. Significance level was considered as $p<0.05$. * denotes significance between cell lines upon treatment whereas # denotes significance between treatment and control groups

### 4.2.5. Confocal Microscopy Studies

#### 4.2.5.1. Visualization of Subcellular Localization

Pc1 did not localize to mitochondria, whereas it still disrupted mitochondrial network, leading to disrupted mitochondrial signal in all cell lines (green arrows) (Figure 4.8). “Rounder” cells were observed compared to untreated controls of each cell line. Pc1 mainly localized to nuclei and nucleoli in all cell lines (red arrows), however, fluorescent deposits around nuclear membranes were also observed in MCF-7 and MDA-MB-231 cells (white arrows).

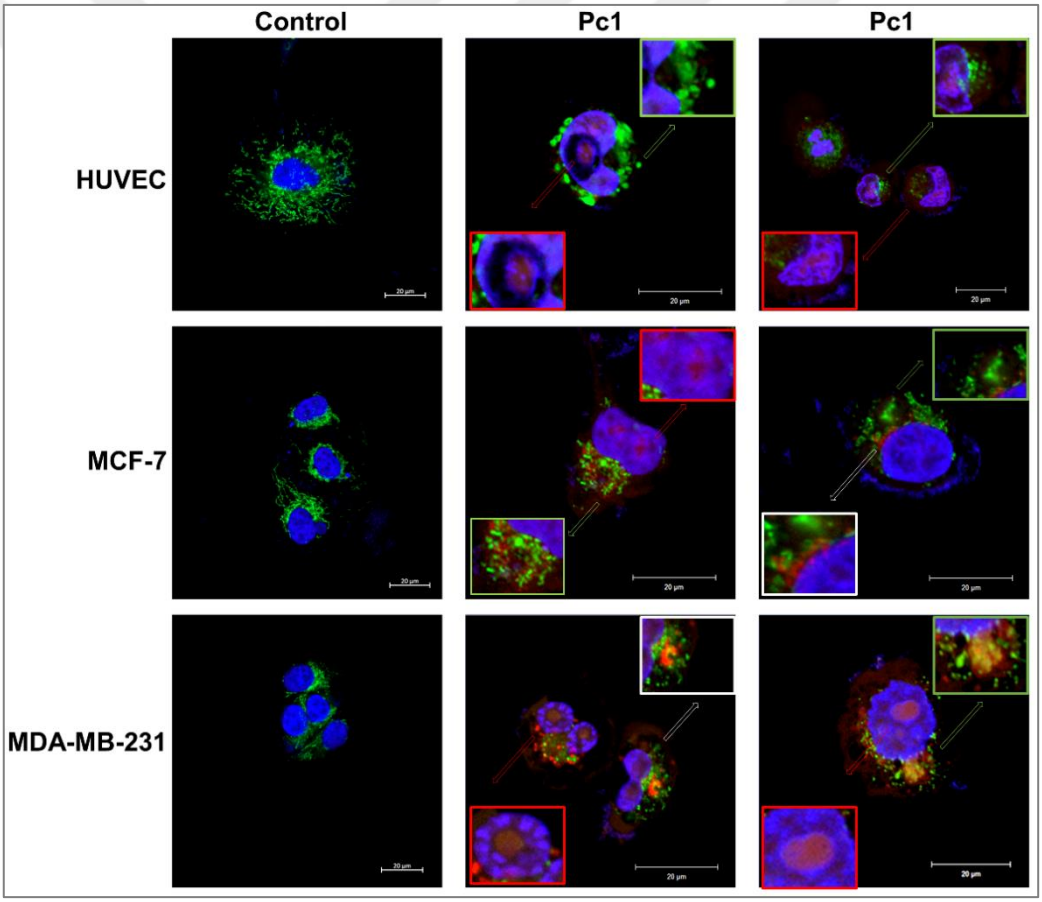


Figure 4.8: Micrographs of untreated (left column) and Pc1 treated (middle and right columns) cells indicating cellular localization. Cells were stained with anti-mitochondria antibody and counterstained with DAPI. Red squares indicate deposits in nuclei and nucleoli whereas white squares indicate fluorescence deposits around nuclei. Disrupted mitochondria are shown in green squares. Scale bars indicate 20 μm. All images were taken at 63X zoom with immersion oil.

### 4.2.5.2. Visualization of Autophagy

We observed homogenous LC3A/B staining in untreated cells where Pc1 treatment led to autophagosome formation in MCF-7 and MDA-MB-231 cells which is observed with puncta formation and indicated in yellow squares (Figure 4.9) Treatment did not induced autophagy in HUVECs.

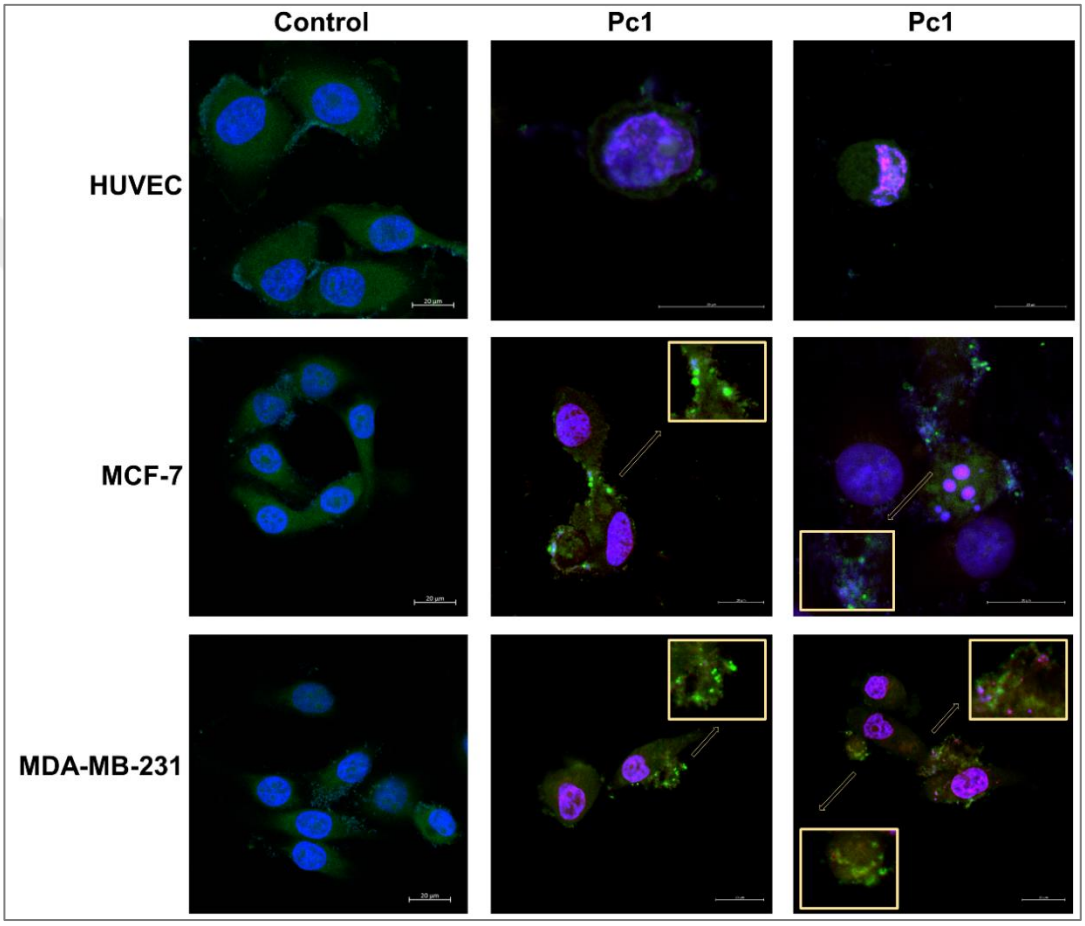


Figure 4.9: Micrographs of untreated (left column) and Pc1 treated (middle and right columns) cells indicating autophagosome formation. Cells were stained with rabbit polyclonal anti-LC3A/B antibody followed by donkey anti-rabbit Alexa Fluor 488 secondary antibody and counterstained with DAPI. Puncta formations are indicated in squares. Scale bars indicate 20 µm. All images were taken at 63X zoom with immersion oil.

### 4.2.6. Evaluation of Mitochondrial Activity

Pc1 treatment induced ROS generation in all cell lines (HUVEC $p<0.01$, MCF-7 and MDA-MB-231 $p<0.0001$) compared to control groups. Comparisons investigating treatment efficacy between cell lines revealed ROS levels in HUVECs were significantly lower than those in MCF-7 and MDA-MB-231 (Figure 4.10), which may indicate a selectivity between healthy and malignant cells.

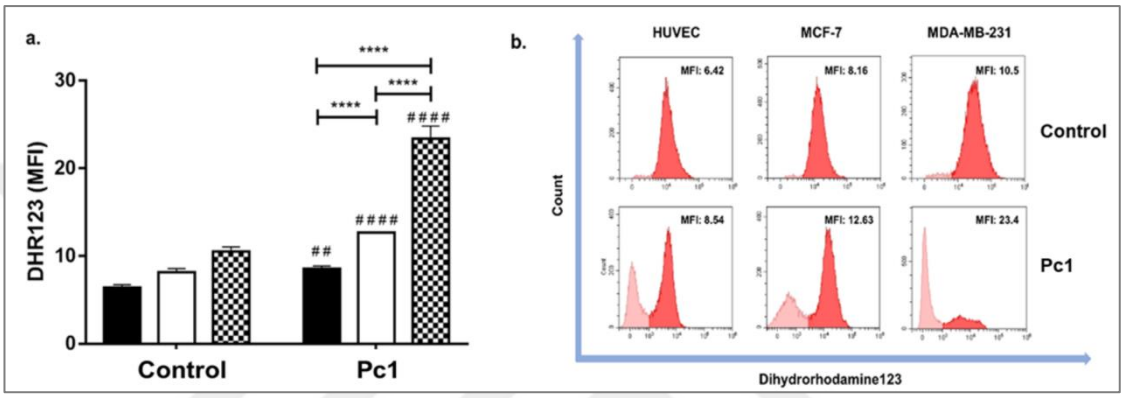


Figure 4.10: Pc1 treatment increases Dihydrorhodamine123 mean fluorescence intensity in all cell lines. a. Quantification of the DHR123 mean fluorescent intensity for control and treated cells. b. Representative histograms for the DHR123 measurements in treated and untreated cells. A p value lower than 0.05 was considered as significant. * denotes significance between cell lines upon treatment whereas # denotes significance between treatment and control groups.

### 4.2.7. Evaluation of CD44, CXCR4 and CCR7 Levels by Flow Cytometry

Pc1 decreased CD44 and CCR7 protein levels in all cell lines significantly ($p<0.0001$) while increasing CXCR4 levels in all cell lines significantly upon treatment (HUVECs and MDA-MB-231; $p<0.01$, MCF-7 $p<0.001$) (Figure 4.11.a). When comparing alterations of protein levels between treatment and control groups, Pc1 decreased CD44 levels by ~39, ~20, ~68% and CCR7+ cell population by ~35, ~21, ~82% in HUVEC, MCF-7 and MDA-MB-231, respectively, compared to their control counterparts (Figure 4.11.b). Percent changes in both CD44 and CCR7 protein levels were significantly higher in MDA-MB-231 cells than MCF-7 and HUVEC ($p<0.0001$), while it was higher in the HUVEC than MCF-7 cells ($p<0.0001$). On the contrary, CXCR4 expression was increased by ~128, ~271 and ~84% in HUVECs,

MCF-7 and MDA-MB-231 cells, respectively, compared to their respective control groups. Percent increase in CXCR4 levels were significantly lower in MDA-MB-231 cells when compared to HUVEC and MCF-7 cells. Representative flow cytometry histograms were given on Figure B1.5.

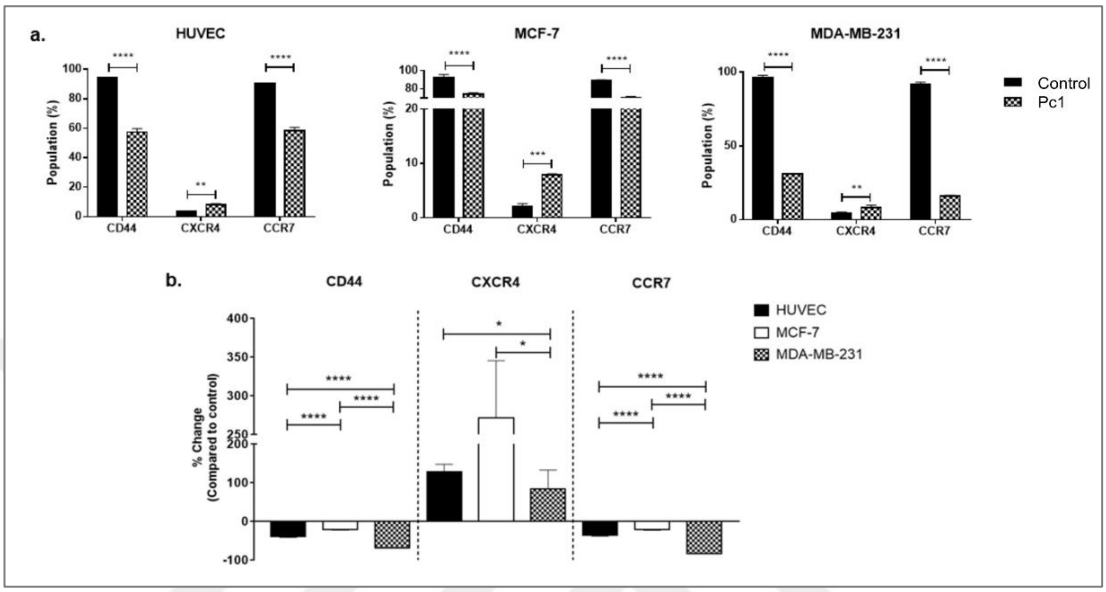


Figure 4.11: Pc1 decreases CD44 and CCR7 but not CXCR4 levels significantly in all cell lines. a. Percentage of CD44, CXCR4 and CCR7 protein levels in control and treatment groups. * denotes significance between control and treatment groups. b. Relative changes in the CD44, CXCR4, and CCR7 levels after treatment. Differences between groups were indicated with *.

## 4.3. Anti-Cancer Properties of Zn(II) Pc Derivatives (Pc2 and Pc3), In(III) Pc Derivatives Phthalocyanines (Pc4 and Pc5)

### 4.3.1. Measurement of Cellular Uptake by Flow Cytometry

Fluorescence positivity percentages for Pc2 were significantly higher than Pc3 in HUVECs ($p<0.01$) and MCF-7 cells ($p<0.05$) yet no significant difference in MDA-MB-231 cells after treatment with Pc2 or Pc3 fluorescence ratios was observed ($p>0.05$) (Figure 4.12.b). Comparisons between cell lines revealed higher Pc2 and Pc3 ratios in HUVECs and MCF-7 cells compared to MDA-MB-231 cells ($p<0.001$ and $p<0.0001$, respectively for Pc2 and $p<0.0001$ for Pc3). When treated with the same compound, MCF-7 cells had higher fluorescence rates compared to MDA-MB-231 cells ($p<0.0001$ for both Pc2 and Pc3), suggesting a lower affinity for ZnPc-HDACi

derivatives towards TNBC cells. When comparing InPc derivatives; Pc4 uptake was significantly higher compared to Pc5 in HUVECs, but no difference after treatment with either Pc4 or Pc5 between MCF-7 and MCDA-MB-231 cell lines was observed ($p>0.05$) which may indicate that non-peripheral or peripheral HDACi substitutions do not have an influence on compound-cancer cell interaction (Figure 4.12.c). Both Pc4 and Pc5 treatments resulted in significantly lower fluorescence ratio in MDA-MB-231 cells compared to HUVECs and MCF-7 cells ($p<0.0001$ for Pc4 and $p<0.01$ and $p<0.0001$ for Pc5, respectively), similarly to ZnPc-HDACi derivatives mentioned above. No difference in terms of Pc4 fluorescence ratios between HUVECs and MCF-7 cells was observed, yet Pc5 percentage of fluorescence positivity was significantly higher in MCF-7 cells compared to HUVECs ($p<0.001$), may suggest a slight specificity towards double positive cancer cells against healthy cells as well as TNBC.

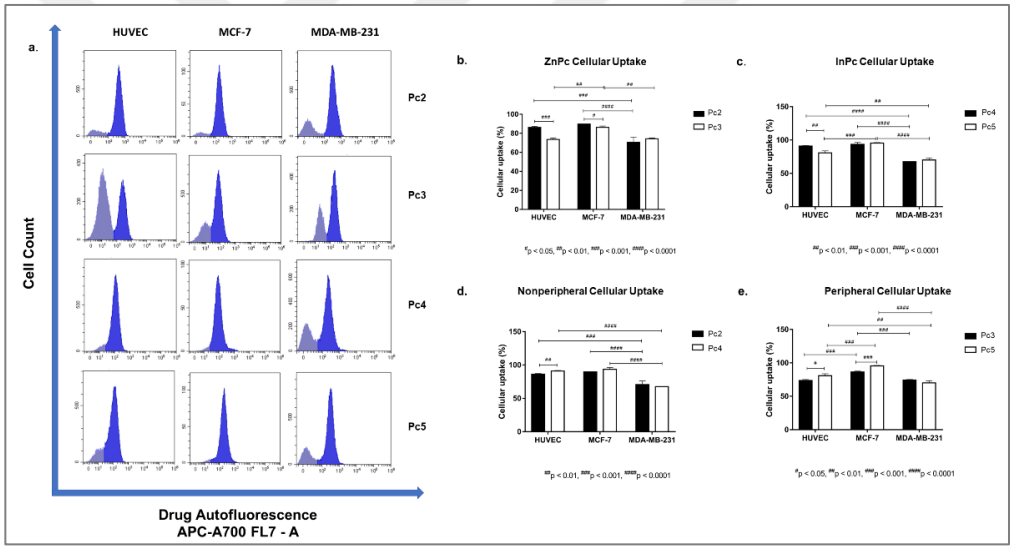


Figure 4.12: Determination of Pc2 - Pc5 intensities on each cell line after treatment with respective $IC_{50}$ doses. a. Representative flow cytometry histograms. b. Comparisons between two ZnPc derivatives' in terms of cellular uptake based on the position of their HDACi moieties. c. Comparisons between two InPc derivatives' in terms of cellular uptake based on the position of their HDACi moieties. d. Comparisons between non-peripheral HDACi substituted Pcs bearing either zinc or indium as core metal. e. Comparisons between peripheral HDACi substituted Pcs bearing either zinc or indium as core metal. # denotes statistical significance between groups.

Comparisons between non-peripheral HDACi substituted ZnPcs and InPcs indicated Pc4 had significantly higher fluorescence positivity rate in HUVECs

compared to Pc2 ($p<0.001$), however, such difference was not observed in MCF-7 or MDA-MB-231 cells ($p>0.05$) (Figure 4.12.d). Both Pc2 and Pc4 treatments led to lower fluorescence positivity in MDA-MB-231 cells compared to HUVECs and MCF-7 cells ($p<0.001$ for HUVECs and $p<0.0001$ MCF-7 cells for Pc2 whereas $p<0.0001$ for Pc4) which may indicate a lower specificity towards for both non-peripheral ZnPc-HDACi and InPc-HDACi derivatives to TNBC. Moreover, no significant difference between non-peripheral InPc-HDACis and ZnPc-HDACis in MCF-7 and MDA-MB-231 cells were observed in terms of compound-cell interaction.

When comparing peripheral HDACi-substituted Pc derivatives, Pc5 positivity ratios were significantly higher in HUVECs and MCF-7 cells than their zinc-bearing counterpart Pc3 ($p<0.01$ and $p<0.0001$, respectively) whereas no difference in MDA-MB-231 cells between Pc3 and Pc5 treatments was observed ($p>0.05$) (Figure 4.12.e). Highest fluorescence ratios were observed in MCF-7 cells for both compounds compared to other cell lines ($p<0.001$ for Pc3, $p<0.001$ and $p<0.0001$ for Pc5, respectively), regardless of the core metal. These findings may suggest that peripheral InPc-HDACi derivatives tend to have a higher cellular uptake percentage compared to their zinc-containing counterparts in HUVECs and MCF-7 cells, but not in MDA-MB-231 cells.

### 4.3.2. Annexin V/Propidium Iodide Staining

Both ZnPc-HDACi derivatives decreased viability significantly for all cell lines compared to control groups while viability rates of all cell lines were significantly higher for Pc2 treated cells compared to Pc3 treatment ($p<0.0001$) (Figure 4.13.b). Pc2 did not induce apoptosis significantly ($p>0.05$); on the other hand, treatment with its peripheral counterpart Pc3 increased apoptotic cell rate in all cells lines ($p<0.0001$). Comparisons between cell lines indicated MCF-7 cells had highest late apoptotic cell population ($p<0.0001$) as well as HUVECs had significantly lower apoptosis compared to both MCF-7 and MDA-MB-231 cells (Figure 4.13.e). Pc2 treatment did not alter late apoptotic cell ratios between different cell lines ($p>0.05$). However, in contrast to Pc3 which did not have any effect on early apoptosis, Pc2 significantly increased early apoptosis rates in all cell lines, most significantly in MCF-7 cells which had higher apoptotic cell rate compared to MDA-MB-231 cells ($p<0.05$) (Figure

4.13.c). Comparisons between treatment and control groups revealed Pc2 treatment did not alter necrotic cell population in all cell lines ($p<0.05$), however, Pc3 induced necrosis significantly on HUVECs and MCF-7 cells but not MDA-MB-231 cells ($p<0.0001$ and $p<0.01$, respectively) (Figure 4.13.d). Necrosis levels of Pc2 treated HUVECs and MCF-7 cells were significantly lower than their Pc3 treated counterparts ($p<0.0001$ and $p<0.01$, respectively). In conclusion, Pc2 treatment led to higher early apoptosis rates while peripheral Pc3 induced late apoptosis in cell lines in addition to necrosis in HUVECs and MCF-7 cells.

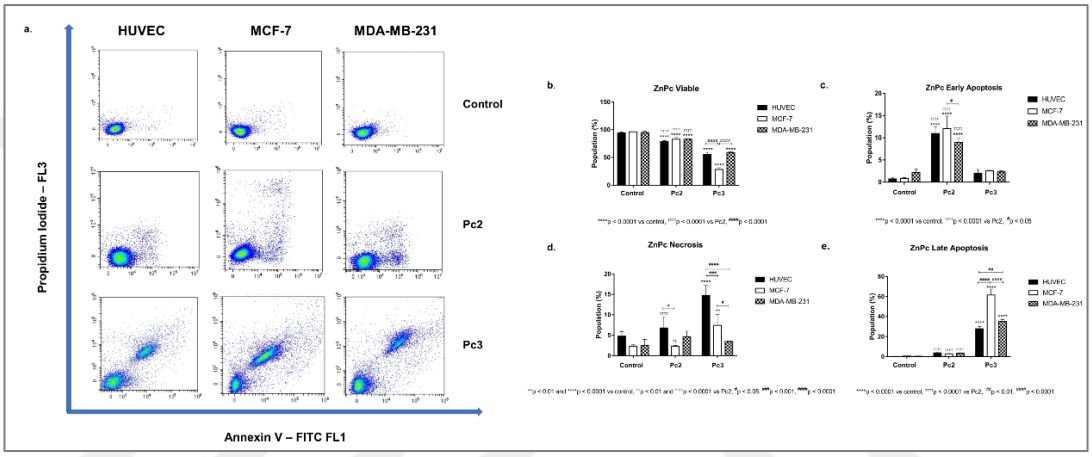


Figure 4.13: Both Pc2 and Pc3 treatment decreases all cell lines' viability while promoting apoptosis. a. Representative flow cytometry histograms. Comparisons between two different ZnPc derivatives in terms of b. viability, c. early apoptosis, d. necrosis and e. late apoptosis revealed that Pc2 treatment increased early apoptosis rates more effectively in all cell lines compared to Pc3; on the other hand, late apoptotic cell populations in all cell lines were significantly higher compared to Pc2 treated counterparts, suggesting non-peripheral and peripheral substitution of HDACi residues may induce different mechanisms of action. * denotes difference between control and treatment groups. # denotes difference between cell lines within the same treatment groups. $\tau$ indicates difference between either peripherally or non-peripheral HDACi substituted Pcs bearing Zn as core metal.

Comparisons between control groups and indium Pc derivatives Pc4 and Pc5 revealed that both compounds decreased viability significantly for all cell lines compared to control groups ($p<0.0001$) while Pc4 treated MCF-7 cells had significantly higher viability percentage compared to its Pc5 treated counterpart ($p<0.0001$) (Figure 4.14.b). The decrease in viability rates as accompanied by an increase in both early (Figure 4.14.c) and late apoptosis (Figure 4.14.e) after Pc4 and Pc5 treatments ($p<0.0001$). While no differences were observed within Pc4 and Pc5

groups in terms of early apoptosis (Figure 4.14.c), Pc4 treated HUVECs as well as MCF-7 cells had significantly lower late apoptosis percentages compared to Pc5 treated counterparts ($p<0.001$ and $p<0.0001$, respectively).

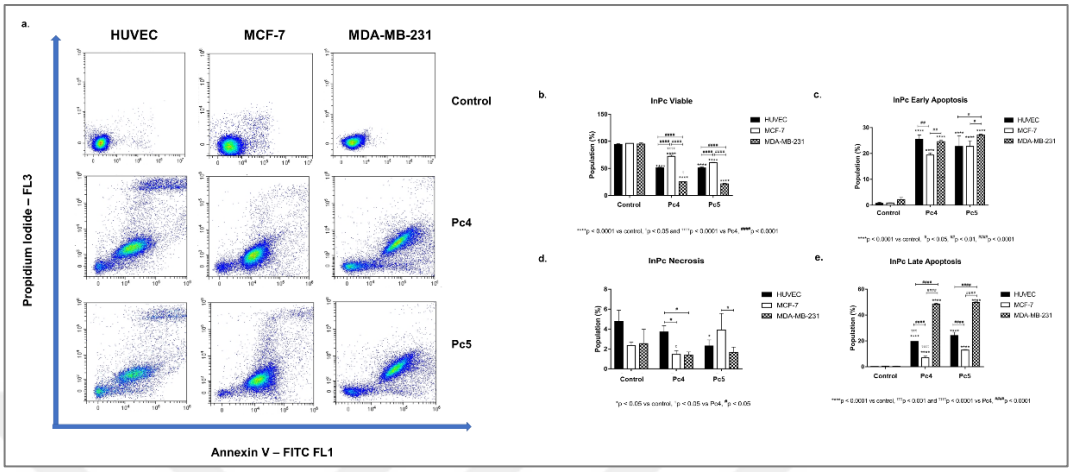


Figure 4.14: Both Pc4 and Pc5 treatments decreases all cell lines' viability while promoting apoptosis. a. Representative flow cytometry histograms. Comparisons between two different InPc derivatives in terms of b. viability, c. early apoptosis, d. necrosis and e. late apoptosis. Data indicated that Pc4 and Pc5 induces both early and late apoptosis in all cell lines. While substation position of HDACi residues have no effect on early apoptosis rates, Pc4 treatment led significantly higher viability accompanied with lower late apoptosis rates in MCF-7 cells compared to Pc5 treatment. * denotes difference between control and treatment groups, # denotes difference between cell lines within the same treatment groups and $\tau$ indicates difference between either peripheral or non-peripheral HDACi substituted Pcs bearing In as core metal.

When comparing non-peripheral Pc derivatives, Pc4 decreased viability while increasing both early and late apoptosis rates in all cell lines more significantly compared to Pc2 ($p<0.0001$) (Figure B1.3). Comparisons between peripheral Pc derivatives revealed Pc3 had a more prominent effects on MCF-7 cells while Pc5 was found more effective on MDA-MB-231 cells with higher late apoptosis rates accompanied with lower viability rates ($p<0.0001$) (Figure B1.4). Early apoptosis rates in all cell lines were significantly higher upon Pc5 treatment ($p<0.0001$) while Pc3 had a slight necrotic effect on HUVECs ($p<0.0001$) and MCF-7 cells ($p<0.05$) compared to Pc5.

### 4.3.3. DNA Content Analysis

ZnPc-HDACi derivatives did not induce cell cycle arrest on HUVECs while Pc2 led to a small but significant decrease in $G_0/G_1$ phase ($p<0.05$). Pc2 induced $G_2$/M-phase arrest in MCF-7 and $G_0/G_1$-phase arrest MDA-MB-231 ($p<0.0001$) cells, which is accompanied by significant decrease of S phase in both cell lines ($p<0.0001$). Pc3 induced $G_2$/M-phase arrest in both cancer cell lines, while in contrary to Pc2, it decreased $G_0/G_1$ phase in MDA-MB-231 cells (Figure 4.15).

Both Pc4 and Pc5 increased $SubG_1$ phase ($p<0.01$), decreased $G_2$/M phase significantly in HUVECs ($p<0.05$ for Pc4 and $p<0.01$ for Pc5, respectively) while no differences between $G_0/G_1$ and S phases compared to control was observed ($p>0.05$). Similarly, both Pc4 and Pc5 increased $SubG_1$ ($p<0.01$) and S phases ($p<0.0001$) accompanied by the decrease of $G_2$/M phase ($p<0.0001$) in MCF-7 cells, suggesting an S-phase arrest. On the other hand, both Pc4 and Pc5 increased $G_0/G_1$ phase ($p<0.01$) in MDA-MB-231 cells and decreased $G_2$/M phase ($p<0.0001$) without altering S phase ($p>0.05$), indicating a $G_0/G_1$ phase arrest (Figure 4.16).

In conclusion, both ZnPc-HDACi derivatives induced $G_2$/M-phase arrest in cancer cell lines while non-peripheral Pc2 also lead to accumulation in $G_0/G_1$ phase in MDA-MB-231 cells. On the other hand, InPc-HDACi derivatives Pc4 and Pc5 led to an S-phase arrest in MCF-7 cells while inducing $G_0/G_1$ accumulation in MDA-MB-231 cells. None of the compounds did not induce cell cycle arrest in HUVECs. These data suggest when considering breast cancer cells, ZnPc-HDACis induce cell cycle arrest at $G_2$/M phase while InPc-HDACis tend to lead accumulation in $G_0/G_1$ or S phases according to the cell line, and the position of HDACi moieties do not have a major impact on cell cycle arrest.

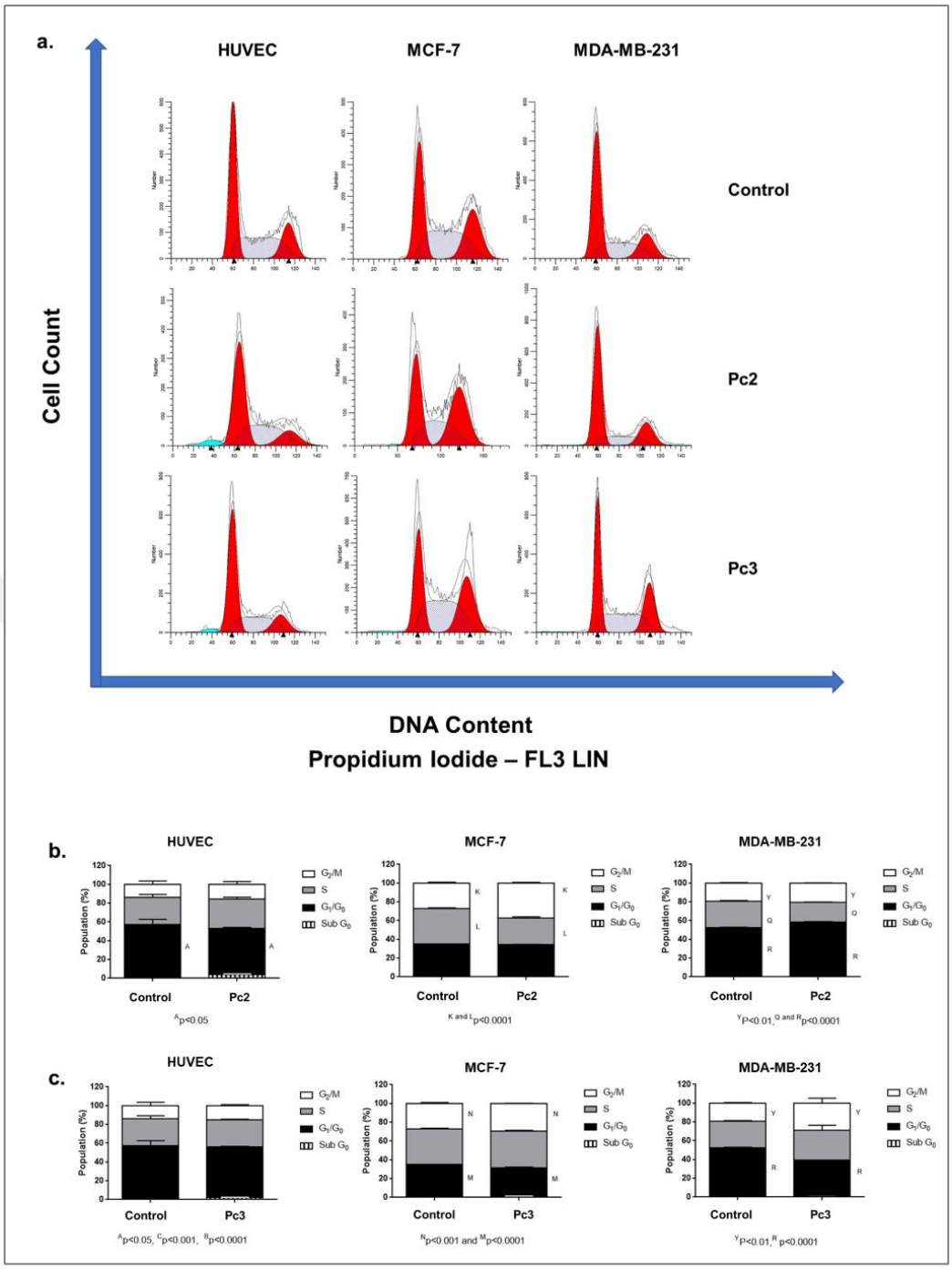


Figure 4.15: DNA content analysis upon treatment with ZnPc-HDACi derivatives. a. Representative histograms of DNA content. b. Pc2 treatment increased $G_2$/M phase in MCF-7 cells and $G_0/G_1$ phase in MDA-MB-231 cells while decreasing $G_0/G_1$ in HUVECs. c. Pc3 treatment led to $G_2$/M arrest in both MCF-7 and MDA-MB-231 cells.

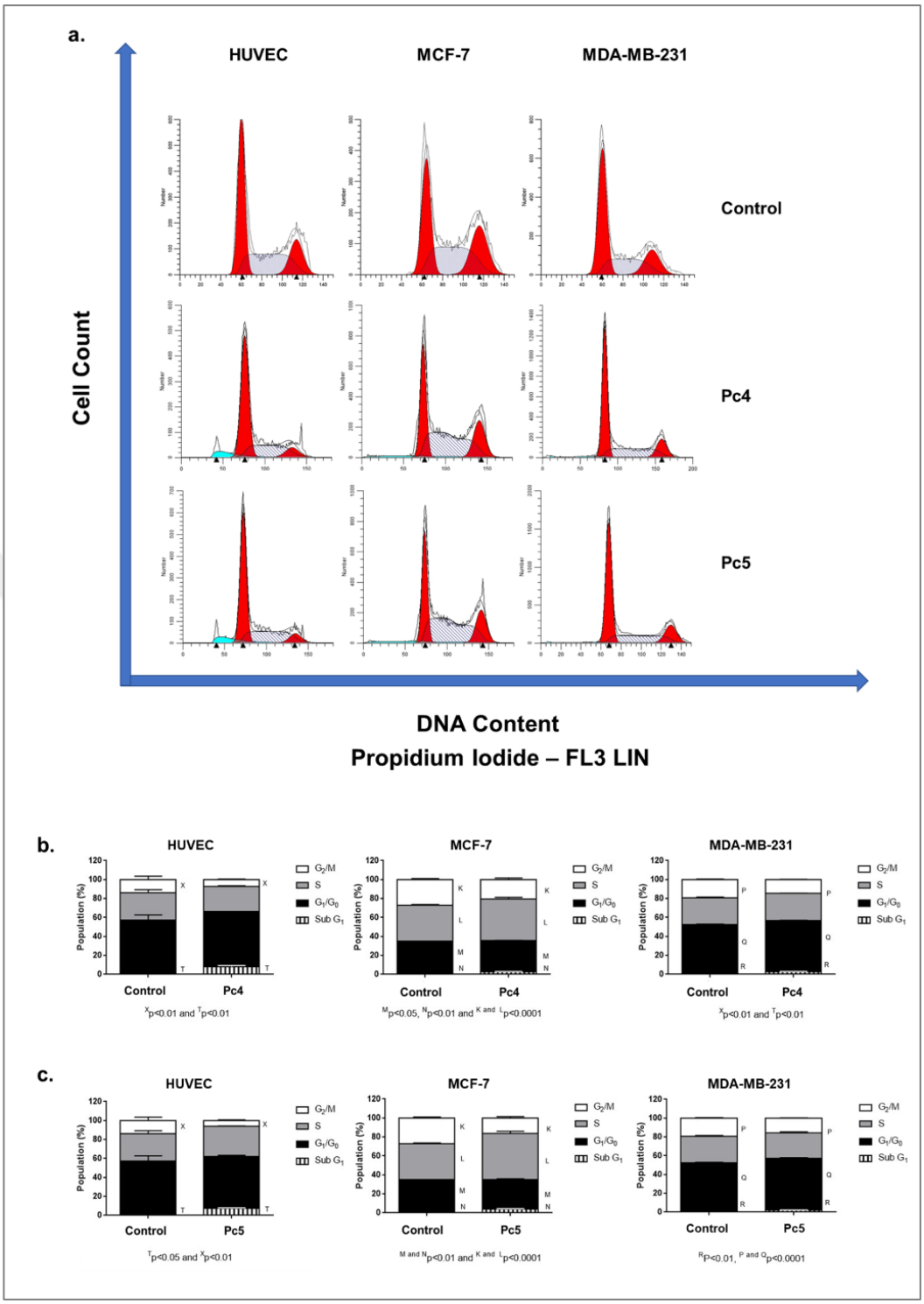


Figure 4.16: DNA content analysis upon treatment with InPc-HDACi derivatives. a. Representative histograms of DNA content. b. Pc4 treatment decreased $G_2$/M phase in all cell lines while inducing S-phase arrest in MCF-7 and $G_0/G_1$ MDA-MB-231 cells. c. Pc5 treatment induced S-phase arrest in MCF-7 cells while led to $G_0/G_1$-phase arrest in MDA-MB-231 cells.

### 4.3.4. Evaluation of HDAC6 and HDAC8 levels by Western Blotting

Both Pc2 ($p<0.001$, $p<0.0001$ and $p<0.01$ for HUVEC, MCF-7 and MDA-MB-231 cell lines, respectively) and Pc3 ($p<0.001$ for all cell lines) treatments significantly decreased HDAC6 levels on all cell lines while both decreasing HDAC8 levels on MDA-MB-231 cells ($p<0.05$), but not on MCF-7 cells or HUVECs (Figure 4.17).

Similar to its zinc counterparts, both Pc4 ($p<0.001$ for all cell lines) and Pc5 ($p<0.05$, $p<0.001$ and $p<0.01$ for HUVECs, MCF-7 and MDA-MB-231 cells) treatments significantly decreased HDAC6 levels on all cell lines. Pc4 did not alter HDAC8 protein levels ($p>0.05$) in contrast to Pc5 which significantly decreased HDAC8 protein levels in both HUVECs ($p<0.05$) and MDA-MB-231 cells ($p<0.01$). When considering 3-HPT has an $IC_{50}$(nM)=306±69 for HDAC6 and $IC_{50}$(nM)=3105±1649 for HDAC 8 [173], our results indicating successful HDAC6 inhibition in addition to a relatively weak effect on HDAC8 is compatible with the literature.

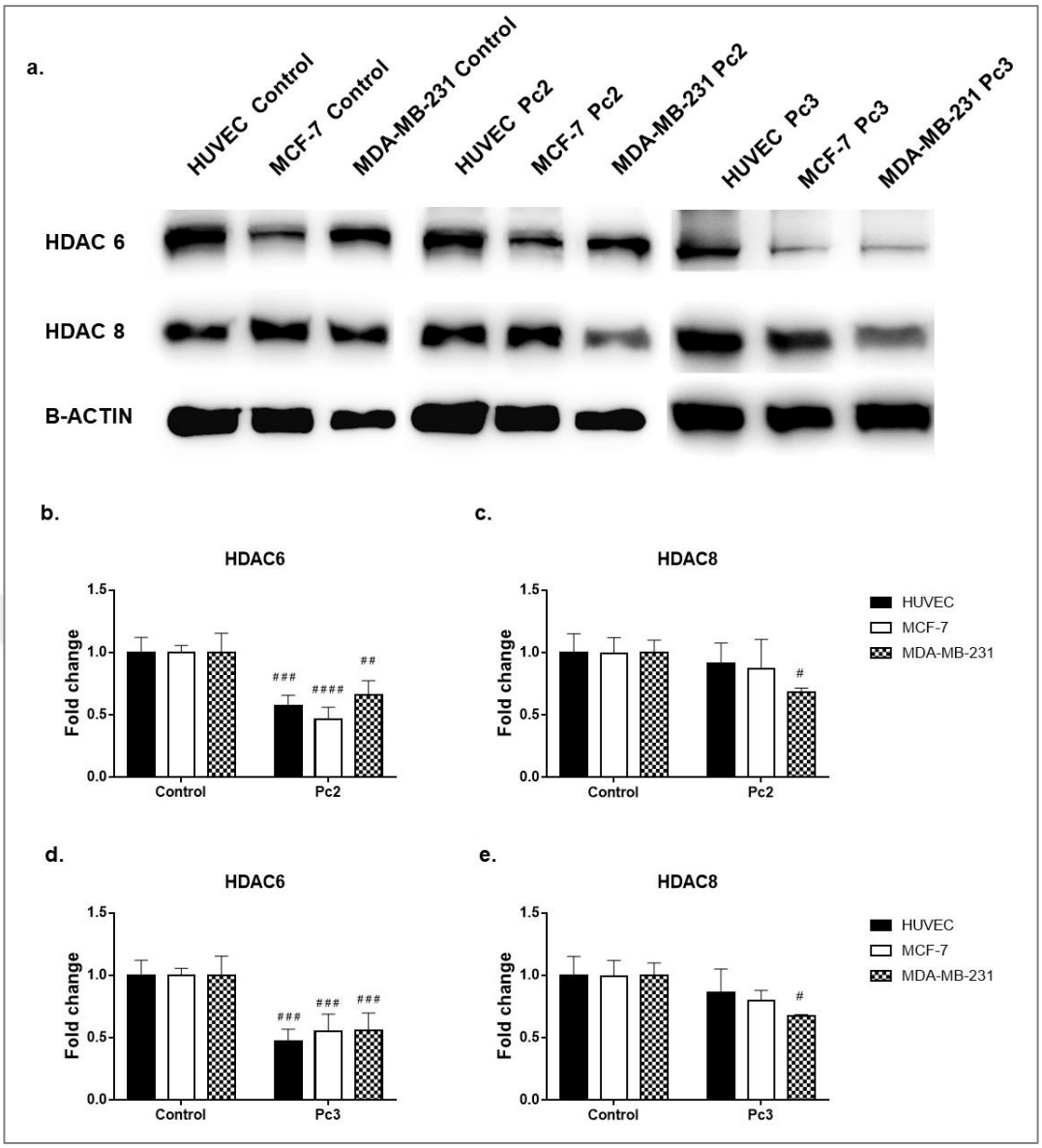


Figure 4.17: Both Pc2 and Pc3 successfully decrease HDAC6 levels in all cell lines while HDAC8 levels were only decreased in MDA-MB-231 cells. a. Representative blot image of Pc2 and Pc3 treated HUVECs, MCF-7 and MDA-MB-231 cells. b. Quantification of HDAC6 upon Pc2 treatment. c. Quantification of HDAC8 upon Pc2 treatment. d. Quantification of HDAC6 upon Pc3 treatment. e. Quantification of HDAC8 upon Pc3 treatment. Significance level was considered as $p<0.05$. * denotes significance between cell lines upon treatment whereas # denotes significance between treatment and control groups

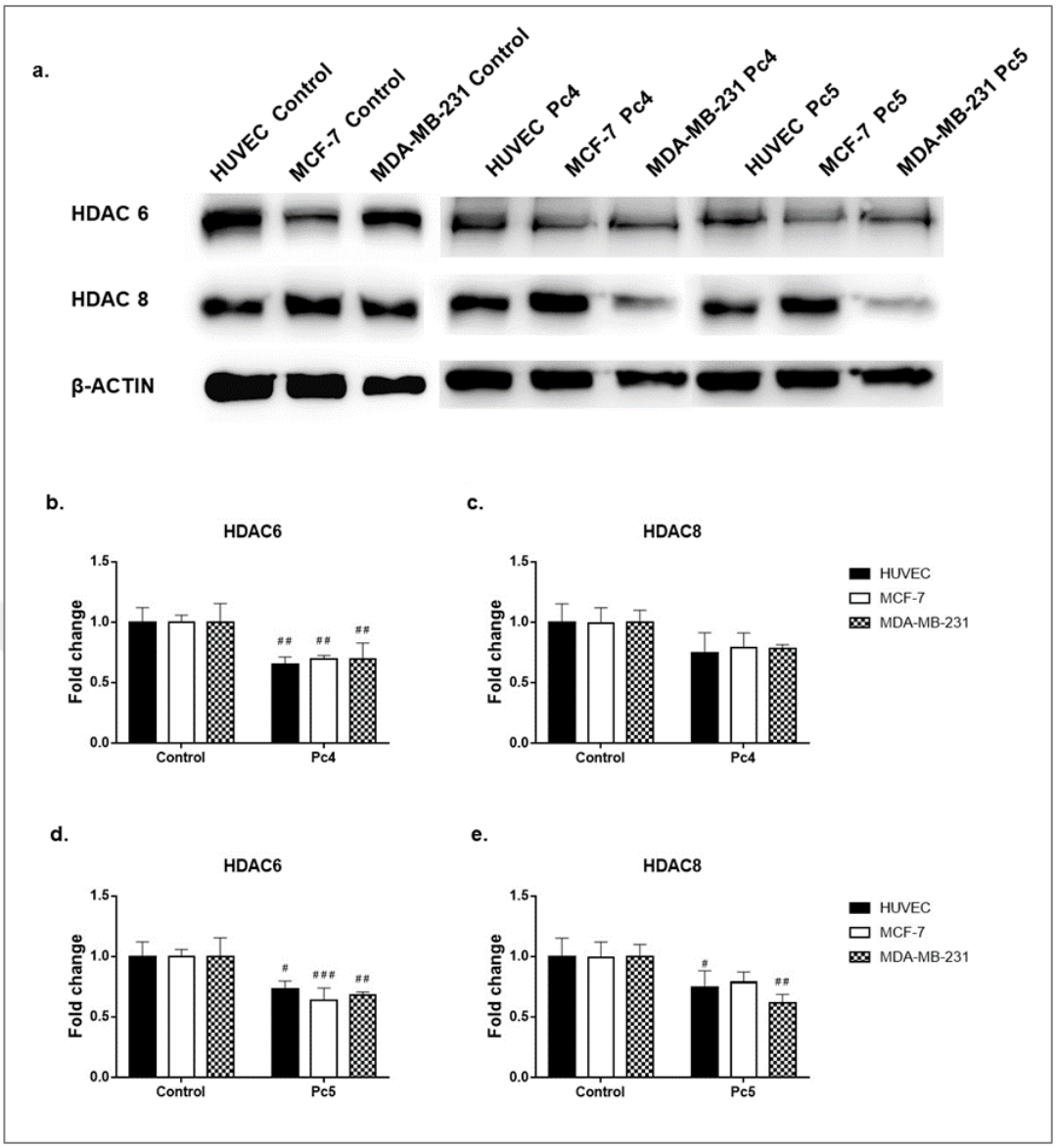


Figure 4.18: Both Pc4 and Pc5 successfully decrease HDAC6 levels in all cell lines while HDAC8 levels were only decreased in HUVECs and MDA-MB-231 cells treated with Pc5. a. Representative blot images of Pc4 and Pc5 treated HUVECs, MCF-7 and MDA-MB-231 cells. b. Quantification of HDAC6 upon Pc4 treatment. c. Quantification of HDAC8 upon Pc4 treatment. d. Quantification of HDAC6 upon Pc5 treatment. e. Quantification of HDAC8 upon Pc5 treatment.

### 4.3.5. Confocal Microscopy Studies

#### 4.3.5.1. Visualization of Cellular Localization

Confocal imaging revealed that Pc2 is either localizes to nucleoli or distributed homogeneous whereas Pc3 is localized into nucleus (Figure 4.19). Homogenous staining suggest that Pc2 localizes to cell membrane and/or cytoplasm which may explain why Pc2 treated cells have significantly lower late apoptosis rates compared to Pc3 as it would induce a different mode of cell death mechanism in contrast to its peripheral counterpart Pc3. Mitochondrial staining revealed that Pc2 disrupts mitochondrial network in HUVECs and MCF-7 cells whereas Pc3 treatment impairs in HUVECs and MDA-MB-231 cells but not MCF-7 cells.

On the contrary, in addition to homogenous staining (shown in white squares), both Pc4 and Pc5 also localized to the mitochondrial network (shown in pale blue squares); which is not observed in compounds Pc1 (nuclear/nucleolar or around the nuclear membrane), Pc2 (membrane/cytoplasmic) and Pc3 (nuclear). Pc5 treatment also decreased mitochondrial signal (shown in green squares).

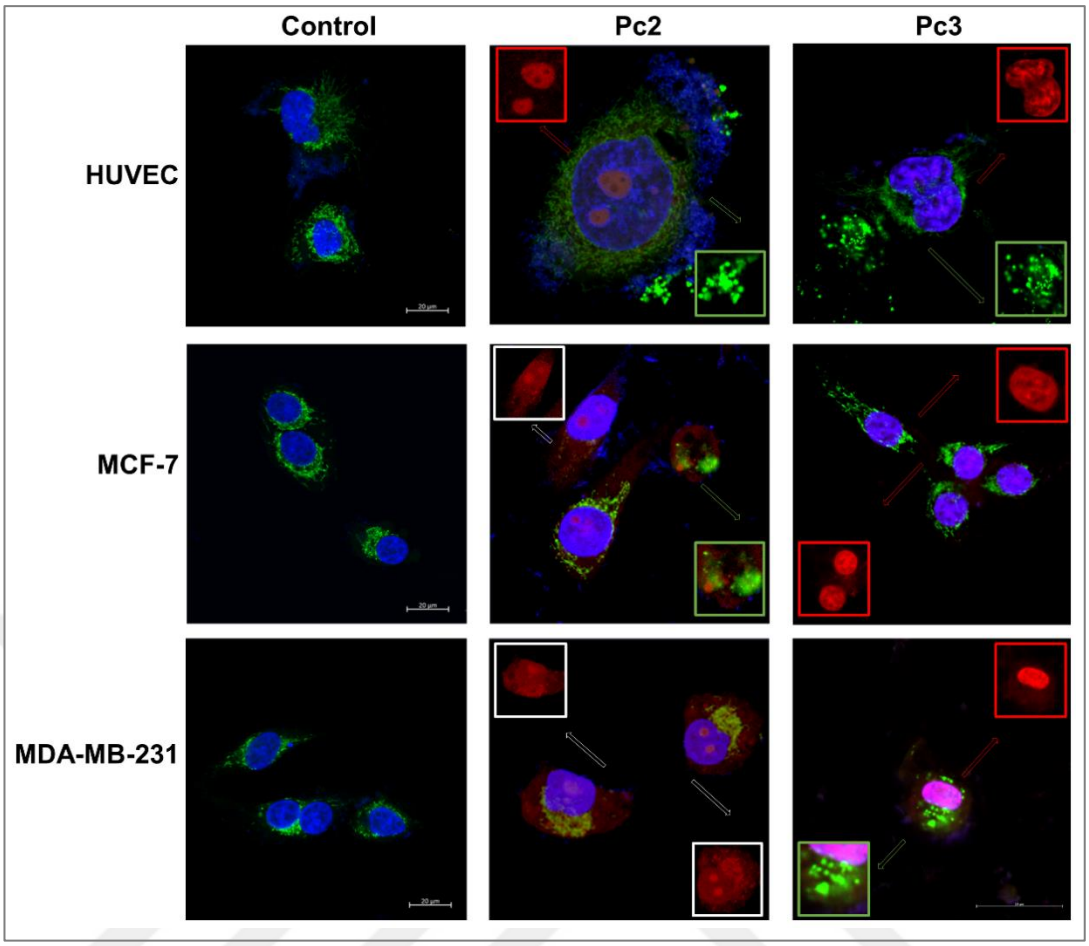


Figure 4.19: Micrographs of untreated and Pc2 or Pc3 treated cells indicating cellular localization. Cells were stained with anti-mitochondria antibody and counterstained with DAPI. Red squares indicate deposits in nuclei and nucleoli whereas white squares indicate homogenous staining that may indicate predominant membrane/cytoplasmic localization. Disrupted mitochondria are shown in green squares. Scale bars indicate 20 µm. All images were taken at 63X zoom with immersion oil.

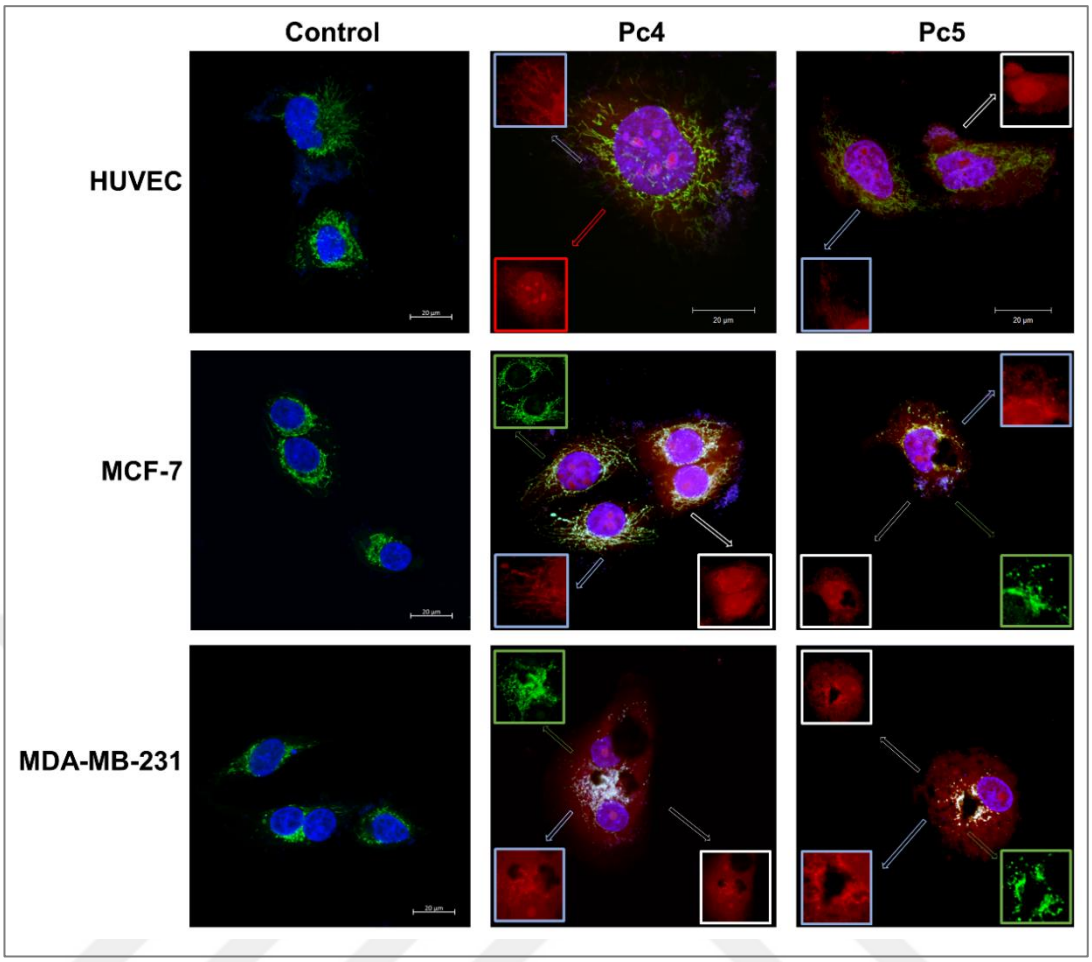


Figure 4.20: Micrographs of untreated and Pc4 or Pc5 treated cells indicating cellular localization. Cells were stained with anti-mitochondria antibody and counterstained with DAPI. Red squares indicate deposits in nuclei and nucleoli whereas white squares indicate homogenous staining that may indicate predominant membrane/cytoplasmic localization. Disrupted mitochondria are shown in green squares. Scale bars indicate 20 µm. All images were taken at 63X zoom with immersion oil.

### 4.3.5.2. Visualization of Autophagy

Confocal microscopy demonstrated that Pc2 treatment induced autophagosome formation that is characterized with green puncta and observed in HUVECs and MCF-7 cells but not MDA-MB-231 cells. Untreated cells exhibit homogenous LC3A/B staining pattern throughout the cytoplasm. Autophagosome formation is indicated with yellow squares. In addition, Pc2 did not localize into autophagosomes and accumulated on either cell membrane or in nucleus which is also indicated above (Figure 4.19-4.21); suggesting Pc2 treatment may induce autophagosome formation but do not directly interact with autophagic lysosomes. On the other hand, Pc3

treatment did not lead to autophagosome formation, yet localized mainly in the nucleus as also indicated (Figure 4.19-4.21).

Pc4 and Pc5 treatment induced autophagy in both cancer cell lines, but not in HUVECs which can be observed in Figure 4.22. Similar to Pc2, neither Pc4 nor Pc5 did not localize to the autophagosomes, but the cyan colour observed in merged photos indicate autophagosomes contain nuclear material, which is not present upon Pc1 or Pc2 treatment.

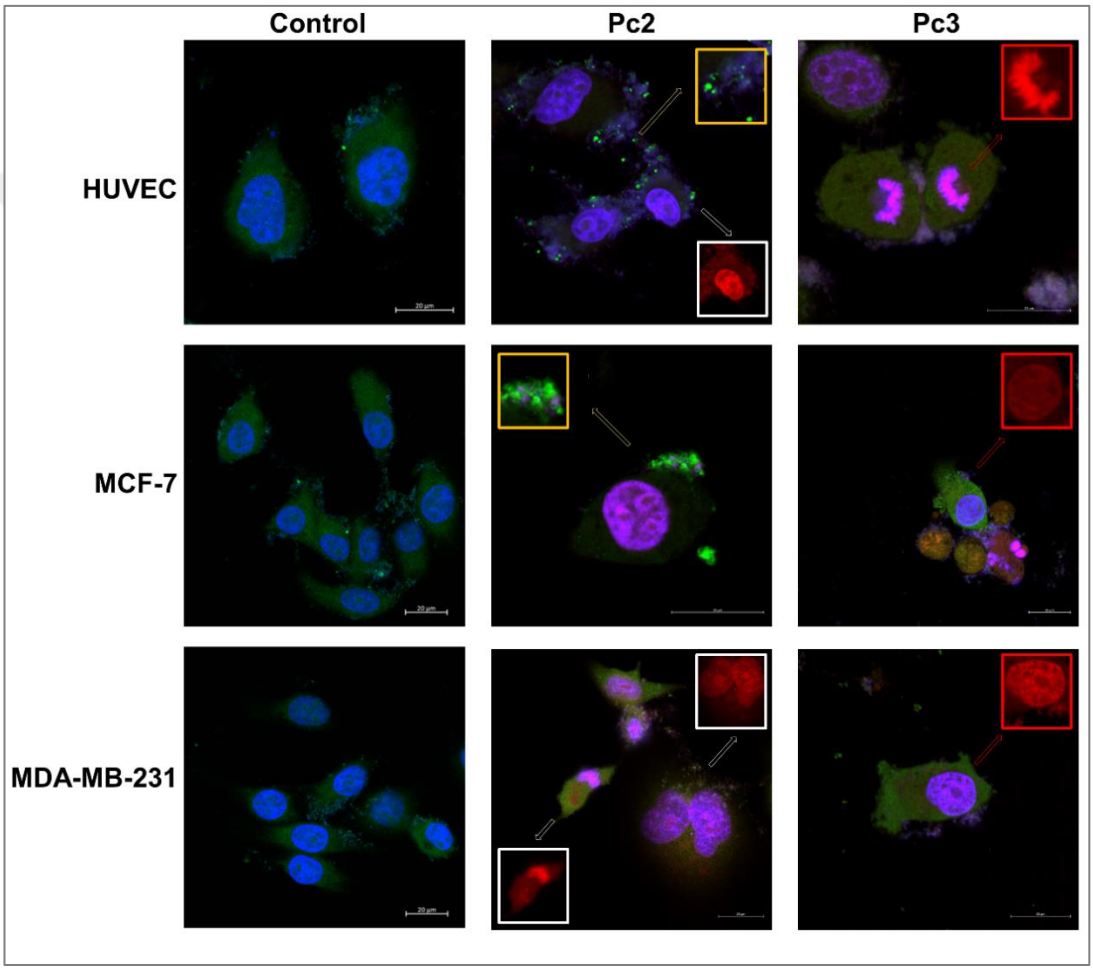


Figure 4.21: Micrographs of untreated and Pc2 or Pc3 treated cells indicating autophagosome formation. Cells were stained with rabbit polyclonal anti-LC3A/B antibody followed by donkey anti-rabbit Alexa Fluor 488 secondary antibody and counterstained with DAPI. Puncta formations are indicated in yellow squares while red squares and white squares indicate nuclear and cytoplasmic/membrane localization, respectively. Scale bars indicate 20 µm. All images were taken at 63X zoom with immersion oil.

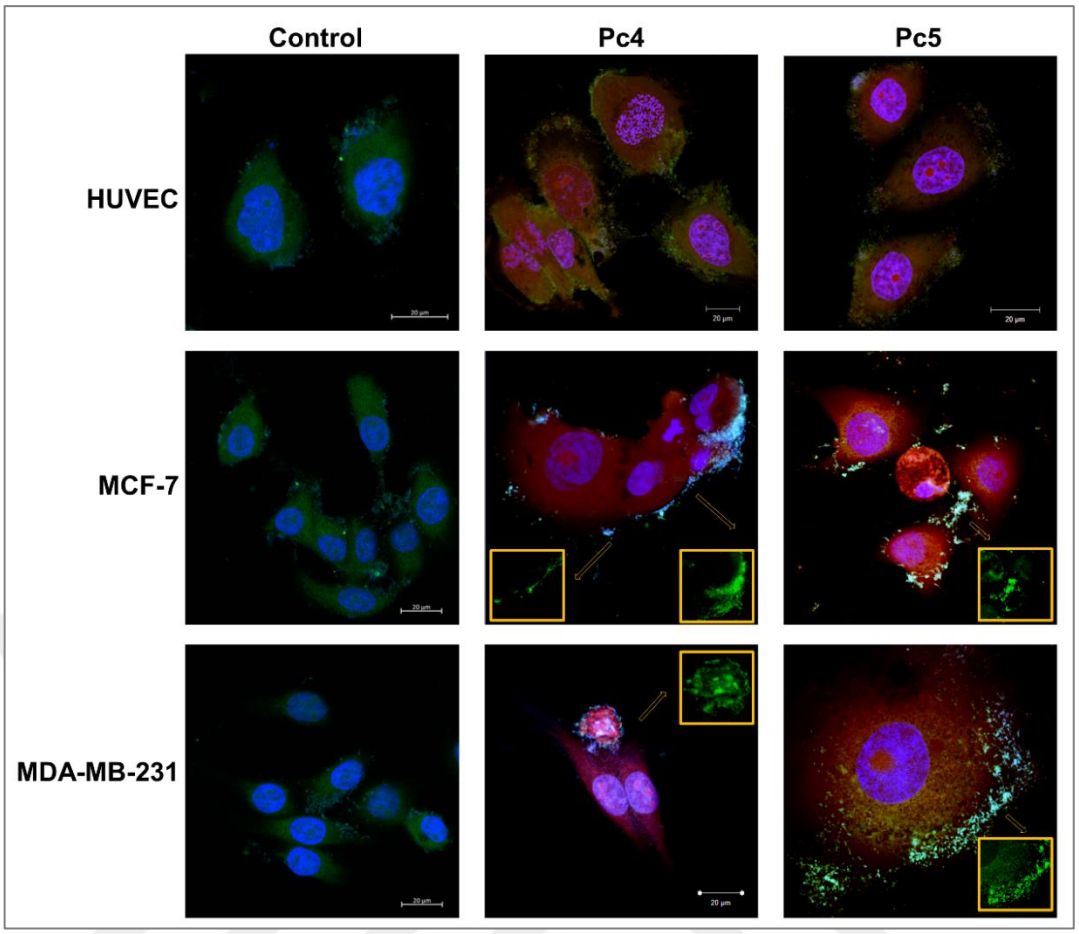


Figure 4.22: Micrographs of untreated and Pc4 or Pc5 treated cells indicating autophagosome formation. Cells were stained with rabbit polyclonal anti-LC3A/B antibody followed by donkey anti-rabbit Alexa Fluor 488 secondary antibody and counterstained with DAPI. Puncta formations are indicated in yellow squares. Scale bars indicate 20 μm. All images were taken at 63X zoom with immersion oil.

### 4.3.6. Evaluation of Mitochondrial Activity

Both Pc2 ($p<0.001$ for HUVECs, $p<0.0001$ for MCF-7 and MDA-MB-231 cells) and Pc3 ($p<0.0001$ for all cell lines) treatments significantly increased DHR-123 MFI in all cell lines (Figure 4.23.b). Comparisons between two compounds indicated Pc3 treatment significantly increased DHR-123 MFI in all cell lines compared to Pc2 treatment ($p<0.0001$). A similar trend for Pc4 ($p<0.0001$ for all cell lines) and Pc5 ($p<0.001$ for HUVECs, $p<0.0001$ for MCF-7 and MDA-MB-231 cells) was observed when treatment and control groups were compared (Figure 4.23.c). Contrary to zinc Pcs, higher DHR-123 MFI values were observed for Pc4 treated HUVECs as well as MCF-7 cells ($p<0.0001$ and $p<0.05$, respectively) in comparison with peripheral Pc5.

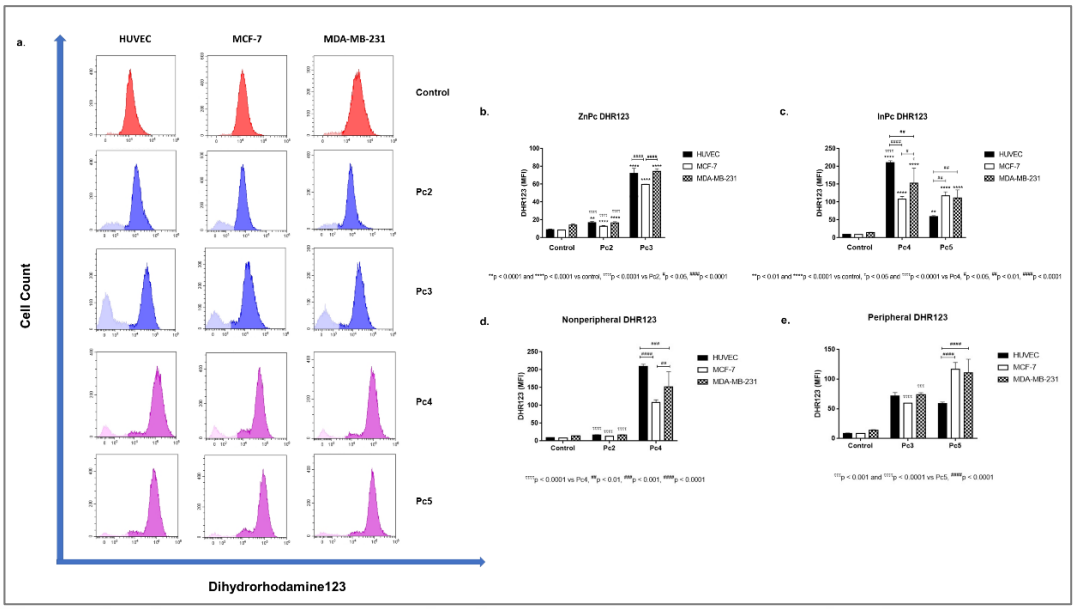


Figure 4.23: Both ZnPc-HDACi and InPc-HDACi derivatives increase Dihydrorhodamine123 mean fluorescence intensity in all cell lines. a. Representative flow cytometry histograms. b. Bar graphics indicating comparisons between cell lines and DHR-123 MFI values for Pc2 and Pc3 treatments. c. Bar graphics indicating comparisons between cell lines and DHR-123 MFI values for Pc4 and Pc5 treatments. d. Comparisons between Pc2 and Pc4 treatments in terms of mitochondrial activity for evaluating zinc or indium as core metals. e. Comparisons between Pc3 and Pc5 treatments in terms of mitochondrial activity for evaluating zinc or indium as core metals.

Comparisons between non-peripheral substituted Pcs that have either Zn or Iv as core metals indicated Pc4 increased DHR-123 MFI in all cell lines compared to its zinc counterpart Pc2 ($p<0.0001$ for all cell lines) (Figure 4.23.d). A similar phenomenon was observed when MCF-7 and MDA-MB-231 cells were compared after Pc3 and Pc5 treatments as peripheral substituted InPc derivative led to significantly increased MFI values in MCF-7 and MDA-MB-231 cells ($p<0.0001$ and $p<0.001$, respectively), but no difference between HUVECs was observed ($p>0.05$.) (Figure 4.23.e).

### 4.3.7. Evaluation of CD44, CXCR4 and CCR7 Levels by Flow Cytometry

Pc2 did not alter CXCR4 protein levels in cell lines ($p>0.05$) while decreasing CD44 and CCR7 protein levels in HUVECs and MDA-MB-231 cells ($p<0.001$ and $p<0.0001$, respectively) (Figure 4.24.a). Percent decrease in CD44 protein levels did

not differ between cell lines ($p>0.05$) though percent decrease in CCR7 levels were significantly higher in MDA-MB-231 cells when compared to MCF-7 cells ($p<0.05$), but not HUVECs ($p>0.05$). The decrease in CXCR4 levels were slightly but significantly increased in HUVECs in comparison with MDA-MB-231 cells ($p>0.05$) (Figure 4.24.b). Representative flow cytometry histograms were given on Figure B1.6.

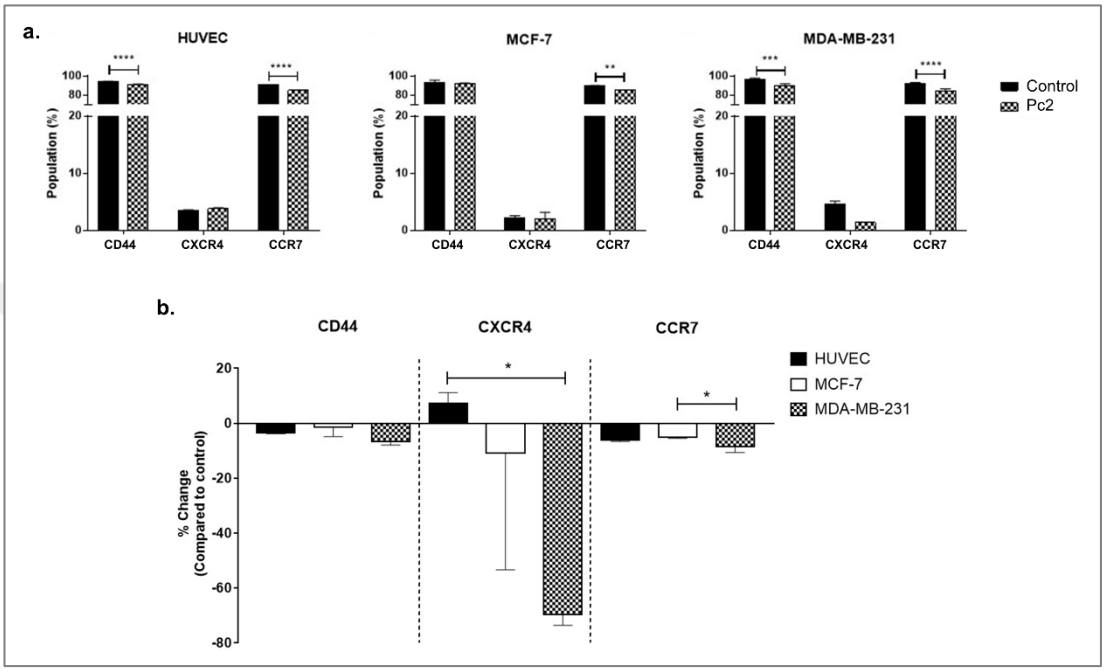


Figure 4.24: Pc2 decreases CCR7 protein levels in all cell lines while increasing CXCR4 in HUVECs and MCF7 cells. a. CD44, CXCR4, and CCR7 protein levels in control and treatment groups. * denotes significance between control and treatment groups. b. Relative changes in the CD44, CXCR4, and CCR7 levels after treatment. Differences between groups were indicated with *.

Pc3 led to a significant decrease in CD44 levels in all cell lines ($p<0.0001$) while increasing CXCR4 levels ($p<0.0001$ for HUVECs and MCF-7 cells, $p<0.01$ MDA-MB-231) (Figure 4.25.a). In addition, Pc3 treatment did not alter CCR7 protein levels in MCF-7 cells while decreasing it both in HUVECs and MDA-MB-231 cells ($p<0.0001$). Comparisons between percent alterations indicated that the decrease in the CD44 levels were slightly but significantly higher in HUVECs and MDA-MB-231 cells compared to MCF-7 cells ($p<0.05$; Figure 4.25.b). On the other hand, CXCR4 protein levels were increased upon Pc3 treatment in MCF-7 cells at a significantly higher rate than both HUVECs and MDA-MB-213 cells ($p<0.001$, Figure 4.25.b). The decrease in the CCR7 levels in HUVECs and MDA-MB-231 upon Pc3 treatment were

significantly more pronounced than MCF7 cells ($p<0.001$ and $p<0.0001$, respectively, Figure 4.25.b). On the other hand, the decrease in CCR7 levels in MDA-MB-231 cells were slightly but significantly higher than HUVECs ($p<0.05$, Figure 4.25.b). Representative flow cytometry histograms were given on Figure B1.7.

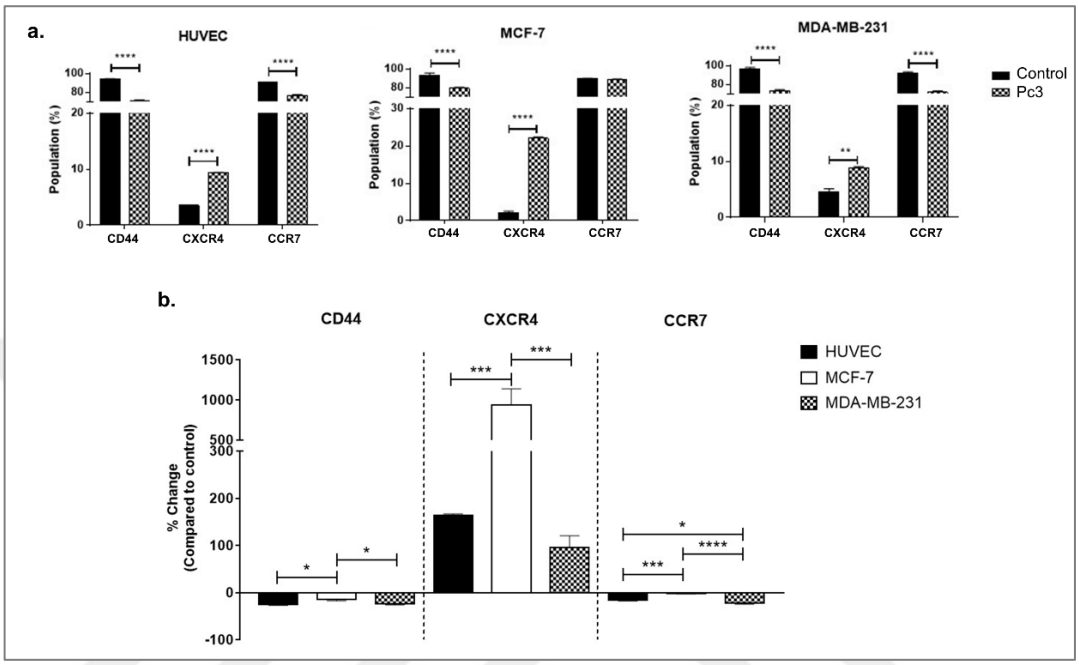


Figure 4.25: Pc3 decreases CD44 protein levels in all cell lines while increasing CXCR4 in HUVECs and MCF7 cells. a. Percentage of CD44, CXCR4, and CCR7 protein levels in control and treatment groups. * denotes significance between control and treatment groups. b. Relative changes in the CD44, CXCR4, and CCR7 levels after treatment. Differences between groups were indicated with *.

Pc4 significantly reduced CD44 protein levels in all cell lines ($p<0.0001$); CCR7 levels were decreased significantly in MCF-7 and MDA-MB-231 cells ($p<0.0001$ and $p<0.001$, respectively) while HUVECs remain unaffected ($p>0.05$). On the other hand, Pc4 significantly increased CXCR4 levels in HUVECs ($p<0.0001$) and MCF-7 cells ($p<0.01$), but not in MDA-MB-231 cells (Figure 4.26.a). The decrease in the CD44 levels was significantly more pronounced in HUVECs than both MCF-7 and MDA-MB-213 cells upon Pc4 treatment ($p<0.01$ and $p<0.001$, respectively; Figure 4.26.b). Additionally, the decrease in CD44 levels was significantly lower in MDA-MB-231 cells compared to MCF-7 cells ($p<0.05$; Figure 4.26.b). Pc4 treatment increased CXCR4 levels in HUVECs significantly compared to MCF-7 cells ($p<0.05$, Figure 4.26.b) while decreasing CXCR4 levels significantly in MDA-MB-231 cells, though

this alteration was not significant. Representative flow cytometry histograms were given on Figure B1.8.

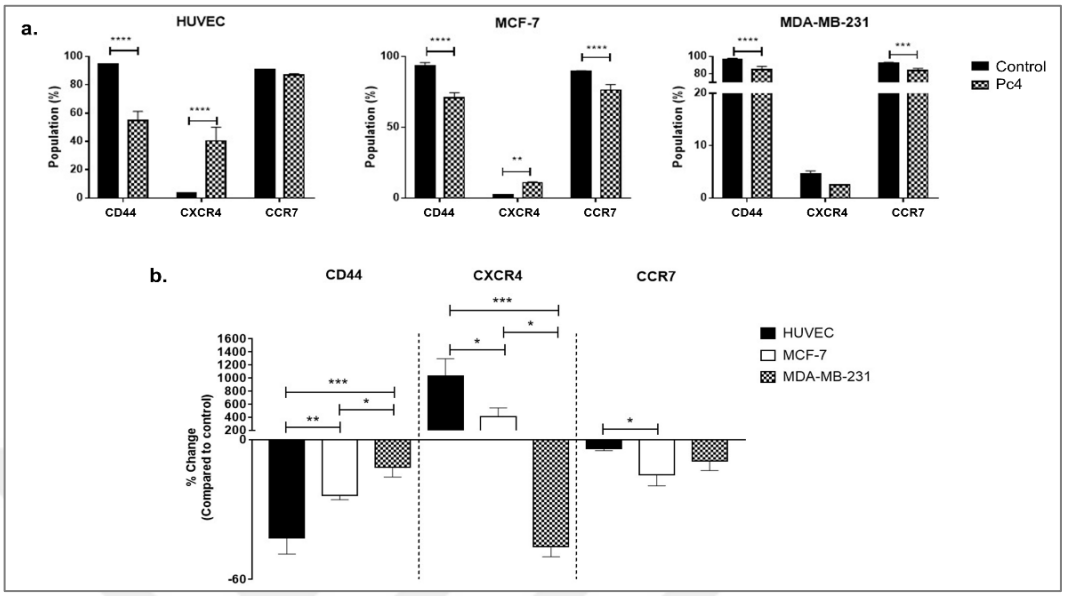


Figure 4.26: Pc4 decreases CD44 protein levels in all cell lines while increasing CXCR4 in HUVECs and MCF7 cells. a. Percentage of CD44, CXCR4, and CCR7 protein levels in control and treatment groups. * denotes significance between control and treatment groups. b. Relative changes in the CD44, CXCR4, and CCR7 positivity after treatment. Differences between groups were indicated with *.

Pc5 altered CD44 and CXCR4 protein levels a similar manner with Pc4 in HUVECs ($p<0.001$) while also decreasing CCR7 levels compared to control ($p<0.0001$). Also, in MCF-7 cells, Pc5 acted in a similar way with its non-peripheral counterpart by decreasing CD44 ($p<0.0001$) and increasing CXCR4 ($p<0.0001$) levels; yet, the decrease in CCR7 levels was not significant ($p>0.05$). In MDA-MB-231 cells, Pc5 slightly but significantly decreased both CD44 and CCR7 protein levels ($p<0.0001$ and $p<0.001$, respectively), but did not alter CXCR4 levels (Figure 4.27.a). Pc5 treatment led to a significantly higher decrease in both HUVEC and MCF-7 cells than MDA-MB-231 cells with regards to CD44 levels ($p<0.01$; Figure 4.27.b). Similar to Pc4 treatment, CXCR4 protein levels were significantly increased at a higher rate in HUVECs compared to MCF-7 cells after Pc5 treatment ($p<0.001$; Figure 4.26.b). On the other hand, the percent decrease in CXCR4 levels in MDA-MB-231 cells were significantly different than both HUVECs and MCF-7 cells upon Pc5 treatment ($p<0.0001$ and $p<0.01$, respectively; Figure 4.27.b). Pc5 treatment led to a significantly

higher decrease in the CCR7 levels in HUVECs compared to MCF-7 and MDA-MB-231 cells ($p<0.0001$, Figure 4.27.b), yet no significant difference between MDA-MB-231 and MCF-7 cells was reported. Representative flow cytometry histograms were given on Figure B1.9.

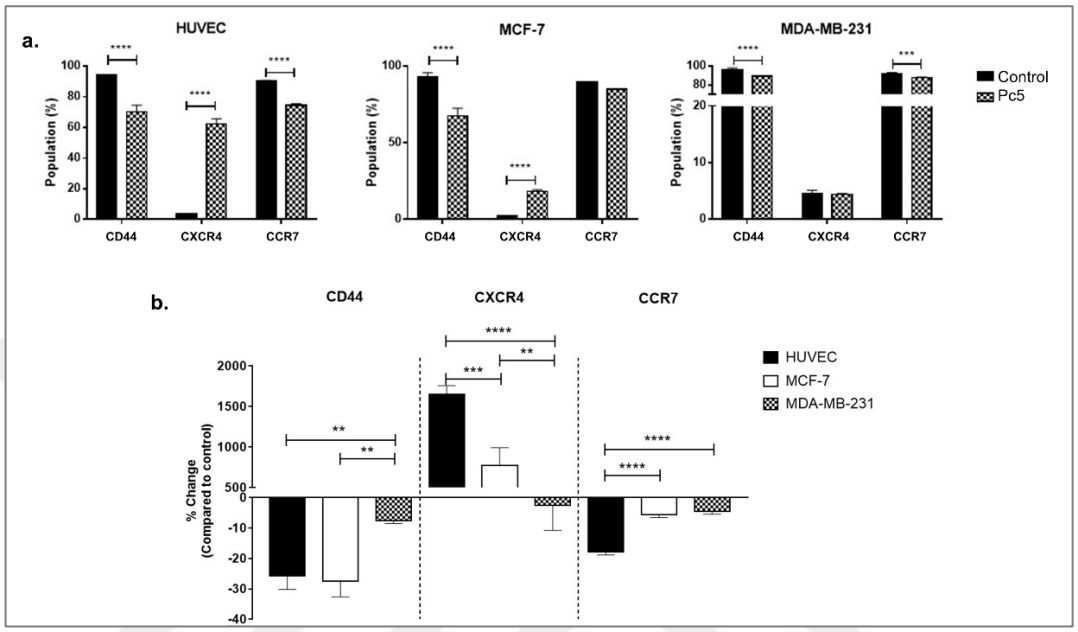


Figure 4.27: Pc5 decreases CD44 protein levels in all cell lines while increasing CXCR4 levels in HUVECs and MCF7 cells. a. CD44, CXCR4, and CCR7 protein lelvels in control and treatment groups. * denotes significance between control and treatment groups. b. Relative changes in the CD44, CXCR4, and CCR7 levels after treatment. Differences between groups were indicated with *.

In conclusion, Pc-HDACi derivatives target different cellular compartments, according to both their core metals and the position of their HDACi moiety; in turn, they activate different modes of programmed cell death pathways. Among all Pc-HDACi derivatives evaluated in this study, SiPc-HDACi derivative stands out as the most promising PDT drug candidate, combining photodynamic action with effective HDAC downregulation.

# 5. DISCUSSION

Small molecule HDACis have successfully altered HDAC activity in pre-clinical models, introducing them to clinical trials. However, as reviewed by Gryder et al., two FDA-approved HDACi, Vorinostat and Romidepsin were found inefficient in solid tumours while exerting toxic side effects [130]. In 2013, Patil et al. were the first to describe 3-HPT as an alternative to non-hydroxamate zinc-binding groups (ZBGs) for inhibition of HDAC6 and HDAC8 [173].

HDAC6 primarily resides in the cytoplasm to regulate various extra-nuclear proteins including tubulin, thus, is involved in cell motility and metastasis [130]. Furthermore, it also involves in aggresome formation, which plays an important role in the elimination of misfolded protein aggregates, and its inhibition has been shown to increase susceptibility to misfolded protein stress [182]. Located on the X chromosome, with its co-factor-independent activity, ability to target non-histone proteins [183] and having lack of C-terminal protein binding domain, HDAC8 differs from other class I HDACs [184]. HDAC8 inhibition decreases the deacetylating activity of HDAC8, in turn, promoting many cellular events including cell cycle arrest and apoptosis [184]. HDAC8 activity is also related to proliferation and resistance to apoptosis in various cancer types. As being unresponsive to most common ZBG, the hydroxamate, HDAC8 is the least inhibited isoform among Class I HDACs [130]. Balasubramanian et al. developed a specific HDAC8 inhibitor, PCI-34051, that induces apoptosis effectively on T-cell lymphoma and in leukaemia cell lines in a calcium-mediated manner; in contrast, same treatment remained ineffective for solid tumours [185].

Studies regarding PSs in combination with HDACi for cancer treatment are limited. In 2014, Ye et al. were the first to report anti-cancer efficiency of four photosensitive cyclometalated Ir(III)-HDACi complexes that exerted phototoxicity against human pulmonary carcinoma cell line A549, cisplatin-resistant cell line A549R and human normal liver cell line LO2 [186]. Mechanistic studies revealed all four complexes induce apoptosis by increasing ROS production, promoting mitochondrial damage and downregulating HDAC activity, which are consistent with our findings. Kasparkova et al. developed a HDACi, suberoyl-bis-hydroxamic acid (SubH)-conjugated photosensitive platinum(IV) complex [187] and evaluated its anti-cancer

properties in ovarian carcinoma cell line A2780. This novel SubH-photosensitive PtIV complex exerted higher cytotoxicity compared to its biologically inactive ligands bearing counterpart or chemotherapeutic platin analogue cisplatin on both cisplatin sensitive and resistant cells; suggesting that HDACi substitution may induce a different cell death mechanism than photosensitive Pt(IV) or cisplatin. Halaburková et al. combined a natural photoactive compound, hypericin, with either pan-HDACis, SAHA and Trichostatin A, or valproic acid and sodium phenylbutyrate that target nuclear HDACs, to evaluate combinatorial effects in two different colorectal cancer cell lines, HCT116 and HT29, that are known to be resistant to hypericin-mediated PDT [188]. Authors revealed that HDACi pre-treatment induces cyclin dependent kinase inhibitor 1A (CDKN1A) expression epigenetically and increases anti-cancer efficacy of hypericin-mediated PDT. Recently Liu et al. developed a nanogel containing second-generation PS chlorin-6 (Ce6) that not only acts as a PS but also facilitates drug delivery to tumour [189]. Hypoxic condition in tumour cells activates HIF-1α pathway that eventually increases *vascular endothelial growth factor* (VEGF) expression to promote angiogenesis and tumour proliferation. Authors further introduced SAHA that was previously proven to inhibit hypoxia signalling pathway to the Ce6-containing nanogel and observed increased anti-tumour efficiency that was accompanied by decreased HIF-1α and VEGF levels. As indicated, studies combining PS and HDACi for anti-cancer treatment are restricted to these studies, and none of them involves a Pc derivative for PDT.

Recently, many advancements have been made in the management of advanced or metastatic breast cancer while they are only ideal if their adverse effects are controlled, and if supportive therapies increase life quality while decreasing long-term toxicities [190]. Today, the majority of approved PDT protocols target superficial skin and luminal organ lesions while interstitial and intra-operative approaches are under investigation for treating solid tumours including breast tumours [191]. Photofrin, a lipophilic agent that can be intravenously administered was clinically tested for the treatment of breast cancer skin metastases; the complete and partial response rates were reported as 13.5% and 35.1% respectively [192]. Phase II/III trials of tin ethyl etiopurpurin (Purlytin) against recurrent cutaneous metastatic breast cancer revealed the overall response rate as 92% [193]. When considering HDACi treatment for breast cancer, according to Rhodes et al., hydroxamic acid-based pan-HDACi Panobinostat was reported to inhibit metastasis in TNBC [194]. Authors also indicated that

Panobinostat is more effective compared to Vorinostat (a class I and II HDACi) and TMP269 (a class IIa HDACi). Chen et al. suggested that a class I, II, and IV HDACi, Pracinostat treatment prevents cell growth and metastasis in breast cancer by supressing HDAC5 and HDAC4 [195]. Park et al. reported inhibition of HDAC1, 6 and 8 play roles in metastasis of MDA-MB-231 cells. MCF-7 cells, overexpressing HDACs mentioned also showed increased invasiveness [196]. On the other hand, Leslie et al. revealed that HDAC11 inhibition is linked with lymph node metastasis in breast cancer [197]. Lin et al. screened 30 different HDACi-treated cancer cell lines and indicated that in addition to activating programmed cell death pathways, treatment promotes motility in a dose dependent manner by inducing *protein kinase C* (PKC) activation, further suggesting PKC inhibition along with HDACs simultaneously induces cell death pathways while inhibiting metastasis [128]. Altogether, while there is an agreement on HDACis death-triggering properties on breast cancer cells *in vitro* and *in vivo*, results focusing on their effect on metastasis and invasion capacities remain controversial.

In this study, we investigated the anti-cancer efficacy of novel HDACi-bearing Si, Zn and In derivatives on breast cancer cell lines, MCF7 and MDA-MB-231 as well as a healthy endothelial cell line (HUVEC). Among all Pc derivatives synthesized, Pc1 had the highest singlet oxygen yield which is followed by ZnPcs (Pc2 and Pc3), and InPcs (Pc4 and Pc5), respectively (data kindly provided by Prof. Dr. Devrim Atilla); Pc2, Pc3, Pc4 and Pc5 contain four HDACi moieties whereas Pc1 had two. When considering dual activity of the compounds, their localization as well as the abundance of the target HDACs in the cells would affect the outcome. None of the compounds did exert any cytotoxic effect under dark while induced cytotoxicity in a dose-dependent manner in all cell lines. For HUVECs and MDA-MB-231 cells, the lowest $IC_{50}$ values were calculated after Pc3 treatment while for MCF-7, it was calculated upon Pc1 treatment. This may be a result of the oestrogen-dependent regulation of HDAC6 and HDAC8, suggesting the treatment of the oestrogen-sensitive cell line may require higher photodynamic activity in combination with HDAC inhibition [183], [198].

Cellular localization is an important factor that determines the anti-cancer effect of this dual system; as along with $^1O_2$ generation, the HDACi moieties should interact with their respective targets to successfully downregulate respective proteins. In our case, the target proteins can be found both in nucleus and cytoplasm [183], [199]. It is

previously stated that photosensitizers that target ER or mitochondria promote apoptosis by inducing oxidative stress while compounds localize to lysosomes or plasma membranes are reported to initiate necrosis [26]. Induction of autophagy is reported to be localization independent, and apoptosis was observed in cells already undergoing autophagy [200]. Role of autophagy upon PDT is controversial since it may either induce resistance to treatment by promoting recycling damaged organelles, or initiate death signals [201]. On the other hand, presence of apoptosis along with autophagy is reported to be crucial for an enhanced cell death response as MCF-7 cells were shown to develop PDT resistance when the autophagic response is inhibited [202], [203]. In conclusion, it is still unclear how exactly autophagy affects the outcome of PDT [200]. We investigated the link between localization of Pc-HDACis and the mode of cell death and demonstrated that both the core metal of the Pc derivative as well as the position of the HDACi moiety influence the compounds' localization, and in turn, the effectivity of the treatment.

Pc1 tend to localize to the nuclei and nucleoli in addition to forming fluorescent deposits (observed as red foci) around nuclear membranes in cancer cells. Comparisons between Pc2 and Pc3 suggested a possible steric effect as Pc3 localized to the nuclei while Pc2 treatment resulted in homogenous staining in cancer cells, indicating the compound's nuclear penetration is limited, and the staining pattern suggested cytoplasmic and/or cell membrane localization. This would also explain the higher $IC_{50}$ values of Pc2 compared to Pc3, as well as induction of different programmed cell death pathways which is discussed below in detail. Compared to Pc3, the compound-derived signal was slightly higher for Pc2 in HUVECs and MCF-7 cells, while similar in MDA-MB-231 cells, suggesting Pc2 effectively interacts with cells, but has lower penetration ability and likely to attach to the cell membrane. None of the compounds mentioned above localized to the mitochondria while they all disrupted the mitochondrial network as irregular green signal was observed in all cells compared to their control counterparts. On the other hand, treatment with both InPc derivatives revealed homogenous staining with additional mitochondrial localization since the compounds' green signal overlaps with the mitochondrial network structure. Due to the absence of a mitochondria-targeting sequence of the compounds, this overlap suggests that the InPc-HDACi derivatives can target mitochondria themselves. $In^{3+}$ is known to induce mitochondrial permeability transition by disrupting proton channels located in the inner mitochondrial membrane, leading to mitochondrial

oxidative stress, cytochrome c release and eventually apoptosis [204], [205]. Neither Pc4 nor Pc5 altered mitochondrial network in HUVECs while decreasing the signal in MDA-MB-231 cells. Pc4 treated MCF-7 cells' mitochondrial network structure resembled control cells while Pc5 treatment reduced the signal, similar to MDA-MB-231 cells. While healthy mitochondria staining result in a stringy structure under microscope, Pc1, Pc2 and Pc3 treatments disrupted this pattern to form speckles. On the other hand, Pc4 and Pc5 were the only compounds showing mitochondrial localization, but their induction of speckle formation (thus disrupting the mitochondrial network) was less prominent compared to SiPc-HDACi and ZnPc-HDACis.

As $^1O_2$ formation depends on the availability of oxygen, mitochondria are important organelles in PDT due to their high oxygen levels [206]. A previous study even suggested that low levels of singlet oxygen produced in the mitochondria are two times more toxic than membrane targeting, and thrice more effective than nuclear targeting [207]. We evaluated mitROS accumulation by DHR123 staining, and as anticipated, Pc4 and Pc5 which target mitochondria along with homogenous localization resulted in higher mitROS accumulation compared to Pc2 and Pc3 (yet, Pc3 was as effective as Pc5 on HUVECs in terms of mitROS induction). It's relatively low DHR123 MFI values (comparable to those observed upon Pc2 treatment) support Pc1's distant localization from mitochondria.

Here, one would question the mechanism behind Pc1, Pc2 and Pc3's disruptive effect on the mitochondrial network without targeting the mitochondria (observed in the confocal microscopy as green speckles), and how its' integrity is preserved after mitochondria localizing Pc4 and Pc5 treatments. One possible explanation is, this result may be an outcome of the general cellular damage induced by $^1O_2$ formation: even if the PS localizes to a different site of the cell (such as Pc3 targeting nucleus), the resulting signalling cascades may alter mitochondrial network. Another possibility is the partial localization of Pc1, Pc2 and Pc3 to mitochondria-associated membranes (MAMs), the junctions where ER and mitochondria are physically connected [208]. Several proteins involve in cellular homeostasis reside at MAMs including the ones take part in programmed cell death mechanisms and tumourigenesis. This also would explain the red foci around the nuclei observed in Pc1 treated cancer cells as the compound localized closely to the mitochondria, but their signal did not overlap. Yet, we cannot confirm this hypothesis as it should be validated with nucleus-ER-

mitochondria-compound quadruple staining. When taken together with compounds' cellular localizations, differences between $IC_{50}$ values of Pc-HDACi derivatives are likely to be a result of not only the singlet oxygen yield of the Pc derivative, but also the target site, as Pc-HDACi derivatives localized to nucleus had lower values while others had relatively higher $IC_{50}$ values. As mentioned before, this localization is expected to affect the mode of cell death.

Apoptosis is a tightly regulated cell death mechanism that is essential for the maintenance of normal cellular homeostasis by either eliminating undesired or potentially harmful cells. Dysregulations in apoptotic pathways are related to various pathological conditions including cancer [209]. Apoptosis is considered as the main cell death pathway in both PDT and HDAC inhibition [186]. Here, Pc1 treatment decreased viability significantly in all cell lines by promoting apoptosis without initiating a necrotic response. While both Pc2 and Pc3 decrease viability compared to the control groups, Pc2 was reported to be less effective in initiating apoptosis (likely to be a result of the poor penetration of the compound) while a prominent difference was not observed between Pc4 and Pc5, although viability rates were slightly higher in cancer cells upon Pc4 treatment. Comparisons between non-peripheral Pc-HDACi derivatives revealed the effect of Pc2 treatment was less prominent compared to Pc4 in terms of decreasing viability and inducing apoptosis (probably as a result of the membrane localization). Peripheral Pc-HDACis suggested a similar result with a difference: Pc3 was reported to be more efficient in MCF-7 cells in contrast to HUVECs and MDA-MB-231 cells which had better results upon Pc5 treatment. This finding is consistent with the hypothesis proposed above as destruction of MCF-7 cells may require higher photodynamic activity along with HDAC inhibition.

In addition, apoptosis was not the only programmed cell death pathway upon treatment with Pc-HDACi derivatives as Pc1, Pc4 and Pc5 initiated autophagosome formation in cancer cell lines while not affecting healthy cells. In Pc4 and Pc5 groups, punctas representing autophagosomes had a unique cyan colour, indicating they contain nuclear material. Induction of autophagy upon DNA damage is suggested by various studies [210], [211]. However, the origin of the nuclear material (genomic DNA, or mitochondrial DNA) inside the autophagosomes remains unknown. When considering ZnPc-HDACi derivatives, Pc2 treatment resulted in autophagosome formation in HUVECs and MCF-7 cells but not MDA-MB-231 cells, yet Pc3 was found ineffective in terms of inducing autophagy in all cell lines, which may be

attributed to two compounds' distinct localization sites. However, as stated above, results of the studies investigating the effect of autophagy on cancer cells remain controversial. It should be kept in mind that *in vitro* approaches may fail to represent the exact role of autophagy in anti-cancer therapy since stromal cells of the tumour and immune cells have a significant impact on the outcome and response to the autophagy-based anticancer therapies [203]. Further *in vivo* studies taking tumour microenvironment into account should be performed in order to define the therapeutic relevance of autophagy in PDT.

DNA damage is another factor promoting apoptosis [212] and autophagy [213]. HDACis are reported not to cause DNA breaks directly, but they suppress DNA repair proteins and induce ROS accumulation leading to DNA damage [214]. PS may promote DNA damage by generating ROS, oxidizing DNA bases, crosslinking DNA strands or inducing sister chromatid exchanges [215]. $^1O_2$ is thought to be not the main inducer of DNA damage due to its short lifespan and limited range unless it is generated close to DNA strands [215]. Flow cytometric analyses of DNA content relies on the differences in DNA amount cells have through cell division stages $G_0/_1$ (pre-replicative cells), S (dividing cells) and $G_2$/M (post replicative plus mitotic cells). Previously Pcs are shown to induce cell cycle arrest on $G_1/G_0$ [216], [217], S [218] and $G_2$/M [219], [220] phases on different cell lines. Similarly, HDACis are reported to induce cell cycle arrest on $G_0/G_1$ [221] - [223] and G2/M [224], [225] phases. When considering studies mentioned above were conducted with different PS as well as different HDACis, their differential effects would be attributed to their unique mechanism of actions. Testing the same compound in different cell lines would even result in different outcomes as cell cycle checkpoint proteins are commonly dysregulated in cancer [226]. In our study, Pc1 led to $G_2$/M phase arrest in all cell lines, including healthy control cells. On the other hand, comparisons between ZnPc-HDACis indicated that both compounds do not induce cell cycle arrest on HUVECs while their differential effects on cancer cells were noteworthy: Pc3 promoted $G_2$/M phase arrest in both cancer cell lines while Pc2, too, led to $G_2$/M accumulation in MCF-7 cells but not in MDA-MB-231 cells which ended up with $G_0/G_1$ phase arrest. This finding reveals that direct nuclear damage caused by the PS may induce $G_2$/M phase arrest as both Pc3 and Pc1 are shown to localize nucleus, and PS targeting non-nuclear cellular compartments may tend to lead $G_1/G_0$ or S phase arrests. In compliance with this phenomenon, localizing to cytoplasm and mitochondria, treatments with Pc4 and

Pc5 induced accumulation in S and $G_0/G_1$ phases in MCF-7 and MDA-MB-231 cells, respectively. Data abovementioned also suggests the promotion of the $G_2/M$ phase arrest after Pc1 treatment in HUVECs is not observed upon Pc3 treatment. This observation underlines a possibility for compounds that target the same cell compartments, compound's $^1O_2$ generation capacity may determine cytotoxicity exerted upon healthy cells. According to our observations, the position of the 3-HPT moieties (non-peripheral vs. peripheral) did not influence DNA content.

All Pc-HDACis decreased HDAC6 levels in cell lines tested, confirming the 3-HPT moieties' success on HDAC downregulation. As stated previously, 3-HPT is reported to be 9.8 folds more selective towards HDAC6 compared to HDAC8 [173]. Along with HDAC6, Pc1 decreased HDAC8 levels in all cell lines while Pc2 and Pc3 were only shown to downregulate it in MDA-MB-231 cells. Pc5 decreased HDAC8 levels in HUVECs and MDA-MB-231 cells, yet Pc4 remained ineffective. Low penetration of Pc2 due to steric effect was further confirmed with the higher efficacy of Pc4 on downregulating HDAC8 levels in MDA-MB-231 cells. Pc3 was reported to be more effective in terms of downregulating HDAC6 levels in HUVECs, and MDA-MB-231 cells compared to Pc5.

In contrast to other assays evaluating the combinatorial anti-cancer activity of compounds, protein levels of HDAC6 and HDAC8 are PDT-independent and only influenced by the intracellular availability of 3-HPT moieties. To exert its inhibitory effects, 3-HPT should interact with its respective targets. Thus, membrane or mitochondrial localization of Pc-HDACis may decrease their ability to inhibit HDACs. However, our HDAC evaluation strategy is limited to the semi-quantitative analysis of the protein levels and does not measure proteins' enzymatic activity. All compounds may still have disruptive effects on HDAC8 and HDAC6 proteins' deacetylating properties while preserving the proteins' integrity, which is not evaluated as a part of this study.

Leading cause of the cancer related deaths is the migration of tumour cells to form secondary lesions in distant organs. Recent studies indicate that chemokine receptor family belonging to G protein-coupled receptors play important roles in this process [169]. While preliminary studies suggested CXCR4 and CCR7 expression facilitates migration of tumour cells towards the chemokine gradient, today it is known that both chemokine receptors also plays role in cellular growth, endothelial adhesion and extravagation [227]. Upon binding to its ligand CXCL12, CXCR4 induces various

signalling pathways that eventually induce gene expression, cellular motility, survival, and proliferation [228]. CXCR4 has been confirmed to form homo- or hetero- dimers [229] which activates JAK/STAT signalling pathway that promotes chemotactic responses [228]. Disruption of CXCL12/CXCR4 interaction significantly impairs breast cancer cells' migration towards regional lymph nodes and [168]. Along with CXCR4, CCR7 is also shown to be highly expressed in certain malignancies including breast cancer [168]. Aberrant CCR7 expression in cancer was first reported in T cell leukaemia patients as CCR7 expression levels of T cell leukaemia cells from adult patients with lymphoid organ infiltration were reported to be higher than normal T cells or leukaemia cells from patients without lymphoid organ involvement [230]. Additionally, CCR7 expression is regulated by lipid derivatives such as cyclooxygenase-2, an enzyme that is expressed in response to certain stimuli including cytokines and tumour enhancers [231] and converts phospholipid-derived arachidonic acid to prostaglandins that also upregulates CCR7 expression in breast cancer cells, thus increase their lymphatic invasion [232]. Both CXCR4 and CCR7 receptors are shown to be associated with higher grades and weak prognosis in breast cancer patients [233]. Holland et al. suggested that CXCR4 and CCR7 levels are directly correlated with invasive and metastatic phenotype in breast cancer, indicating the potential role of these proteins in tumour progression [234]. Kochetkova et al. revealed that functional activation of CXCR4 and CCR7 has a direct impact on cell death pathways, and inhibition of these molecules can promote detachment-induced cell death (anoikis) [169]. CD44, a large protein family that regulates cell-ECM interactions can contribute to cancer progression including cell growth, angiogenesis, cell migration and invasion [235], in addition, it also modulates CXCR4-CXCL12 signalling [164].

In our study, all Pc-HDACis are shown to downregulate either CD44 or CCR7 protein levels, or both, suggesting that PDT along with HDAC inhibition may have an inhibitory effect on migration. While the effect of PDT on tumour cells' CCR7 expression is not evaluated previously, the response of immune cells to PDT in cancer, especially dendritic cells is well studied [236], [237], suggesting PDT promotes normal function of dendritic cells to possess anti-cancer functions compared to their untreated, tumour-educated, immunosuppressive counterparts, further underlining the importance of the presence of immune system while evaluating the efficacy of PDT in cancer treatment.

HDACis are already known to decrease CD44 levels in different cancer cells [238], [239]. Interestingly PDT alone also shown to decrease CD44 [240] though the vast majority of the studies focus on CD44 as a target molecule, rather than evaluating the sole effect of PDT on CD44 [241] - [244]. On the other hand, it should be noted that CD44 mediated signalling pathways are especially hard to simulate *in vitro* since cells tend to express higher levels of CD44 due to culture conditions and CD44 mediated signalling relies on cell-ECM interactions, which is not present in conventional monolayer cell culture. Yet, the alterations in CD44 levels compared to their control counterparts would provide insight regarding Pc-HDACis' effect on CD44 expression [235].

However, treatment-induced alterations in CXCR4 protein levels were not in line between compounds as both Pc1 and Pc3 increased CXCR4 levels in all cell lines, especially in MCF-7. In a similar manner, Pc4 and Pc5 also induced CXCR4 protein expression in HUVECs and MCF-7 cells, but not MDA-MB-231 cells. On the other hand, Pc2 remained ineffective in terms of CXCR4 expression. Effects of various HDACis on CXCR4 levels in different cancers were previously investigated by many groups, and results were conflicting as butyrate and Vorinostat decreased CXCR4 levels in acute lymphoblastic leukaemia (ALL) and chronic lymphocytic leukaemia (CLL) cells [245,246] whereas VPA increased CXCR4 expression and chemotaxis in immature CD34-positive AML (acute myelogenous leukaemia) cells while decreasing in CD34-negative AML cells [247]. In melanoma cells, TSA increased CXCR4 levels after 24 hours-treatment and downregulated after 48 hours [248]. Ierano et al. hypothesized that HDACi treatment would result in decreased migration capacity due to HDACs role in cellular motility, and revealed that treatment of different cell lines (including breast, colon, lung and renal cancer) with various HDACis lead to CXCR4 mRNA expression along with disrupting CXCL12-mediated signalling cascades to prevent metastasis [249]. According to this study, increased CXCR4 levels upon Pc-HDACi treatment is an expected outcome and should be evaluated together with the other components of CXCL12 signalling pathway.

It should be taken into account that this study design involves a 24 hours incubation of cells with respective compounds (for allowing all cells in the population to enter division when considering HUVECs, MCF-7 cells and MDA-MB-231 cells' doubling times are 27, 24 and 25.1 hours [250] - [252], respectively) followed by irradiation and further 24 hours incubation to enable programmed cell death pathways'

activation. Longer or shorter incubation periods under dark conditions as well as after irradiation may result in different outcomes. Similarly, irradiation with higher or lower optical doses may also show different effects. Another point is the HDACi used in this study, 3-HPT, is a relatively new compound, and its mechanism of action in cancer is not as well documented as other HDACis under preclinical trials, or in clinical use. More comprehensive studies for discovering anti-cancer efficacy of 3-HPT on cancer cells are required for this compound to be used as in further studies.

## 5.1. Challenges and Future Aspects

As mentioned above, PDT has three components: the PS, light, and oxygen [3], which the latter may decrease below critical levels in solid tumours [253]. While normal tissue partial $O_2$ ($pO_2$) levels differ between 40–60 mm Hg, this level can drop less than 10 mm Hg in the hypoxic zone of solid tumours [254]. Adaptation of tumour cells to the hypoxic conditions are mainly driven by HIF-1α [253], which modulates tumour microenvironment to promote dysfunctional neovascularization, cell mobility, metastasis and invasion in addition to facilitating immune escape [254]. Similarly to radiotherapy, the efficacy of the PDT is directly associated with tissue oxygenation as without oxygen PDT remains ineffective [255], [256]. Different approaches including increasing tumour $pO_2$ and modifying tumour microenvironment are being employed to overcome this drawback. In terms of increasing tumour oxygenation, one example is the administration of nanoparticles containing perfluorocarbons (PFCs), organofluorine compounds that are used as oxygen carriers [257] - [259]. Incorporation of tumour-specific molecules to the nanoparticles can further increase the drug efficacy [260], [261]. Nanoparticles combining PS molecules with components that react with hydrogen peroxide ($H_2O_2$), a common by-product present in the tumour microenvironment due to the high metabolic rate of the malignant cells, to generate $O_2$ is another approach to increase the efficacy of PDT under hypoxia [262], [263] which also can be combined with chemotherapy [264].

The major drawback of our study is to conduct all experiments under standard cell culture environment with traditional 2-dimensional (monolayer) cell culture method. While monolayer cell culture is still commonly used during preclinical stages of drug development, it suffers from the insufficient representation of the cell-cell and

cell-ECM interactions and nutrient and oxygen gradient naturally present in the tumour mass [265]. Cell-cell and cell-ECM interactions play an active role in cell growth, differentiation, gene and protein expressions, and cell death, in addition, they determine cellular responses to various drugs [266]. Monolayer cancer cell cultures also lack a hypoxic core, which is observed in up to 60% of solid tumours [267]. When considering more than half of all drugs fail during clinical phases due to low efficacy or safety issues [268], the requirement of advanced cell culture methods that represent tumour microenvironment during preclinical drug testing is clear. Three-dimensional (3D) cell culture which involves the development of multicellular structures that forms cell-cell and cell-ECM interactions similar to the tumour mass is an alternative to monolayer culture. This approach also allows researchers to combine different cell types, e.g. stromal and epithelial in the same spheroid structure to simulate heterogenous tumour [269] and stands out as a promising technique between monolayer culture and animal models [266]. As stated, tissue oxygenation is one of the key elements for the success of PDT, and testing PDT agents in monolayer cell culture may lead to overestimating the effect of the drug. Another point is the limited drug availability in 3D cultures, unlike monolayer cultures where cells have equal access to the drug that may decrease outcomes' precision.

Cell-ECM interactions, too, play role in drug resistance. Bulysheva et al. revealed that cells grown on 3D scaffolds are more resistant to paclitaxel treatment compared to monolayer counterparts as $IC_{90}$ values obtained from monolayer cultures are reported to have minimal effect on cells cultured on scaffolds [270]. These findings are likely to arise from activation of various signalling cascades including chromatin modifications which are also diminished in 2D cultures, and shown to be related to radiation resistance [271]. Higher levels of heterochromatin protect DNA against radiotherapy-induced double strand DNA breaks to a certain extent in cells cultured on scaffolds, and HDAC inhibition may alleviate this phenomenon. Altogether, these data suggest that evaluating anti-cancer efficacy of Pc-HDACi derivatives on 3D culture systems may provide more accurate data compared to monolayer culture, both in terms of photodynamic activity and HDAC inhibition. However, it should be noted that there is no consensus on 3D culture protocols while even some systems may not fulfil the requirements of drug screening, especially when considering, unlike chemotherapeutics, PDT consists of two stages, drug incubation and irradiation. Examples include low media volume and difficulties of media exchange in hanging

drop method, or high lot-to-lot variances in hydrogel-based 3D cultures [272]. On the other hand, low attachment plates, bioreactors or 3D-printed scaffolds are relatively expensive approaches. Thus, the proper 3D culture method should be carefully chosen according to the needs of the study, and it should be kept in mind that a wrong model may lead to inaccurate results.

Another key point that would affect the clinical outcome is the penetration of the light to the tissue, which depends on the wavelength and intensity of the light as well as the optical features of the target [273]. Clinically approved PSs are mostly porphyrin derivatives and are excited outside the optical therapeutic window (700–1000 nm). On the other hand, near infrared (NIR) light has better tissue penetration in addition to its minimal absorbance by biological components. Thus, the introduction of PSs that absorb light in the 650–750 nm region to the clinical practice may be more effective in the treatment of non-superficial tumours. Besides, absorption in higher wavelengths also enables the utilization of two-photon excitation (TPE), which is generally provided by pulsed lasers, relies on the absorption of two photons simultaneously instead of one to reach an excited state. TPE also excites the PS located in a restricted area (1 $mm^3$) compared to conventional light sources, hence may increase the precision of the irradiation process and prevent the healthy tissue. Yet, this technique is relatively slow as scanning the malignant lesion would be time consuming [274]. This limitation may be overcome by Temporal Focusing, enabling illumination of several points at a time.

## 5.2. Conclusions

- Due to its several advantages over conventional therapeutic options, PDT is regarded as a favourable treatment alternative for cancer. In this study, we explored biological effects of a novel 3- hydroxypyridin-2-thione substituted Si, Zn and In Pc derivatives that combines chemotherapeutic benefit of HDAC6 and HDAC8 downregulation with PDT.
- Our results indicate that Pc-HDACi derivatives deserve further attention for developing successful PS drug candidates.
- Our findings also underline the importance of the Pc derivatives' core metal on the activity of the molecule, not only for the photodynamic action, but also for

cellular localization and chemotherapeutic action. Hence, different Pc derivatives may be combined with various HDACis according to the target cancer types.

- In our study, Pc1 is reported to be the most promising Pc-HDACi, due to it's high singlet oxygen yield, ability to induce multiple programmed cell death pathways simultaneously, and HDAC inhibiting action.
- In comparison with MCF-7 cells and HUVECs, TNBC cell line MDA-MB-231 gave the most prominent response to Pc1 treatment as when treated with their respective $IC_{50}$ values, lowest viable cell rate among highest late apoptotic cell population and highest DHR123 fluorescence intensity was observed in this cell line.
- Comparisons between ZnPc-HDACis revealed that non-peripheral positioning of HDACi moieties in Pc2 resulted in a steric effect; thus, higher $IC_{50}$ values, weak penetration into the cell, lower mitROS accumulation, and in turn, relatively lower anti-cancer activity compared to peripheral Pc3 was reported.
- A steric effect was not observed in Pc4 and Pc5. Both compounds showed a distinct localization pattern that also targets the mitochondrial network, induced mitROS accumulation effectively and led to cell cycle arrest in different phases during cell cycle compared to other Pc-HDACis.
- The slightly lower response rate of MCF-7 cells to treatment suggests that PS-chemotherapeutics combinatorial treatments may have to offer higher photoactivity if the target protein of the chemotherapeutic moiety regulates pathways directly contribute to respective cancer types' progression.
- Another interesting result is the preservation of DNA content upon ZnPc- and InPc-HDACis treatments in healthy cells, HUVECs as no cell cycle arrest was observed in this cell line, which possibly indicates that healthy cells can cope with $^1O_2$-induced DNA damage to a greater extent in comparison with cancer cells.
- More research is required to develop new PDT agents targeting tumour cells to increase treatment efficiency. For this purpose, differences between various Pc derivatives' cellular impacts including their target programmed cell death pathways and localizations should be well documented in order to determine right PS for the photodynamic action according to the respective cancer type. Different positions for introduced HDACis (peripheral vs. non-peripheral and/or asymmetrical vs. symmetrical) may be evaluated in order to achieve optimum cellular penetration.

- Different HDACis may be considered according to the targeted cancers' transcription profiles. Due to the PSs' oxygen dependency, *in vivo* models that can accurately reflect the outcomes of the treatment in humans to be employed for a complete evaluation of PDT drug candidates is crucial.
- Such evaluations would also provide insight to the compounds' effects on different cell types of the tumour, immune system, tumour vasculature, and many other components play role in cancer progression, and cannot be represented *in vitro*. Finally, switchable/changeable light sources may be developed to achieve a more precise irradiation pattern that would exert minimum harm to neighbouring healthy tissues for a more effective PDT.

# REFERENCES


[1] Kübler A. C., (2005), “Photodynamic therapy”, Medical Laser Application, 20 (1), 37-45.

[2] Mitra A., Stables G. I., (2006), “Topical photodynamic therapy for non-cancerous skin conditions”, Photodiagnosis and photodynamic therapy, 3 (2), 116-127.

[3] Agostinis P., Berg K., Cengel K. A., Foster T. H., Girotti A. W., Gollnick S. O., Hahn S. M., Hamblin M. R., Juzeniene A., Kessel D., Korbelik M., Moan J., Mroz P., Nowis D., Piette J., Wilson B. C., Golab J., (2011), “Photodynamic therapy of cancer: an update”, CA: a cancer journal for clinicians, 61 (4), 250-281.

[4] Schuitmaker J. J., Baas P., van Leengoed H. L., van der Meulen F. W., Star W. M., van Zandwijk N., (1996), “Photodynamic therapy: a promising new modality for the treatment of cancer”, Journal of Photochemistry and Photobiology B: Biology, 34 (1), 3-12.

[5] Castano A. P., Demidova T. N., Hamblin M. R., (2005), “Mechanisms in photodynamic therapy: part two-cellular signaling, cell metabolism and modes of cell death”, Photodiagnosis and photodynamic therapy, 2 (1), 1-23.

[6] Brown S. B., Brown E. A., Walker I., (2004), “The present and future role of photodynamic therapy in cancer treatment”, The Lancet Oncology, 5 (8), 497-508.

[7] De Rosa F. S., Bentley M. V., (2000), “Photodynamic therapy of skin cancers: sensitizers, clinical studies and future directives”, Pharmaceutical research, 17 (12), 1447-1455.

[8] Alexiades-Armenakas M., (2006), “Laser-mediated photodynamic therapy”, Clinics in dermatology, 24 (1), 16-25.

[9] Dougherty T. J., Gomer C. J., Henderson B. W., Jori G., Kessel D., Korbelik M., Moan J., Peng Q., (1998), “Photodynamic therapy”, Journal of the National Cancer Institute, 90 (12), 889-905.

[10] Niedre M., Patterson M. S., Wilson B. C., (2002), “Direct near-infrared luminescence detection of singlet oxygen generated by photodynamic therapy in cells in vitro and tissues in vivo”, Photochemistry and photobiology, 75 (4), 382-391.

[11] Henderson B. W., Dougherty T. J., (1992), “How does photodynamic therapy work?”, Photochemistry and photobiology, 55 (1), 145-157.

[12] Dolmans D. E., Fukumura D., Jain R. K., (2003), “Photodynamic therapy for cancer”, Nature reviews. Cancer, 3 (5), 380-387.

[13] Zhorina L. V., Elena B. C., Agronskaya A. V., Maria G. G., (1994), "Phthalocyanines as second generation photosensitizers for the photodynamic therapy of cancer: fluorescence and absorption spectroscopy", Proceedings of SPIE, 2100.

[14] Zhang Y., Lovell J. F., (2017), "Recent applications of phthalocyanines and naphthalocyanines for imaging and therapy", Wiley Interdisciplinary Reviews - Nanomedicine and Nanobiotechnology, 9 (1).

[15] Juzeniene A., Moan J., (2007), "The history of PDT in Norway Part one: Identification of basic mechanisms of general PDT", Photodiagnosis and photodynamic therapy, 4 (1), 3-11.

[16] Mashayekhi V., Op 't Hoog C., Oliveira S., (2019), "Vascular targeted photodynamic therapy: A review of the efforts towards molecular targeting of tumor vasculature", Journal of Porphyrins and Phthalocyanines, 23 (11n12), 1229-1240.

[17] MacCormack M. A., (2008), "Photodynamic therapy in dermatology: an update on applications and outcomes", Seminars in cutaneous medicine and surgery, 27 (1), 52-62.

[18] Hamblin M. R., Newman E. L., (1994), "On the mechanism of the tumour-localising effect in photodynamic therapy", Journal of Photochemistry and Photobiology B: Biology, 23 (1), 3-8.

[19] Iyer A. K., Greish K., Seki T., Okazaki S., Fang J., Takeshita K., Maeda H., (2007), "Polymeric micelles of zinc protoporphyrin for tumor targeted delivery based on EPR effect and singlet oxygen generation", Journal of drug targeting, 15 (7-8), 496-506.

[20] Sibani S. A., McCarron P. A., Woolfson A. D., Donnelly R. F., (2008), "Photosensitiser delivery for photodynamic therapy. Part 2: systemic carrier platforms", Expert opinion on drug delivery, 5 (11), 1241-1254.

[21] Alpugan S., Topkaya D., Atilla D., Ahsen V., Niazi J. H., Dumoulin F., (2017), "Zn phthalocyanine conjugation to H2-ul aptamer for HER2-targeted breast cancer photodynamic therapy: Design, optimization and properties", Journal of Porphyrins and Phthalocyanines, 21 (12), 887-892.

[22] Lazaro-Carrillo A., Simões B., Clarke R., Villanueva A., PO-010 Dual chemotherapy and photodynamic therapy: a synergistic strategy to improve cancer treatment. 2018, BMJ Publishing Group Limited.

[23] Peng C. L., Lai P. S., Lin F. H., Yueh-Hsiu Wu S., Shieh M. J., (2009), "Dual chemotherapy and photodynamic therapy in an HT-29 human colon cancer xenograft model using SN-38-loaded chlorin-core star block copolymer micelles", Biomaterials, 30 (21), 3614-3625.

[24] Peterson C. M., Lu J. M., Sun Y., Peterson C. A., Shiah J. G., Straight R. C., Kopecek J., (1996), "Combination chemotherapy and photodynamic therapy with N-(2-hydroxypropyl) methacrylamide copolymer-bound anticancer drugs

inhibit human ovarian carcinoma heterotransplanted in nude mice", Cancer research, 56 (17), 3980-3985.

[25] Mfouo-Tynga I., Houreld N. N., Abrahamse H., (2014), "Induced cell death pathway post photodynamic therapy using a metallophthalocyanine photosensitizer in breast cancer cells", Photomedicine and laser surgery, 32 (4), 205-211.

[26] Manisova B., Binder S., Malina L., Jiravova J., Langova K., Kolarova H., (2015), "Phthalocyanine-mediated Photodynamic Treatment of Tumoural and Non-tumoural cell lines", Anticancer research, 35 (7), 3943-3951.

[27] Giorgi C., Bonora M., Missiroli S., Poletti F., Ramirez F. G., Morciano G., Morganti C., Pandolfi P. P., Mammano F., Pinton P., (2015), "Intravital imaging reveals p53-dependent cancer cell death induced by phototherapy via calcium signaling", Oncotarget, 6 (3), 1435-1445.

[28] Agarwal M. L., Larkin H. E., Zaidi S. I., Mukhtar H., Oleinick N. L., (1993), "Phospholipase activation triggers apoptosis in photosensitized mouse lymphoma cells", Cancer research, 53 (24), 5897-5902.

[29] Separovic D., He J., Oleinick N. L., (1997), "Ceramide generation in response to photodynamic treatment of L5178Y mouse lymphoma cells", Cancer research, 57 (9), 1717-1721.

[30] Cho Y., McQuade T., Zhang H., Zhang J., Chan F. K., (2011), "RIP1-dependent and independent effects of necrostatin-1 in necrosis and T cell activation", PloS one, 6 (8), e23209.

[31] Coupienne I., Fettweis G., Piette J., (2011), "RIP3 expression induces a death profile change in U2OS osteosarcoma cells after 5-ALA-PDT", Lasers in surgery and medicine, 43 (7), 557-564.

[32] Hotchkiss R. S., Strasser A., McDunn J. E., Swanson P. E., (2009), "Cell death", The New England journal of medicine, 361 (16), 1570-1583.

[33] Wyllie A. H., (2010), ""Where, O death, is thy sting?" A brief review of apoptosis biology", Molecular neurobiology, 42 (1), 4-9.

[34] Vicencio J. M., Galluzzi L., Tajeddine N., Ortiz C., Criollo A., Tasdemir E., Morselli E., Ben Younes A., Maiuri M. C., Lavandero S., Kroemer G., (2008), "Senescence, apoptosis or autophagy? When a damaged cell must decide its path--a mini-review", Gerontology, 54 (2), 92-99.

[35] Libera L. D., Vescovo G., (2004), "Muscle wastage in chronic heart failure, between apoptosis, catabolism and altered anabolism: a chimaeric view of inflammation?", Current Opinion in Clinical Nutrition & Metabolic Care, 7 (4), 435-441.

[36] Zheng M., Zhu W., Han Q., Xiao R. P., (2005), "Emerging concepts and therapeutic implications of beta-adrenergic receptor subtype signaling", Pharmacology & therapeutics, 108 (3), 257-268.

[37] Dalla Libera L., Vescovo G., Volterrani M., (2008), “Physiological basis for contractile dysfunction in heart failure”, Current pharmaceutical design, 14 (25), 2572-2581.

[38] Sprick M. R., Walczak H., (2004), “The interplay between the Bcl-2 family and death receptor-mediated apoptosis”, Biochimica et biophysica acta, 1644 (2-3), 125-132.

[39] Whelan R. S., Kaplinskiy V., Kitsis R. N., (2010), “Cell death in the pathogenesis of heart disease: mechanisms and significance”, Annual review of physiology, 72, 19-44.

[40] Duprez L., Wirawan E., Vanden Berghe T., Vandenabeele P., (2009), “Major cell death pathways at a glance”, Microbes and infection, 11 (13), 1050-1062.

[41] Karp G., Cell and Molecular Biology: Concepts and Experiments. 5th ed. 2007: John Wiley & Sons Canada, Limited.

[42] Szegezdi E., Fitzgerald U., Samali A., (2003), “Caspase-12 and ER-stress-mediated apoptosis: the story so far”, Annals of the New York Academy of Sciences, 1010, 186-194.

[43] Lalier L., Cartron P. F., Juin P., Nedelkina S., Manon S., Bechinger B., Vallette F. M., (2007), “Bax activation and mitochondrial insertion during apoptosis”, Apoptosis : an international journal on programmed cell death, 12 (5), 887-896.

[44] Chipuk J. E., Green D. R., (2008), “How do BCL-2 proteins induce mitochondrial outer membrane permeabilization?”, Trends in cell biology, 18 (4), 157-164.

[45] Khoury C. M., Greenwood M. T., (2008), “The pleiotropic effects of heterologous Bax expression in yeast”, Biochimica et biophysica acta, 1783 (7), 1449-1465.

[46] Majno G., Joris I., (1995), “Apoptosis, oncosis, and necrosis. An overview of cell death”, The American journal of pathology, 146 (1), 3-15.

[47] Kroemer G., Galluzzi L., Vandenabeele P., Abrams J., Alnemri E. S., Baehrecke E. H., Blagosklonny M. V., El-Deiry W. S., Golstein P., Green D. R., Hengartner M., Knight R. A., Kumar S., Lipton S. A., Malorni W., Nuñez G., Peter M. E., Tschopp J., Yuan J., Piacentini M., Zhivotovsky B., Melino G., (2009), “Classification of cell death: recommendations of the Nomenclature Committee on Cell Death 2009”, Cell death and differentiation, 16 (1), 3-11.

[48] Christofferson D. E., Yuan J., (2010), “Necroptosis as an alternative form of programmed cell death”, Current opinion in cell biology, 22 (2), 263-268.

[49] Degterev A., Yuan J., (2008), “Expansion and evolution of cell death programmes”, Nature reviews. Molecular cell biology, 9 (5), 378-390.

[50] Henriquez M., Armisén R., Stutzin A., Quest A. F., (2008), “Cell death by necrosis, a regulated way to go”, Current molecular medicine, 8 (3), 187-206.

[51] Nikoletopoulou V., Markaki M., Palikaras K., Tavernarakis N., (2013), “Crosstalk between apoptosis, necrosis and autophagy”, Biochimica et biophysica acta, 1833 (12), 3448-3459.

[52] Dhuriya Y. K., Sharma D., (2018), “Necroptosis: a regulated inflammatory mode of cell death”, Journal of neuroinflammation, 15 (1), 199.

[53] Marshall K. D., Baines C. P., (2014), “Necroptosis: is there a role for mitochondria?”, Frontiers in physiology, 5, 323.

[54] Fan H., Tang H. B., Kang J., Shan L., Song H., Zhu K., Wang J., Ju G., Wang Y. Z., (2015), “Involvement of endoplasmic reticulum stress in the necroptosis of microglia/macrophages after spinal cord injury”, Neuroscience, 311, 362-373.

[55] Holler N., Zaru R., Micheau O., Thome M., Attinger A., Valitutti S., Bodmer J. L., Schneider P., Seed B., Tschopp J., (2000), “Fas triggers an alternative, caspase-8-independent cell death pathway using the kinase RIP as effector molecule”, Nature immunology, 1 (6), 489-495.

[56] Kim S. O., Ono K., Han J., (2001), “Apoptosis by pan-caspase inhibitors in lipopolysaccharide-activated macrophages”, American journal of physiology. Lung cellular and molecular physiology, 281 (5), L1095-1105.

[57] Wang H., Sun L., Su L., Rizo J., Liu L., Wang L. F., Wang F. S., Wang X., (2014), “Mixed lineage kinase domain-like protein MLKL causes necrotic membrane disruption upon phosphorylation by RIP3”, Molecular cell, 54 (1), 133-146.

[58] Wegner K. W., Saleh D., Degterev A., (2017), “Complex Pathologic Roles of RIPK1 and RIPK3: Moving Beyond Necroptosis”, Trends in pharmacological sciences, 38 (3), 202-225.

[59] Kadigamuwa C., Choksi S., Xu Q., Cataisson C., Greenbaum S. S., Yuspa S. H., Liu Z. G., (2019), “Role of Retinoic Acid Receptor-γ in DNA Damage-Induced Necroptosis”, iScience, 17, 74-86.

[60] Mizushima N., Komatsu M., (2011), “Autophagy: renovation of cells and tissues”, Cell, 147 (4), 728-741.

[61] Li W. W., Li J., Bao J. K., (2012), “Microautophagy: lesser-known self-eating”, Cellular and molecular life sciences : CMLS, 69 (7), 1125-1136.

[62] Cuervo A. M., Wong E., (2014), “Chaperone-mediated autophagy: roles in disease and aging”, Cell research, 24 (1), 92-104.

[63] Lamb C. A., Yoshimori T., Tooze S. A., (2013), “The autophagosome: origins unknown, biogenesis complex”, Nature reviews. Molecular cell biology, 14 (12), 759-774.

[64] Huang R., Xu Y., Wan W., Shou X., Qian J., You Z., Liu B., Chang C., Zhou T., Lippincott-Schwartz J., Liu W., (2015), “Deacetylation of nuclear LC3 drives autophagy initiation under starvation”, Molecular cell, 57 (3), 456-466.

[65] Liang X. H., Jackson S., Seaman M., Brown K., Kempkes B., Hibshoosh H., Levine B., (1999), "Induction of autophagy and inhibition of tumorigenesis by beclin 1", Nature, 402 (6762), 672-676.

[66] Michaud M., Martins I., Sukkurwala A. Q., Adjemian S., Ma Y., Pellegatti P., Shen S., Kepp O., Scoazec M., Mignot G., Rello-Varona S., Tailler M., Menger L., Vacchelli E., Galluzzi L., Ghiringhelli F., di Virgilio F., Zitvogel L., Kroemer G., (2011), "Autophagy-dependent anticancer immune responses induced by chemotherapeutic agents in mice", Science (New York, N.Y.), 334 (6062), 1573-1577.

[67] Kimmelman A. C., White E., (2017), "Autophagy and Tumor Metabolism", Cell metabolism, 25 (5), 1037-1043.

[68] Apel A., Herr I., Schwarz H., Rodemann H. P., Mayer A., (2008), "Blocked autophagy sensitizes resistant carcinoma cells to radiation therapy", Cancer research, 68 (5), 1485-1494.

[69] Zou Z., Yuan Z., Zhang Q., Long Z., Chen J., Tang Z., Zhu Y., Chen S., Xu J., Yan M., Wang J., Liu Q., (2012), "Aurora kinase A inhibition-induced autophagy triggers drug resistance in breast cancer cells", Autophagy, 8 (12), 1798-1810.

[70] Hu Y. L., Jahangiri A., Delay M., Aghi M. K., (2012), "Tumor cell autophagy as an adaptive response mediating resistance to treatments such as antiangiogenic therapy", Cancer research, 72 (17), 4294-4299.

[71] Mariño-Ramírez L., Kann M. G., Shoemaker B. A., Landsman D., (2005), "Histone structure and nucleosome stability", Expert review of proteomics, 2 (5), 719-729.

[72] Barnes C. E., English D. M., Cowley S. M., (2019), "Acetylation & Co: an expanding repertoire of histone acylations regulates chromatin and transcription", Essays in biochemistry, 63 (1), 97-107.

[73] Eberharter A., Becker P. B., (2002), "Histone acetylation: a switch between repressive and permissive chromatin. Second in review series on chromatin dynamics", EMBO reports, 3 (3), 224-229.

[74] Luger K., Dechassa M. L., Tremethick D. J., (2012), "New insights into nucleosome and chromatin structure: an ordered state or a disordered affair?", Nature reviews. Molecular cell biology, 13 (7), 436-447.

[75] Tremethick D. J., (2007), "Higher-order structures of chromatin: the elusive 30 nm fiber", Cell, 128 (4), 651-654.

[76] Ropero S., Esteller M., (2007), "The role of histone deacetylases (HDACs) in human cancer", Molecular oncology, 1 (1), 19-25.

[77] Allfrey V. G., Faulkner R., Mirsky A. E., (1964), "Acetylation and Methylation of Histones and Their Possible Role in the Regulation of Rna Synthesis",

Proceedings of the National Academy of Sciences of the United States of America, 51 (5), 786-794.

[78] Inoue A., Fujimoto D., (1969), "Enzymatic deacetylation of histone", Biochemical and biophysical research communications, 36 (1), 146-150.

[79] Dutta A., Abmayr S. M., Workman J. L., (2016), "Diverse Activities of Histone Acylations Connect Metabolism to Chromatin Function", Molecular cell, 63 (4), 547-552.

[80] Brownell J. E., Zhou J., Ranalli T., Kobayashi R., Edmondson D. G., Roth S. Y., Allis C. D., (1996), "Tetrahymena histone acetyltransferase A: a homolog to yeast Gcn5p linking histone acetylation to gene activation", Cell, 84 (6), 843-851.

[81] Taunton J., Hassig C. A., Schreiber S. L., (1996), "A mammalian histone deacetylase related to the yeast transcriptional regulator Rpd3p", Science (New York, N.Y.), 272 (5260), 408-411.

[82] Seto E., Yoshida M., (2014), "Erasers of histone acetylation: the histone deacetylase enzymes", Cold Spring Harbor perspectives in biology, 6 (4), a018713.

[83] Lin H. Y., Chen C. S., Lin S. P., Weng J. R., Chen C. S., (2006), "Targeting histone deacetylase in cancer therapy", Medicinal research reviews, 26 (4), 397-413.

[84] Yang W. M., Inouye C., Zeng Y., Bearss D., Seto E., (1996), "Transcriptional repression by YY1 is mediated by interaction with a mammalian homolog of the yeast global regulator RPD3", Proceedings of the National Academy of Sciences of the United States of America, 93 (23), 12845-12850.

[85] Yang W. M., Yao Y. L., Sun J. M., Davie J. R., Seto E., (1997), "Isolation and characterization of cDNAs corresponding to an additional member of the human histone deacetylase gene family", The Journal of biological chemistry, 272 (44), 28001-28007.

[86] Hu E., Chen Z., Fredrickson T., Zhu Y., Kirkpatrick R., Zhang G. F., Johanson K., Sung C. M., Liu R., Winkler J., (2000), "Cloning and characterization of a novel human class I histone deacetylase that functions as a transcription repressor", The Journal of biological chemistry, 275 (20), 15254-15264.

[87] Grozinger C. M., Hassig C. A., Schreiber S. L., (1999), "Three proteins define a class of human histone deacetylases related to yeast Hda1p", Proceedings of the National Academy of Sciences of the United States of America, 96 (9), 4868-4873.

[88] Kao H. Y., Downes M., Ordentlich P., Evans R. M., (2000), "Isolation of a novel histone deacetylase reveals that class I and class II deacetylases promote SMRT-mediated repression", Genes & development, 14 (1), 55-66.

[89] Zhou X., Marks P. A., Rifkind R. A., Richon V. M., (2001), "Cloning and characterization of a histone deacetylase, HDAC9", Proceedings of the National Academy of Sciences of the United States of America, 98 (19), 10572-10577.

[90] Kao H. Y., Lee C. H., Komarov A., Han C. C., Evans R. M., (2002), "Isolation and characterization of mammalian HDAC10, a novel histone deacetylase", The Journal of biological chemistry, 277 (1), 187-193.

[91] Frye R. A., (1999), "Characterization of five human cDNAs with homology to the yeast SIR2 gene: Sir2-like proteins (sirtuins) metabolize NAD and may have protein ADP-ribosyltransferase activity", Biochemical and biophysical research communications, 260 (1), 273-279.

[92] Du J., Zhou Y., Su X., Yu J. J., Khan S., Jiang H., Kim J., Woo J., Kim J. H., Choi B. H., He B., Chen W., Zhang S., Cerione R. A., Auwerx J., Hao Q., Lin H., (2011), "Sirt5 is a NAD-dependent protein lysine demalonylase and desuccinylase", Science (New York, N.Y.), 334 (6057), 806-809.

[93] Gao L., Cueto M. A., Asselbergs F., Atadja P., (2002), "Cloning and functional characterization of HDAC11, a novel member of the human histone deacetylase family", The Journal of biological chemistry, 277 (28), 25748-25755.

[94] Bates S. E., (2020), "Epigenetic Therapies for Cancer", The New England journal of medicine, 383 (7), 650-663.

[95] Esteller M., (2002), "CpG island hypermethylation and tumor suppressor genes: a booming present, a brighter future", Oncogene, 21 (35), 5427-5440.

[96] Mariadason J. M., Corner G. A., Augenlicht L. H., (2000), "Genetic reprogramming in pathways of colonic cell maturation induced by short chain fatty acids: comparison with trichostatin A, sulindac, and curcumin and implications for chemoprevention of colon cancer", Cancer research, 60 (16), 4561-4572.

[97] Li G., Margueron R., Hu G., Stokes D., Wang Y. H., Reinberg D., (2010), "Highly compacted chromatin formed in vitro reflects the dynamics of transcription activation in vivo", Molecular cell, 38 (1), 41-53.

[98] Wang Z., Zang C., Cui K., Schones D. E., Barski A., Peng W., Zhao K., (2009), "Genome-wide mapping of HATs and HDACs reveals distinct functions in active and inactive genes", Cell, 138 (5), 1019-1031.

[99] Bradner J. E., West N., Grachan M. L., Greenberg E. F., Haggarty S. J., Warnow T., Mazitschek R., (2010), "Chemical phylogenetics of histone deacetylases", Nature chemical biology, 6 (3), 238-243.

[100] Eckschlager T., Plch J., Stiborova M., Hrabeta J., (2017), "Histone Deacetylase Inhibitors as Anticancer Drugs", International journal of molecular sciences, 18 (7).

[101] Dawson M. A., Kouzarides T., (2012), "Cancer epigenetics: from mechanism to therapy", Cell, 150 (1), 12-27.

[102] Kretsovali A., Hadjimichael C., Charmpilas N., (2012), "Histone deacetylase inhibitors in cell pluripotency, differentiation, and reprogramming", Stem cells international, 2012, 184154.

[103] Oh M., Choi I. K., Kwon H. J., (2008), "Inhibition of histone deacetylase1 induces autophagy", Biochemical and biophysical research communications, 369 (4), 1179-1183.

[104] Zhang J., Ng S., Wang J., Zhou J., Tan S. H., Yang N., Lin Q., Xia D., Shen H. M., (2015), "Histone deacetylase inhibitors induce autophagy through FOXO1-dependent pathways", Autophagy, 11 (4), 629-642.

[105] Liu Y. L., Yang P. M., Shun C. T., Wu M. S., Weng J. R., Chen C. C., (2010), "Autophagy potentiates the anti-cancer effects of the histone deacetylase inhibitors in hepatocellular carcinoma", Autophagy, 6 (8), 1057-1065.

[106] Hrzenjak A., Kremser M. L., Strohmeier B., Moinfar F., Zatloukal K., Denk H., (2008), "SAHA induces caspase-independent, autophagic cell death of endometrial stromal sarcoma cells by influencing the mTOR pathway", The Journal of pathology, 216 (4), 495-504.

[107] Chiao M. T., Cheng W. Y., Yang Y. C., Shen C. C., Ko J. L., (2013), "Suberoylanilide hydroxamic acid (SAHA) causes tumor growth slowdown and triggers autophagy in glioblastoma stem cells", Autophagy, 9 (10), 1509-1526.

[108] Fröhlich L. F., Mrakovcic M., Smole C., Zatloukal K., (2016), "Molecular mechanism leading to SAHA-induced autophagy in tumor cells: evidence for a p53-dependent pathway", Cancer cell international, 16 (1), 68.

[109] Yuan P. X., Huang L. D., Jiang Y. M., Gutkind J. S., Manji H. K., Chen G., (2001), "The mood stabilizer valproic acid activates mitogen-activated protein kinases and promotes neurite growth", The Journal of biological chemistry, 276 (34), 31674-31683.

[110] Cieslik K., Abrams C. S., Wu K. K., (2001), "Up-regulation of endothelial nitric-oxide synthase promoter by the phosphatidylinositol 3-kinase gamma /Janus kinase 2/MEK-1-dependent pathway", The Journal of biological chemistry, 276 (2), 1211-1219.

[111] Blaheta R. A., Cinatl J., Jr., (2002), "Anti-tumor mechanisms of valproate: a novel role for an old drug", Medicinal research reviews, 22 (5), 492-511.

[112] Logan C. Y., Nusse R., (2004), "The Wnt signaling pathway in development and disease", Annual review of cell and developmental biology, 20, 781-810.

[113] Brest P., Lassalle S., Hofman V., Bordone O., Gavric Tanga V., Bonnetaud C., Moreilhon C., Rios G., Santini J., Barbry P., Svanborg C., Mograbi B., Mari B., Hofman P., (2011), "MiR-129-5p is required for histone deacetylase inhibitor-induced cell death in thyroid cancer cells", Endocrine-related cancer, 18 (6), 711-719.

[114] Cho J. H., Dimri M., Dimri G. P., (2015), "MicroRNA-31 is a transcriptional target of histone deacetylase inhibitors and a regulator of cellular senescence", The Journal of biological chemistry, 290 (16), 10555-10567.

[115] Brockdorff N., (2013), "Noncoding RNA and Polycomb recruitment", RNA (New York, N.Y.), 19 (4), 429-442.

[116] Gibb E. A., Brown C. J., Lam W. L., (2011), "The functional role of long non-coding RNA in human carcinomas", Molecular cancer, 10, 38.

[117] Sabbatino F., Schwab J. H., Ferrone S., Ferrone C. R., (2013), "Evolution of studies of HLA class I antigen processing machinery (APM) components in malignant cells", Clinical transplants, 453-463.

[118] Kortenhorst M. S., Wissing M. D., Rodríguez R., Kachhap S. K., Jans J. J., Van der Groep P., Verheul H. M., Gupta A., Aiyetan P. O., van der Wall E., Carducci M. A., Van Diest P. J., Marchionni L., (2013), "Analysis of the genomic response of human prostate cancer cells to histone deacetylase inhibitors", Epigenetics, 8 (9), 907-920.

[119] Gameiro S. R., Malamas A. S., Tsang K. Y., Ferrone S., Hodge J. W., (2016), "Inhibitors of histone deacetylase 1 reverse the immune evasion phenotype to enhance T-cell mediated lysis of prostate and breast carcinoma cells", Oncotarget, 7 (7), 7390-7402.

[120] Woan K. V., Lienlaf M., Perez-Villaroel P., Lee C., Cheng F., Knox T., Woods D. M., Barrios K., Powers J., Sahakian E., Wang H. W., Canales J., Marante D., Smalley K. S. M., Bergman J., Seto E., Kozikowski A., Pinilla-Ibarz J., Sarnaik A., Celis E., Weber J., Sotomayor E. M., Villagra A., (2015), "Targeting histone deacetylase 6 mediates a dual anti-melanoma effect: Enhanced antitumor immunity and impaired cell proliferation", Molecular oncology, 9 (7), 1447-1457.

[121] Cheng F., Lienlaf M., Wang H. W., Perez-Villarroel P., Lee C., Woan K., Rock-Klotz J., Sahakian E., Woods D., Pinilla-Ibarz J., Kalin J., Tao J., Hancock W., Kozikowski A., Seto E., Villagra A., Sotomayor E. M., (2014), "A novel role for histone deacetylase 6 in the regulation of the tolerogenic STAT3/IL-10 pathway in APCs", Journal of immunology (Baltimore, Md. : 1950), 193 (6), 2850-2862.

[122] Kroesen M., Gielen P., Brok I. C., Armandari I., Hoogerbrugge P. M., Adema G. J., (2014), "HDAC inhibitors and immunotherapy; a double edged sword?", Oncotarget, 5 (16), 6558-6572.

[123] Montgomery R. L., Davis C. A., Potthoff M. J., Haberland M., Fielitz J., Qi X., Hill J. A., Richardson J. A., Olson E. N., (2007), "Histone deacetylases 1 and 2 redundantly regulate cardiac morphogenesis, growth, and contractility", Genes & development, 21 (14), 1790-1802.

[124] Montgomery R. L., Potthoff M. J., Haberland M., Qi X., Matsuzaki S., Humphries K. M., Richardson J. A., Bassel-Duby R., Olson E. N., (2008), "Maintenance of cardiac energy metabolism by histone deacetylase 3 in mice", The Journal of clinical investigation, 118 (11), 3588-3597.

[125] Deroanne C. F., Bonjean K., Servotte S., Devy L., Colige A., Clausse N., Blacher S., Verdin E., Foidart J. M., Nusgens B. V., Castronovo V., (2002), "Histone deacetylases inhibitors as anti-angiogenic agents altering vascular endothelial growth factor signaling", Oncogene, 21 (3), 427-436.

[126] Chelluri R., Caza T., Woodford M. R., Reeder J. E., Bratslavsky G., Byler T., (2016), "Valproic Acid Alters Angiogenic and Trophic Gene Expression in Human Prostate Cancer Models", Anticancer research, 36 (10), 5079-5086.

[127] Jeong J. W., Bae M. K., Ahn M. Y., Kim S. H., Sohn T. K., Bae M. H., Yoo M. A., Song E. J., Lee K. J., Kim K. W., (2002), "Regulation and destabilization of HIF-1alpha by ARD1-mediated acetylation", Cell, 111 (5), 709-720.

[128] Lin K. T., Wang Y. W., Chen C. T., Ho C. M., Su W. H., Jou Y. S., (2012), "HDAC inhibitors augmented cell migration and metastasis through induction of PKCs leading to identification of low toxicity modalities for combination cancer therapy", Clinical cancer research : an official journal of the American Association for Cancer Research, 18 (17), 4691-4701.

[129] Halsall J. A., Turner B. M., (2016), "Histone deacetylase inhibitors for cancer therapy: An evolutionarily ancient resistance response may explain their limited success", BioEssays : news and reviews in molecular, cellular and developmental biology, 38 (11), 1102-1110.

[130] Gryder B. E., Sodji Q. H., Oyelere A. K., (2012), "Targeted cancer therapy: giving histone deacetylase inhibitors all they need to succeed", Future medicinal chemistry, 4 (4), 505-524.

[131] Vansteenkiste J., Van Cutsem E., Dumez H., Chen C., Ricker J. L., Randolph S. S., Schöffski P., (2008), "Early phase II trial of oral vorinostat in relapsed or refractory breast, colorectal, or non-small cell lung cancer", Investigational new drugs, 26 (5), 483-488.

[132] Woyach J. A., Kloos R. T., Ringel M. D., Arbogast D., Collamore M., Zwiebel J. A., Grever M., Villalona-Calero M., Shah M. H., (2009), "Lack of therapeutic effect of the histone deacetylase inhibitor vorinostat in patients with metastatic radioiodine-refractory thyroid carcinoma", The Journal of clinical endocrinology and metabolism, 94 (1), 164-170.

[133] Wu S., Luo Z., Yu P. J., Xie H., He Y. W., (2016), "Suberoylanilide hydroxamic acid (SAHA) promotes the epithelial mesenchymal transition of triple negative breast cancer cells via HDAC8/FOXA1 signals", Biological chemistry, 397 (1), 75-83.

[134] Whitehead R. P., Rankin C., Hoff P. M., Gold P. J., Billingsley K. G., Chapman R. A., Wong L., Ward J. H., Abbruzzese J. L., Blanke C. D., (2009), "Phase II trial of romidepsin (NSC-630176) in previously treated colorectal cancer patients with advanced disease: a Southwest Oncology Group study (S0336)", Investigational new drugs, 27 (5), 469-475.

[135] Haigentz M., Jr., Kim M., Sarta C., Lin J., Keresztes R. S., Culliney B., Gaba A. G., Smith R. V., Shapiro G. I., Chirieac L. R., Mariadason J. M., Belbin T. J.,

Greally J. M., Wright J. J., Haddad R. I., (2012), "Phase II trial of the histone deacetylase inhibitor romidepsin in patients with recurrent/metastatic head and neck cancer", Oral oncology, 48 (12), 1281-1288.

[136] Robertson F. M., Chu K., Boley K. M., Ye Z., Liu H., Wright M. C., Moraes R., Zhang X., Green T. L., Barsky S. H., Heise C., Cristofanilli M., (2013), "The class I HDAC inhibitor Romidepsin targets inflammatory breast cancer tumor emboli and synergizes with paclitaxel to inhibit metastasis", Journal of experimental therapeutics & oncology, 10 (3), 219-233.

[137] Shen J., Huang C., Jiang L., Gao F., Wang Z., Zhang Y., Bai J., Zhou H., Chen Q., (2007), "Enhancement of cisplatin induced apoptosis by suberoylanilide hydroxamic acid in human oral squamous cell carcinoma cell lines", Biochemical pharmacology, 73 (12), 1901-1909.

[138] Lassen U., Molife L. R., Sorensen M., Engelholm S. A., Vidal L., Sinha R., Penson R. T., Buhl-Jensen P., Crowley E., Tjornelund J., Knoblauch P., de Bono J. S., (2010), "A phase I study of the safety and pharmacokinetics of the histone deacetylase inhibitor belinostat administered in combination with carboplatin and/or paclitaxel in patients with solid tumours", British journal of cancer, 103 (1), 12-17.

[139] Halsall J. A., Turan N., Wiersma M., Turner B. M., (2015), "Cells adapt to the epigenomic disruption caused by histone deacetylase inhibitors through a coordinated, chromatin-mediated transcriptional response", Epigenetics & chromatin, 8, 29.

[140] Coleman M. P., Quaresma M., Berrino F., Lutz J. M., De Angelis R., Capocaccia R., Baili P., Rachet B., Gatta G., Hakulinen T., Micheli A., Sant M., Weir H. K., Elwood J. M., Tsukuma H., Koifman S., GA E. S., Francisci S., Santaquilani M., Verdecchia A., Storm H. H., Young J. L., (2008), "Cancer survival in five continents: a worldwide population-based study (CONCORD)", The Lancet. Oncology, 9 (8), 730-756.

[141] DeSantis C. E., Ma J., Gaudet M. M., Newman L. A., Miller K. D., Goding Sauer A., Jemal A., Siegel R. L., (2019), "Breast cancer statistics, 2019", CA: a cancer journal for clinicians, 69 (6), 438-451.

[142] Ozmen V., Fidaner C., Aksaz E., Bayol U., Dede İ., Goker E., Gulluoglu B. M., Işıkdoğan A., Topa U., Uhri M., (2009), "Organizing early diagnosis and screening programs for breast cancer in Turkey "The report of breast cancer early detection and screening sub-committee, National Cancer Advisory Board, The Ministry of Health of Turkey"", Journal of Breast Health, 5, 125-134.

[143] Tsang J. Y. S., Tse G. M., (2020), "Molecular Classification of Breast Cancer", Advances in anatomic pathology, 27 (1), 27-35.

[144] Hammond M. E., Hayes D. F., Dowsett M., Allred D. C., Hagerty K. L., Badve S., Fitzgibbons P. L., Francis G., Goldstein N. S., Hayes M., Hicks D. G., Lester S., Love R., Mangu P. B., McShane L., Miller K., Osborne C. K., Paik S., Perlmutter J., Rhodes A., Sasano H., Schwartz J. N., Sweep F. C., Taube S.,

Torlakovic E. E., Valenstein P., Viale G., Visscher D., Wheeler T., Williams R. B., Wittliff J. L., Wolff A. C., (2010), "American Society of Clinical Oncology/College Of American Pathologists guideline recommendations for immunohistochemical testing of estrogen and progesterone receptors in breast cancer", Journal of clinical oncology : official journal of the American Society of Clinical Oncology, 28 (16), 2784-2795.

[145] Cui X., Schiff R., Arpino G., Osborne C. K., Lee A. V., (2005), "Biology of progesterone receptor loss in breast cancer and its implications for endocrine therapy", Journal of clinical oncology : official journal of the American Society of Clinical Oncology, 23 (30), 7721-7735.

[146] Ethier J. L., Ocaña A., Rodríguez Lescure A., Ruíz A., Alba E., Calvo L., Ruíz-Borrego M., Santaballa A., Rodríguez C. A., Crespo C., Ramos M., Gracia Marco J., Lluch A., Álvarez I., Casas M., Sánchez-Aragó M., Carrasco E., Caballero R., Amir E., Martin M., (2018), "Outcomes of single versus double hormone receptor-positive breast cancer. A GEICAM/9906 sub-study", European journal of cancer (Oxford, England : 1990), 94, 199-205.

[147] Bedard P. L., Cardoso F., Piccart-Gebhart M. J., (2009), "Stemming resistance to HER-2 targeted therapy", Journal of mammary gland biology and neoplasia, 14 (1), 55-66.

[148] Redig A. J., McAllister S. S., (2013), "Breast cancer as a systemic disease: a view of metastasis", Journal of internal medicine, 274 (2), 113-126.

[149] DeSantis C., Siegel R., Bandi P., Jemal A., (2011), "Breast cancer statistics, 2011", CA: a cancer journal for clinicians, 61 (6), 409-418.

[150] O'Shaughnessy J., (2005), "Extending survival with chemotherapy in metastatic breast cancer", The oncologist, 10 Suppl 3, 20-29.

[151] Griffith J. W., Sokol C. L., Luster A. D., (2014), "Chemokines and chemokine receptors: positioning cells for host defense and immunity", Annual review of immunology, 32, 659-702.

[152] Dewan M. Z., Ahmed S., Iwasaki Y., Ohba K., Toi M., Yamamoto N., (2006), "Stromal cell-derived factor-1 and CXCR4 receptor interaction in tumor growth and metastasis of breast cancer", Biomedicine & pharmacotherapy = Biomedecine & pharmacotherapie, 60 (6), 273-276.

[153] Nagarsheth N., Wicha M. S., Zou W., (2017), "Chemokines in the cancer microenvironment and their relevance in cancer immunotherapy", Nature reviews. Immunology, 17 (9), 559-572.

[154] Chow M. T., Luster A. D., (2014), "Chemokines in cancer", Cancer immunology research, 2 (12), 1125-1131.

[155] Gustavsson M., Dyer D. P., Zhao C., Handel T. M., (2019), "Kinetics of CXCL12 binding to atypical chemokine receptor 3 reveal a role for the receptor N terminus in chemokine binding", Science signaling, 12 (598).

[156] Thompson S., Martínez-Burgo B., Sepuru K. M., Rajarathnam K., Kirby J. A., Sheerin N. S., Ali S., (2017), "Regulation of Chemokine Function: The Roles of GAG-Binding and Post-Translational Nitration", International journal of molecular sciences, 18 (8).

[157] Bonecchi R., Graham G. J., (2016), "Atypical Chemokine Receptors and Their Roles in the Resolution of the Inflammatory Response", Frontiers in immunology, 7, 224.

[158] Terasaki M., Sugita Y., Arakawa F., Okada Y., Ohshima K., Shigemori M., (2011), "CXCL12/CXCR4 signaling in malignant brain tumors: a potential pharmacological therapeutic target", Brain tumor pathology, 28 (2), 89-97.

[159] Ruffini P. A., Morandi P., Cabioglu N., Altundag K., Cristofanilli M., (2007), "Manipulating the chemokine-chemokine receptor network to treat cancer", Cancer, 109 (12), 2392-2404.

[160] Wald O., (2018), "CXCR4 Based Therapeutics for Non-Small Cell Lung Cancer (NSCLC)", Journal of clinical medicine, 7 (10).

[161] Xu C., Zhao H., Chen H., Yao Q., (2015), "CXCR4 in breast cancer: oncogenic role and therapeutic targeting", Drug design, development and therapy, 9, 4953-4964.

[162] Orian-Rousseau V., (2015), "CD44 Acts as a Signaling Platform Controlling Tumor Progression and Metastasis", Frontiers in immunology, 6, 154.

[163] Orian-Rousseau V., Sleeman J., (2014), "CD44 is a multidomain signaling platform that integrates extracellular matrix cues with growth factor and cytokine signals", Advances in cancer research, 123, 231-254.

[164] Fuchs K., Hippe A., Schmaus A., Homey B., Sleeman J. P., Orian-Rousseau V., (2013), "Opposing effects of high- and low-molecular weight hyaluronan on CXCL12-induced CXCR4 signaling depend on CD44", Cell death & disease, 4 (10), e819.

[165] Bao W., Fu H. J., Xie Q. S., Wang L., Zhang R., Guo Z. Y., Zhao J., Meng Y. L., Ren X. L., Wang T., Li Q., Jin B. Q., Yao L. B., Wang R. A., Fan D. M., Chen S. Y., Jia L. T., Yang A. G., (2011), "HER2 interacts with CD44 to up-regulate CXCR4 via epigenetic silencing of microRNA-139 in gastric cancer cells", Gastroenterology, 141 (6), 2076-2087.e2076.

[166] Xu B., Zhou M., Qiu W., Ye J., Feng Q., (2017), "CCR7 mediates human breast cancer cell invasion, migration by inducing epithelial-mesenchymal transition and suppressing apoptosis through AKT pathway", Cancer medicine, 6 (5), 1062-1071.

[167] Tutunea-Fatan E., Majumder M., Xin X., Lala P. K., (2015), "The role of CCL21/CCR7 chemokine axis in breast cancer-induced lymphangiogenesis", Molecular cancer, 14, 35.

[168] Müller A., Homey B., Soto H., Ge N., Catron D., Buchanan M. E., McClanahan T., Murphy E., Yuan W., Wagner S. N., Barrera J. L., Mohar A., Verástegui E., Zlotnik A., (2001), "Involvement of chemokine receptors in breast cancer metastasis", Nature, 410 (6824), 50-56.

[169] Kochetkova M., Kumar S., McColl S. R., (2009), "Chemokine receptors CXCR4 and CCR7 promote metastasis by preventing anoikis in cancer cells", Cell death and differentiation, 16 (5), 664-673.

[170] Pieslinger A., Plaetzer K., Oberdanner C. B., Berlanda J., Mair H., Krammer B., Kiesslich T., (2006), "Characterization of a simple and homogeneous irradiation device based on light-emitting diodes: A possible low-cost supplement to conventional light sources for photodynamic treatment", Medical Laser Application, 21 (4), 277-283.

[171] Breslin S., O'Driscoll L., (2016), "The relevance of using 3D cell cultures, in addition to 2D monolayer cultures, when evaluating breast cancer drug sensitivity and resistance", Oncotarget, 7 (29), 45745-45756.

[172] Atilla D., Saydan N., Durmus M., Gurek A. G., Khan T., Ruck A., Walt H., Nyokong T., Ahsen V., (2007), "Synthesis and photodynamic potential of tetra- and octa-triethyleneoxysulfonyl substituted zinc phthalocyanines", Journal of Photochemistry and Photobiology A: Chemistry, 186 (2-3), 298-307.

[173] Patil V., Sodji Q. H., Kornacki J. R., Mrksich M., Oyelere A. K., (2013), "3-Hydroxypyridin-2-thione as novel zinc binding group for selective histone deacetylase inhibition", Journal of medicinal chemistry, 56 (9), 3492-3506.

[174] Nishida M., Horiuchi H., Momotake A., Nishimura Y., Hiratsuka H., Arai T., (2011), "Singlet molecular oxygen generation by water-soluble phthalocyanine dendrimers with different aggregation behavior", Journal of Porphyrins and Phthalocyanines, 15 (1), 47-53.

[175] Şahin B., Topal S. Z., Atilla D., (2017), "Synthesis, Photophysical and Photochemical Properties of a Set of Silicon Phthalocyanines Bearing Anti-Inflammatory Groups", Journal of fluorescence, 27 (1), 407-416.

[176] Byth H. A., McHunu B. I., Dubery I. A., Bornman L., (2001), "Assessment of a simple, non-toxic Alamar blue cell survival assay to monitor tomato cell viability", Phytochemical analysis : PCA, 12 (5), 340-346.

[177] Gelles J. D., Chipuk J. E., (2016), "Robust high-throughput kinetic analysis of apoptosis with real-time high-content live-cell imaging", Cell death & disease, 7 (12), e2493.

[178] Eray M., Mättö M., Kaartinen M., Andersson L., Pelkonen J., (2001), "Flow cytometric analysis of apoptotic subpopulations with a combination of annexin V-FITC, propidium iodide, and SYTO 17", Cytometry, 43 (2), 134-142.

[179] Darzynkiewicz Z., (2011), "Critical aspects in analysis of cellular DNA content", Current protocols in cytometry, Chapter 7, Unit 7.2.

[180] Sobreira C., Davidson M., King M. P., Miranda A. F., (1996), "Dihydrorhodamine 123 identifies impaired mitochondrial respiratory chain function in cultured cells harboring mitochondrial DNA mutations", The journal of histochemistry and cytochemistry : official journal of the Histochemistry Society, 44 (6), 571-579.

[181] Djiadeu P., Azzouz D., Khan M. A., Kotra L. P., Sweezey N., Palaniyar N., (2017), "Ultraviolet irradiation increases green fluorescence of dihydrorhodamine (DHR) 123: false-positive results for reactive oxygen species generation", Pharmacology research & perspectives, 5 (2), e00303.

[182] Kawaguchi Y., Kovacs J. J., McLaurin A., Vance J. M., Ito A., Yao T. P., (2003), "The deacetylase HDAC6 regulates aggresome formation and cell viability in response to misfolded protein stress", Cell, 115 (6), 727-738.

[183] Chakrabarti A., Oehme I., Witt O., Oliveira G., Sippl W., Romier C., Pierce R. J., Jung M., (2015), "HDAC8: a multifaceted target for therapeutic interventions", Trends in pharmacological sciences, 36 (7), 481-492.

[184] Banerjee S., Adhikari N., Amin S. A., Jha T., (2019), "Histone deacetylase 8 (HDAC8) and its inhibitors with selectivity to other isoforms: An overview", Eur J Med Chem, 164, 214-240.

[185] Balasubramanian S., Ramos J., Luo W., Sirisawad M., Verner E., Buggy J. J., (2008), "A novel histone deacetylase 8 (HDAC8)-specific inhibitor PCI-34051 induces apoptosis in T-cell lymphomas", Leukemia, 22 (5), 1026-1034.

[186] Ye R. R., Tan C. P., He L., Chen M. H., Ji L. N., Mao Z. W., (2014), "Cyclometalated Ir(III) complexes as targeted theranostic anticancer therapeutics: combining HDAC inhibition with photodynamic therapy", Chem Commun (Camb), 50 (75), 10945-10948.

[187] Kasparkova J., Kostrhunova H., Novakova O., Krikavova R., Vanco J., Travnicek Z., Brabec V., (2015), "A Photoactivatable Platinum(IV) Complex Targeting Genomic DNA and Histone Deacetylases", Angew Chem Int Ed Engl, 54 (48), 14478-14482.

[188] Halaburkova A., Jendzelovsky R., Koval J., Herceg Z., Fedorocko P., Ghantous A., (2017), "Histone deacetylase inhibitors potentiate photodynamic therapy in colon cancer cells marked by chromatin-mediated epigenetic regulation of CDKN1A", Clin Epigenetics, 9, 62.

[189] Liu N., Liu H., Chen H., Wang G., Teng H., Chang Y., (2020), "Polyphotosensitizer nanogels for GSH-responsive histone deacetylase inhibitors delivery and enhanced cancer photodynamic therapy", Colloids Surf B Biointerfaces, 188, 110753.

[190] Lüftner D., Schneeweiss A., Hartkopf A. D., Müller V., Wöckel A., Janni W., Ettl J., Belleville E., Schütz F., Thill M., Huober J., Fasching P. A., Kolberg H. C., Pöschke P., Welslau M., Overkamp F., Tesch H., Fehm T. N., Lux M. P., (2020), "Update Breast Cancer 2020 Part 2 - Advanced Breast Cancer: New

Treatments and Implementation of Therapies with Companion Diagnostics", Geburtshilfe und Frauenheilkunde, 80 (4), 391-398.

[191] Master A., Livingston M., Sen Gupta A., (2013), "Photodynamic nanomedicine in the treatment of solid tumors: perspectives and challenges", Journal of controlled release : official journal of the Controlled Release Society, 168 (1), 88-102.

[192] Khan S. A., Dougherty T. J., Mang T. S., (1993), "An evaluation of photodynamic therapy in the management of cutaneous metastases of breast cancer", European journal of cancer (Oxford, England : 1990), 29a (12), 1686-1690.

[193] Mang T. S., Allison R., Hewson G., Snider W., Moskowitz R., (1998), "A phase II/III clinical study of tin ethyl etiopurpurin (Purlytin)-induced photodynamic therapy for the treatment of recurrent cutaneous metastatic breast cancer", The cancer journal from Scientific American, 4 (6), 378-384.

[194] Rhodes L. V., Tate C. R., Segar H. C., Burks H. E., Phamduy T. B., Hoang V., Elliott S., Gilliam D., Pounder F. N., Anbalagan M., Chrisey D. B., Rowan B. G., Burow M. E., Collins-Burow B. M., (2014), "Suppression of triple-negative breast cancer metastasis by pan-DAC inhibitor panobinostat via inhibition of ZEB family of EMT master regulators", Breast cancer research and treatment, 145 (3), 593-604.

[195] Chen J., Li N., Liu B., Ling J., Yang W., Pang X., Li T., (2020), "Pracinostat (SB939), a histone deacetylase inhibitor, suppresses breast cancer metastasis and growth by inactivating the IL-6/STAT3 signalling pathways", Life sciences, 248, 117469.

[196] Park S. Y., Jun J. A., Jeong K. J., Heo H. J., Sohn J. S., Lee H. Y., Park C. G., Kang J., (2011), "Histone deacetylases 1, 6 and 8 are critical for invasion in breast cancer", Oncology reports, 25 (6), 1677-1681.

[197] Leslie P. L., Chao Y. L., Tsai Y. H., Ghosh S. K., Porrello A., Van Swearingen A. E. D., Harrison E. B., Cooley B. C., Parker J. S., Carey L. A., Pecot C. V., (2019), "Histone deacetylase 11 inhibition promotes breast cancer metastasis from lymph nodes", Nature communications, 10 (1), 4192.

[198] Saji S., Kawakami M., Hayashi S., Yoshida N., Hirose M., Horiguchi S., Itoh A., Funata N., Schreiber S. L., Yoshida M., Toi M., (2005), "Significance of HDAC6 regulation via estrogen signaling for cell motility and prognosis in estrogen receptor-positive breast cancer", Oncogene, 24 (28), 4531-4539.

[199] Liu Y., Peng L., Seto E., Huang S., Qiu Y., (2012), "Modulation of histone deacetylase 6 (HDAC6) nuclear import and tubulin deacetylase activity through acetylation", The Journal of biological chemistry, 287 (34), 29168-29174.

[200] Mroz P., Yaroslavsky A., Kharkwal G. B., Hamblin M. R., (2011), "Cell death pathways in photodynamic therapy of cancer", Cancers, 3 (2), 2516-2539.

[201] Mfouo-Tynga I., Abrahamse H., (2015), "Cell death pathways and phthalocyanine as an efficient agent for photodynamic cancer therapy", International journal of molecular sciences, 16 (5), 10228-10241.

[202] Xue L. Y., Chiu S. M., Oleinick N. L., (2010), "Atg7 deficiency increases resistance of MCF-7 human breast cancer cells to photodynamic therapy", Autophagy, 6 (2), 248-255.

[203] Garg A. D., Maes H., Romano E., Agostinis P., (2015), "Autophagy, a major adaptation pathway shaping cancer cell death and anticancer immunity responses following photodynamic therapy", Photochemical & photobiological sciences : Official journal of the European Photochemistry Association and the European Society for Photobiology, 14 (8), 1410-1424.

[204] Yuan L., Zhang J., Liu Y., Zhao J., Jiang F., Liu Y., (2017), "Indium (III) induces isolated mitochondrial permeability transition by inhibiting proton influx and triggering oxidative stress", Journal of inorganic biochemistry, 177, 17-26.

[205] Tsai P. K., Wu S. W., Chiang C. Y., Lee M. W., Chen H. Y., Chen W. Y., Chen C. J., Yang S. F., Yeh C. B., Kuan Y. H., (2020), "Evaluation of cytotoxicity, apoptosis, and genotoxicity induced by indium chloride in macrophages through mitochondrial dysfunction and reactive oxygen species generation", Ecotoxicology and environmental safety, 193, 110348.

[206] Mahalingam S. M., Ordaz J. D., Low P. S., (2018), "Targeting of a Photosensitizer to the Mitochondrion Enhances the Potency of Photodynamic Therapy", ACS omega, 3 (6), 6066-6074.

[207] Rubio N., Fleury S. P., Redmond R. W., (2009), "Spatial and temporal dynamics of in vitro photodynamic cell killing: extracellular hydrogen peroxide mediates neighbouring cell death", Photochemical & photobiological sciences : Official journal of the European Photochemistry Association and the European Society for Photobiology, 8 (4), 457-464.

[208] Missiroli S., Patergnani S., Caroccia N., Pedriali G., Perrone M., Previati M., Wieckowski M. R., Giorgi C., (2018), "Mitochondria-associated membranes (MAMs) and inflammation", Cell death & disease, 9 (3), 329.

[209] Elmore S., (2007), "Apoptosis: a review of programmed cell death", Toxicol Pathol, 35 (4), 495-516.

[210] Orlotti N. I., Cimino-Reale G., Borghini E., Pennati M., Sissi C., Perrone F., Palumbo M., Daidone M. G., Folini M., Zaffaroni N., (2012), "Autophagy acts as a safeguard mechanism against G-quadruplex ligand-mediated DNA damage", Autophagy, 8 (8), 1185-1196.

[211] Eapen V. V., Haber J. E., (2013), "DNA damage signaling triggers the cytoplasm-to-vacuole pathway of autophagy to regulate cell cycle progression", Autophagy, 9 (3), 440-441.

[212] Redza-Dutordoir M., Averill-Bates D. A., (2016), "Activation of apoptosis signalling pathways by reactive oxygen species", Biochim Biophys Acta, 1863 (12), 2977-2992.

[213] Eliopoulos A. G., Havaki S., Gorgoulis V. G., (2016), "DNA Damage Response and Autophagy: A Meaningful Partnership", Frontiers in genetics, 7, 204.

[214] Lee J. H., Choy M. L., Ngo L., Foster S. S., Marks P. A., (2010), "Histone deacetylase inhibitor induces DNA damage, which normal but not transformed cells can repair", Proc Natl Acad Sci U S A, 107 (33), 14639-14644.

[215] El-Hussein A., Harith M., Abrahamse H., (2012), "Assessment of DNA Damage after Photodynamic Therapy Using a Metallophthalocyanine Photosensitizer", Int. J. Photoenergy, 281068 1-10.

[216] Haywood-Small S. L., Vernon D. I., Griffiths J., Schofield J., Brown S. B., (2006), "Phthalocyanine-mediated photodynamic therapy induces cell death and a G0/G1 cell cycle arrest in cervical cancer cells", Biochem Biophys Res Commun, 339 (2), 569-576.

[217] Ahmad N., Feyes D. K., Agarwal R., Mukhtar H., (1998), "Photodynamic therapy results in induction of WAF1/CIP1/P21 leading to cell cycle arrest and apoptosis", Proc Natl Acad Sci U S A, 95 (12), 6977-6982.

[218] Xia C., Wang Y., Chen W., Yu W., Wang B., Li T., (2011), "New hydrophilic/lipophilic tetra-α-(4-carboxyphenoxy) phthalocyanine zinc-mediated photodynamic therapy inhibits the proliferation of human hepatocellular carcinoma Bel-7402 cells by triggering apoptosis and arresting cell cycle", Molecules (Basel, Switzerland), 16 (2), 1389-1401.

[219] Schmidt J., Kuzyniak W., Berkholz J., Steinemann G., Ogbodu R., Hoffmann B., Nouailles G., Gürek A. G., Nitzsche B., Höpfner M., (2018), "Novel zinc- and silicon-phthalocyanines as photosensitizers for photodynamic therapy of cholangiocarcinoma", Int J Mol Med, 42 (1), 534-546.

[220] Shao J., Xue J., Dai Y., Liu H., Chen N., Jia L., Huang J., (2012), "Inhibition of human hepatocellular carcinoma HepG2 by phthalocyanine photosensitiser PHOTOCYANINE: ROS production, apoptosis, cell cycle arrest", Eur J Cancer, 48 (13), 2086-2096.

[221] Finzer P., Kuntzen C., Soto U., zur Hausen H., Rösl F., (2001), "Inhibitors of histone deacetylase arrest cell cycle and induce apoptosis in cervical carcinoma cells circumventing human papillomavirus oncogene expression", Oncogene, 20 (35), 4768-4776.

[222] Bernhart E., Stuendl N., Kaltenegger H., Windpassinger C., Donohue N., Leithner A., Lohberger B., (2017), "Histone deacetylase inhibitors vorinostat and panobinostat induce G1 cell cycle arrest and apoptosis in multidrug resistant sarcoma cell lines", Oncotarget, 8 (44), 77254-77267.

[223] Hrgovic I., Doll M., Kleemann J., Wang X. F., Zoeller N., Pinter A., Kippenberger S., Kaufmann R., Meissner M., (2016), "The histone deacetylase

inhibitor trichostatin a decreases lymphangiogenesis by inducing apoptosis and cell cycle arrest via p21-dependent pathways", BMC cancer, 16 (1), 763.

[224] Roy S., Packman K., Jeffrey R., Tenniswood M., (2005), "Histone deacetylase inhibitors differentially stabilize acetylated p53 and induce cell cycle arrest or apoptosis in prostate cancer cells", Cell death and differentiation, 12 (5), 482-491.

[225] Dong Z., Yang Y., Liu S., Lu J., Huang B., Zhang Y., (2018), "HDAC inhibitor PAC-320 induces G2/M cell cycle arrest and apoptosis in human prostate cancer", Oncotarget, 9 (1), 512-523.

[226] Gordon E. M., Ravicz J. R., Liu S., Chawla S. P., Hall F. L., (2018), "Cell cycle checkpoint control: The cyclin G1/Mdm2/p53 axis emerges as a strategic target for broad-spectrum cancer gene therapy - A review of molecular mechanisms for oncologists", Molecular and clinical oncology, 9 (2), 115-134.

[227] Kakinuma T., Hwang S. T., (2006), "Chemokines, chemokine receptors, and cancer metastasis", Journal of leukocyte biology, 79 (4), 639-651.

[228] Chatterjee S., Behnam Azad B., Nimmagadda S., (2014), "The intricate role of CXCR4 in cancer", Advances in cancer research, 124, 31-82.

[229] Ge B., Lao J., Li J., Chen Y., Song Y., Huang F., (2017), "Single-molecule imaging reveals dimerization/oligomerization of CXCR4 on plasma membrane closely related to its function", Scientific reports, 7 (1), 16873.

[230] Hasegawa H., Nomura T., Kohno M., Tateishi N., Suzuki Y., Maeda N., Fujisawa R., Yoshie O., Fujita S., (2000), "Increased chemokine receptor CCR7/EBI1 expression enhances the infiltration of lymphoid organs by adult T-cell leukemia cells", Blood, 95 (1), 30-38.

[231] Davies G., Martin L. A., Sacks N., Dowsett M., (2002), "Cyclooxygenase-2 (COX-2), aromatase and breast cancer: a possible role for COX-2 inhibitors in breast cancer chemoprevention", Annals of oncology : official journal of the European Society for Medical Oncology, 13 (5), 669-678.

[232] Pan M. R., Hou M. F., Chang H. C., Hung W. C., (2008), "Cyclooxygenase-2 up-regulates CCR7 via EP2/EP4 receptor signaling pathways to enhance lymphatic invasion of breast cancer cells", The Journal of biological chemistry, 283 (17), 11155-11163.

[233] Zlotnik A., (2006), "Chemokines and cancer", International journal of cancer, 119 (9), 2026-2029.

[234] Holland J. D., Kochetkova M., Akekawatchai C., Dottore M., Lopez A., McColl S. R., (2006), "Differential functional activation of chemokine receptor CXCR4 is mediated by G proteins in breast cancer cells", Cancer research, 66 (8), 4117-4124.

[235] Louderbough J. M., Schroeder J. A., (2011), “Understanding the dual nature of CD44 in breast cancer progression”, Molecular cancer research : MCR, 9 (12), 1573-1586.

[236] Trempolec N., Doix B., Degavre C., Brusa D., Bouzin C., Riant O., Feron O., (2020), “Photodynamic Therapy-Based Dendritic Cell Vaccination Suited to Treat Peritoneal Mesothelioma”, Cancers, 12 (3).

[237] Zhang F., Zhu Y., Fan G., Hu S., (2018), “Photodynamic therapy reduces the inhibitory effect of osteosarcoma cells on dendritic cells by upregulating HSP70”, Oncology letters, 16 (4), 5034-5040.

[238] Canella A., Cordero Nieves H., Sborov D. W., Cascione L., Radomska H. S., Smith E., Stiff A., Consiglio J., Caserta E., Rizzotto L., Zanesi N., Stefano V., Kaur B., Mo X., Byrd J. C., Efebera Y. A., Hofmeister C. C., Pichiorri F., (2015), “HDAC inhibitor AR-42 decreases CD44 expression and sensitizes myeloma cells to lenalidomide”, Oncotarget, 6 (31), 31134-31150.

[239] Schech A., Kazi A., Yu S., Shah P., Sabnis G., (2015), “Histone Deacetylase Inhibitor Entinostat Inhibits Tumor-Initiating Cells in Triple-Negative Breast Cancer Cells”, Molecular cancer therapeutics, 14 (8), 1848-1857.

[240] Yu C. H., Yu C. C., (2014), “Photodynamic therapy with 5-aminolevulinic acid (ALA) impairs tumor initiating and chemo-resistance property in head and neck cancer-derived cancer stem cells”, PloS one, 9 (1), e87129.

[241] Gaio E., Conte C., Esposito D., Reddi E., Quaglia F., Moret F., (2020), “CD44 Targeting Mediated by Polymeric Nanoparticles and Combination of Chlorine TPCS(2a)-PDT and Docetaxel-Chemotherapy for Efficient Killing of Breast Differentiated and Stem Cancer Cells In Vitro”, Cancers, 12 (2).

[242] Kim D. M., Shim Y. H., Kwon H., Kim J. P., Park J. I., Kim D. H., Kim D. H., Kim J. H., Jeong Y. I., (2019), “CD44 Receptor-Specific and Redox-Sensitive Nanophotosensitizers of Hyaluronic Acid-Chlorin e6 Tetramer Having Diselenide Linkages for Photodynamic Treatment of Cancer Cells”, Journal of pharmaceutical sciences, 108 (11), 3713-3722.

[243] Park S. B., Jang H. H., Lee H. L., Kim J., Nah J. W., Kim D. H., Jeong Y. I., Kang D. H., (2019), “Redox and CD44 Dual-Responsive Nanophotosensitizer Composed of Chlorin e6-Conjugated Hyaluronic Acid via Disulfide Linkage for Targeted Photodynamic Treatment of Cancer Cells”, Bulletin of the Korean Chemical Society, 40 (5), 439-445.

[244] Maiolino S., Moret F., Conte C., Fraix A., Tirino P., Ungaro F., Sortino S., Reddi E., Quaglia F., (2015), “Hyaluronan-decorated polymer nanoparticles targeting the CD44 receptor for the combined photo/chemo-therapy of cancer”, Nanoscale, 7 (13), 5643-5653.

[245] Crazzolara R., Jöhrer K., Johnstone R. W., Greil R., Kofler R., Meister B., Bernhard D., (2002), “Histone deacetylase inhibitors potently repress CXCR4 chemokine receptor expression and function in acute lymphoblastic leukaemia”, British journal of haematology, 119 (4), 965-969.

[246] Stamatopoulos B., Meuleman N., De Bruyn C., Delforge A., Bron D., Lagneaux L., (2010), "The histone deacetylase inhibitor suberoylanilide hydroxamic acid induces apoptosis, down-regulates the CXCR4 chemokine receptor and impairs migration of chronic lymphocytic leukemia cells", Haematologica, 95 (7), 1136-1143.

[247] Gul H., Marquez-Curtis L. A., Jahroudi N., Larratt L. M., Janowska-Wieczorek A., (2010), "Valproic acid exerts differential effects on CXCR4 expression in leukemic cells", Leukemia research, 34 (2), 235-242.

[248] Mori T., Kim J., Yamano T., Takeuchi H., Huang S., Umetani N., Koyanagi K., Hoon D. S., (2005), "Epigenetic up-regulation of C-C chemokine receptor 7 and C-X-C chemokine receptor 4 expression in melanoma cells", Cancer research, 65 (5), 1800-1807.

[249] Ierano C., Basseville A., To K. K., Zhan Z., Robey R. W., Wilkerson J., Bates S. E., Scala S., (2013), "Histone deacetylase inhibitors induce CXCR4 mRNA but antagonize CXCR4 migration", Cancer biology & therapy, 14 (2), 175-183.

[250] Bagley R. G., Walter-Yohrling J., Cao X., Weber W., Simons B., Cook B. P., Chartrand S. D., Wang C., Madden S. L., Teicher B. A., (2003), "Endothelial precursor cells as a model of tumor endothelium: characterization and comparison with mature endothelial cells", Cancer research, 63 (18), 5866-5873.

[251] Sutherland R. L., Hall R. E., Taylor I. W., (1983), "Cell proliferation kinetics of MCF-7 human mammary carcinoma cells in culture and effects of tamoxifen on exponentially growing and plateau-phase cells", Cancer research, 43 (9), 3998-4006.

[252] Sagara A., Igarashi K., Otsuka M., Kodama A., Yamashita M., Sugiura R., Karasawa T., Arakawa K., Narita M., Kuzumaki N., Narita M., Kato Y., (2017), "Endocan as a prognostic biomarker of triple-negative breast cancer", Breast cancer research and treatment, 161 (2), 269-278.

[253] Masoud G. N., Li W., (2015), "HIF-1α pathway: role, regulation and intervention for cancer therapy", Acta pharmaceutica Sinica. B, 5 (5), 378-389.

[254] Sun Y., Zhao D., Wang G., Wang Y., Cao L., Sun J., Jiang Q., He Z., (2020), "Recent progress of hypoxia-modulated multifunctional nanomedicines to enhance photodynamic therapy: opportunities, challenges, and future development", Acta pharmaceutica Sinica. B, 10 (8), 1382-1396.

[255] Huang Z., Xu H., Meyers A. D., Musani A. I., Wang L., Tagg R., Barqawi A. B., Chen Y. K., (2008), "Photodynamic therapy for treatment of solid tumors--potential and technical challenges", Technology in cancer research & treatment, 7 (4), 309-320.

[256] Larue L., Myrzakhmetov B., Ben-Mihoub A., Moussaron A., Thomas N., Arnoux P., Baros F., Vanderesse R., Acherar S., Frochot C., (2019), "Fighting Hypoxia to Improve PDT", Pharmaceuticals (Basel, Switzerland), 12 (4).

[257] Cheng Y., Cheng H., Jiang C., Qiu X., Wang K., Huan W., Yuan A., Wu J., Hu Y., (2015), "Perfluorocarbon nanoparticles enhance reactive oxygen levels and tumour growth inhibition in photodynamic therapy", Nature communications, 6, 8785.

[258] Day R. A., Estabrook D. A., Logan J. K., Sletten E. M., (2017), "Fluorous photosensitizers enhance photodynamic therapy with perfluorocarbon nanoemulsions", Chemical communications (Cambridge, England), 53 (97), 13043-13046.

[259] Liu C., Dong H., Wu N., Cao Y., Zhang X., (2018), "Plasmonic Resonance Energy Transfer Enhanced Photodynamic Therapy with Au@SiO(2)@Cu(2)O/Perfluorohexane Nanocomposites", ACS applied materials & interfaces, 10 (8), 6991-7002.

[260] Zhao C., Tong Y., Li X., Shao L., Chen L., Lu J., Deng X., Wang X., Wu Y., (2018), "Photosensitive Nanoparticles Combining Vascular-Independent Intratumor Distribution and On-Demand Oxygen-Depot Delivery for Enhanced Cancer Photodynamic Therapy", Small (Weinheim an der Bergstrasse, Germany), 14 (12), e1703045.

[261] Hu D. R., Zhong L., Wang M. Y., Li H. H., Qu Y., Liu Q. Y., Han R. X., Yuan L. P., Shi K., Peng J. R., Qian Z. Y., (2019), "Perfluorocarbon-Loaded and Redox-Activatable Photosensitizing Agent with Oxygen Supply for Enhancement of Fluorescence/Photoacoustic Imaging Guided Tumor Photodynamic Therapy", Advanced Functional Materials, 29 (9), 1806199.

[262] Gao S., Wang G., Qin Z., Wang X., Zhao G., Ma Q., Zhu L., (2017), "Oxygen-generating hybrid nanoparticles to enhance fluorescent/photoacoustic/ultrasound imaging guided tumor photodynamic therapy", Biomaterials, 112, 324-335.

[263] Hao Y., Zhang B., Zheng C., Niu M., Guo H., Zhang H., Chang J., Zhang Z., Wang L., Zhang Y., (2017), "Multifunctional nanoplatform for enhanced photodynamic cancer therapy and magnetic resonance imaging", Colloids and surfaces. B, Biointerfaces, 151, 384-393.

[264] Chen Q., Chen J., Liang C., Feng L., Dong Z., Song X., Song G., Liu Z., (2017), "Drug-induced co-assembly of albumin/catalase as smart nano-theranostics for deep intra-tumoral penetration, hypoxia relieve, and synergistic combination therapy", Journal of controlled release : official journal of the Controlled Release Society, 263, 79-89.

[265] Pampaloni F., Reynaud E. G., Stelzer E. H., (2007), "The third dimension bridges the gap between cell culture and live tissue", Nature reviews. Molecular cell biology, 8 (10), 839-845.

[266] Kapałczyńska M., Kolenda T., Przybyła W., Zajączkowska M., Teresiak A., Filas V., Ibbs M., Bliźniak R., Łuczewski Ł., Lamperska K., (2018), "2D and 3D cell cultures - a comparison of different types of cancer cell cultures", Archives of medical science : AMS, 14 (4), 910-919.

[267] Breslin S., O'Driscoll L., (2013), "Three-dimensional cell culture: the missing link in drug discovery", Drug discovery today, 18 (5-6), 240-249.

[268] Arrowsmith J., Miller P., (2013), "Trial watch: phase II and phase III attrition rates 2011-2012", Nature reviews. Drug discovery, 12 (8), 569.

[269] Yip D., Cho C. H., (2013), "A multicellular 3D heterospheroid model of liver tumor and stromal cells in collagen gel for anti-cancer drug testing", Biochemical and biophysical research communications, 433 (3), 327-332.

[270] Bulysheva A. A., Bowlin G. L., Petrova S. P., Yeudall W. A., (2013), "Enhanced chemoresistance of squamous carcinoma cells grown in 3D cryogenic electrospun scaffolds", Biomedical materials (Bristol, England), 8 (5), 055009.

[271] Storch K., Eke I., Borgmann K., Krause M., Richter C., Becker K., Schröck E., Cordes N., (2010), "Three-dimensional cell growth confers radioresistance by chromatin density modification", Cancer research, 70 (10), 3925-3934.

[272] Chaicharoenaudomrung N., Kunhorm P., Noisa P., (2019), "Three-dimensional cell culture systems as an in vitro platform for cancer and stem cell modeling", World journal of stem cells, 11 (12), 1065-1083.

[273] Bolze F., Jenni S., Sour A., Heitz V., (2017), "Molecular photosensitisers for two-photon photodynamic therapy", Chemical communications (Cambridge, England), 53 (96), 12857-12877.

[274] Rowlands C. J., Wu J., Uzel S. G., Klein O., Evans C. L., So P. T., (2014), "3D-resolved targeting of photodynamic therapy using temporal focusing", Laser physics letters, 11 (11).

# BIOGRAPHY

Başak Aru has graduated from İstanbul University, Biology Department, Molecular and Cellular Biology Division in 2013. Same year, she started her Master's Degree in Yeditepe University, Molecular Medicine Department under supervision of Prof. Dr. Gülderen Yanıkkaya Demirel. She received her M.Sc. degree in January, 2016 and enrolled to Gebze Technical University, Molecular Biology and Genetics Doctorate Programme within the same year. Since September 2017, she has been working as Specialist Biologist in Yeditepe University, Faculty of Medicine, Immunology Department.

# APPENDICES

## APPENDIX A: The Paper Published within the Context of the Thesis

Aru B., Günay A., Şenkuytu E., Yanıkkaya Demirel G., Gürek AG., and Atilla D., (2020), A Translational Study of a Silicon Phthalocyanine Substituted with a Histone Deacetylase Inhibitor for Photodynamic Therapy, ACS Omega. doi.org/10.1021/acsomega.0c03180

## APPENDIX B: Supporting Information

$$\text{Viability (\%)} = \frac{(O2 \times A1) - (O1 \times A2)}{(O2 \times P1) - (O1 \times P2)} \times 100 \qquad \text{(B.1)}$$

- O1 = molar extinction coefficient of oxidized AB at 570 nm (80586)
- O2 = molar extinction coefficient of oxidized AB at 600 nm (117216)
- A1 = absorbance of test wells at 570 nm
- A2 = absorbance of test wells at 600 nm
- P1 = absorbance of positive control well (cells plus Alamar Blue but no test agent) at 570 nm
- P2 = absorbance of positive control well (cells plus Alamar Blue but no test agent) at 600 nm

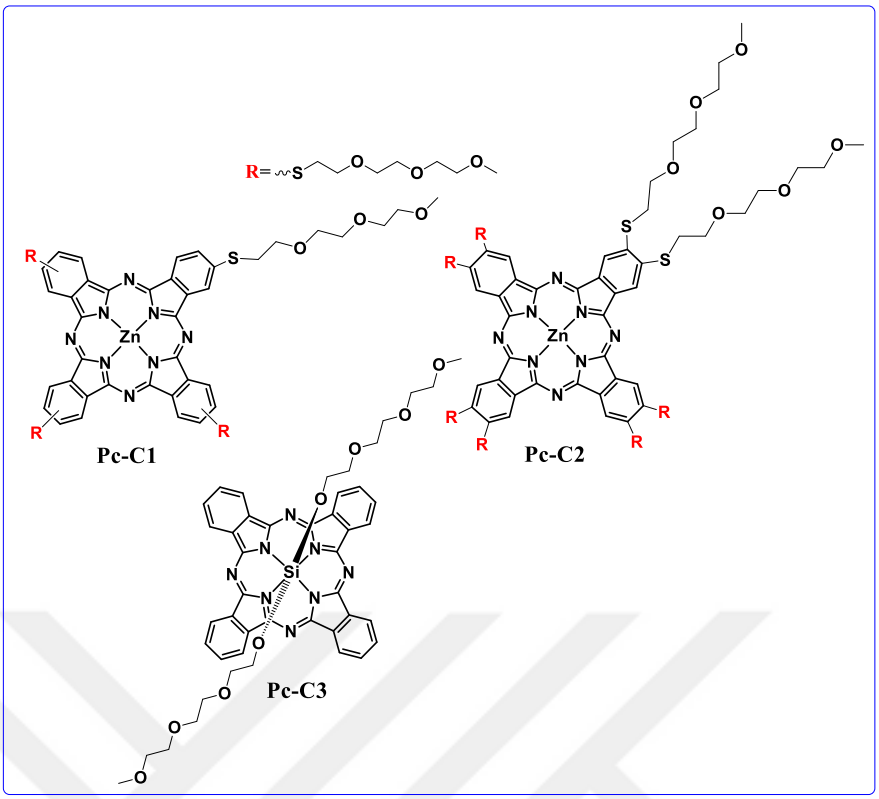


Figure B1.1: Molecular structures of Pc-C1, Pc-C2 and Pc-C3; positive controls used in this study.

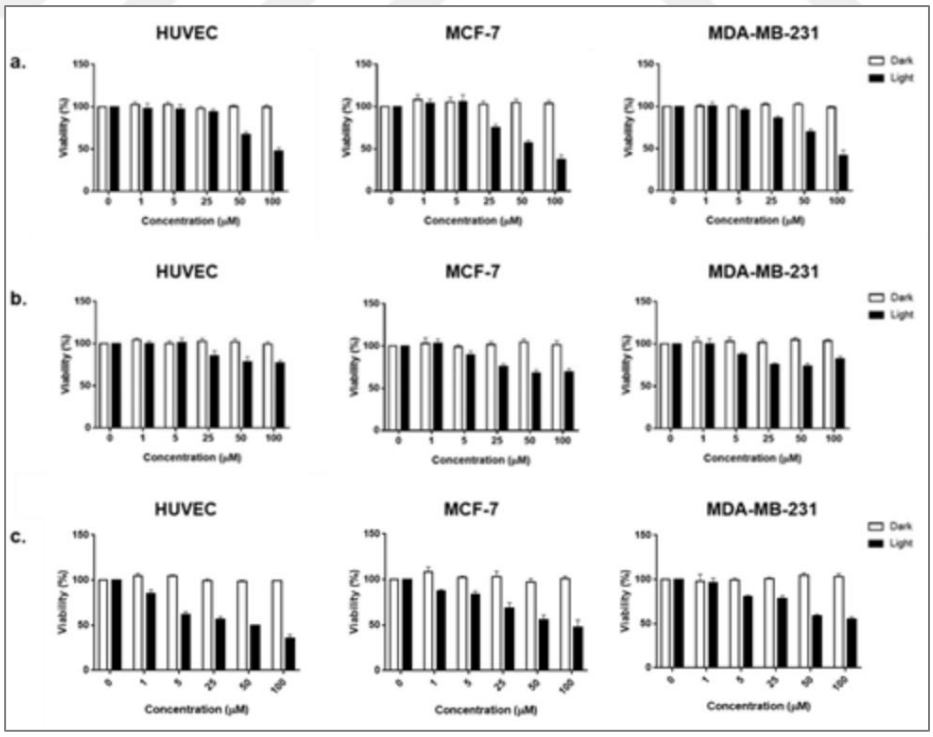


Figure B1.2: Dose-dependent viability graphics for Pc-C1, Pc-C2 and Pc-C3; positive controls used in this study.

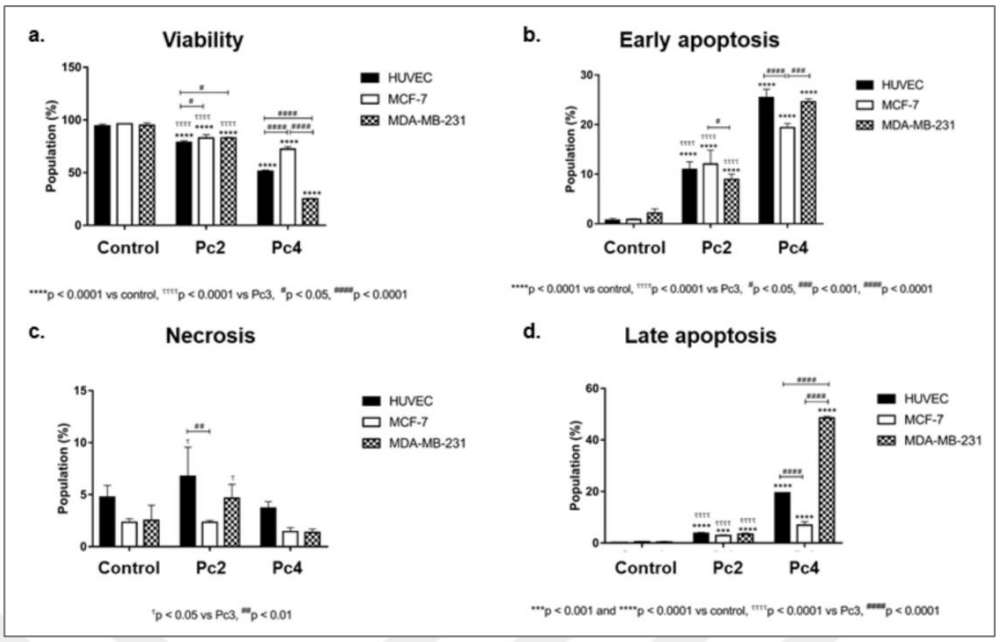


Figure B1.3: Bar graphics comparing a. viability, b. early apoptosis, c. necrosis and d. late apoptosis rates between non-peripheral Pc derivatives Pc2 and Pc4. ***** denotes difference between control and treatment groups. # denotes difference between cell lines within the same treatment groups. $\tau$ indicates difference between either Zn or In Pcs.

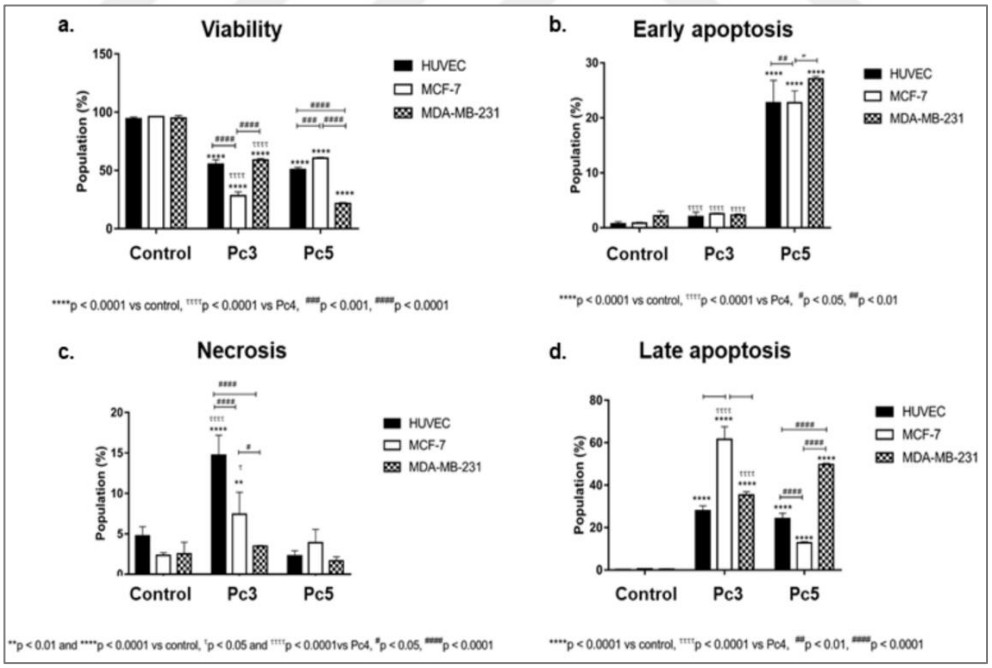


Figure B1.4: Bar graphics comparing a. viability, b. early apoptosis, c. necrosis and d. late apoptosis rates between peripheral Pc derivatives Pc3 and Pc5. * denotes difference between control and treatment groups. # denotes difference between cell lines within the same treatment groups. $\tau$ indicates difference between between either Zn or In Pcs.

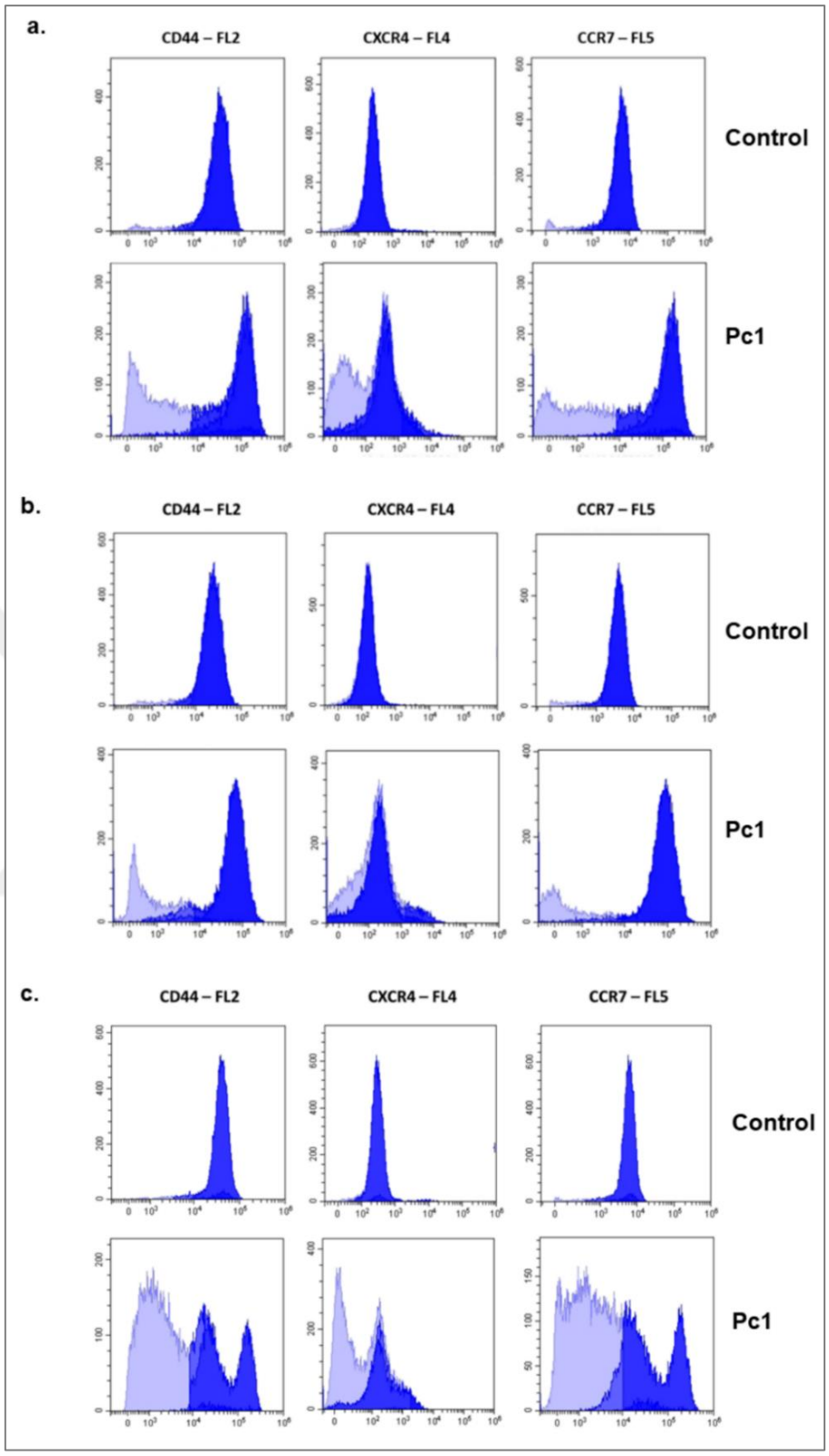


Figure B1.5: Representative flow cytometry histograms demonstrating CD44, CXCR4 and CCR7 protein levels of untreated and Pc1 treated a. HUVECs, b. MCF-7 cells, c. MDA-MB-231 cells.

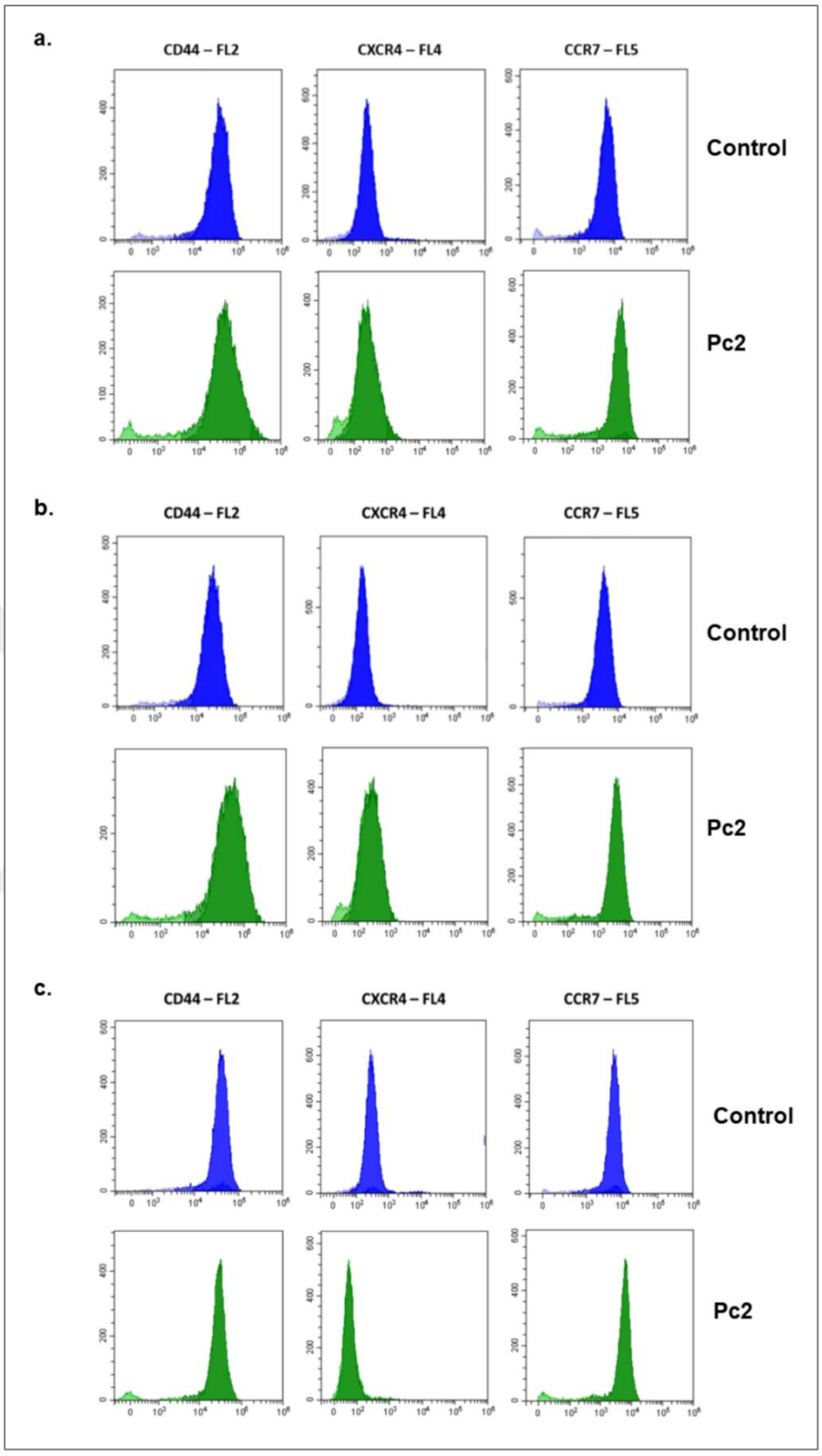


Figure B1.6: Representative flow cytometry histograms demonstrating CD44, CXCR4 and CCR7 protein levels of untreated and Pc2 treated a. HUVECs, b. MCF-7 cells, c.MDA-MB-231 cells.

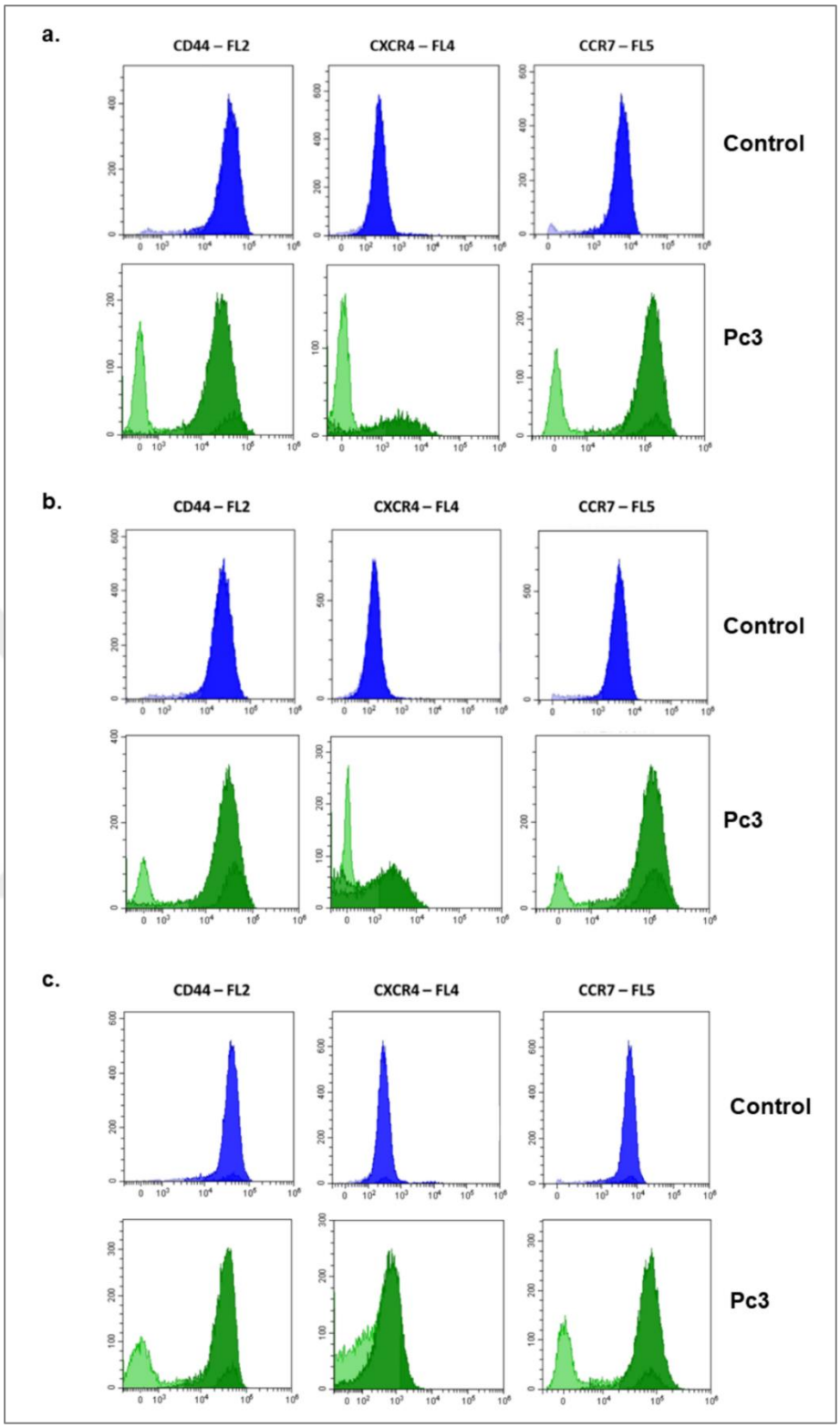


Figure B1.7: Representative flow cytometry histograms demonstrating CD44, CXCR4 and CCR7 protein levels of untreated and Pc3 treated a. HUVECs, b. MCF-7 cells, c. MDA-MB-231 cells.

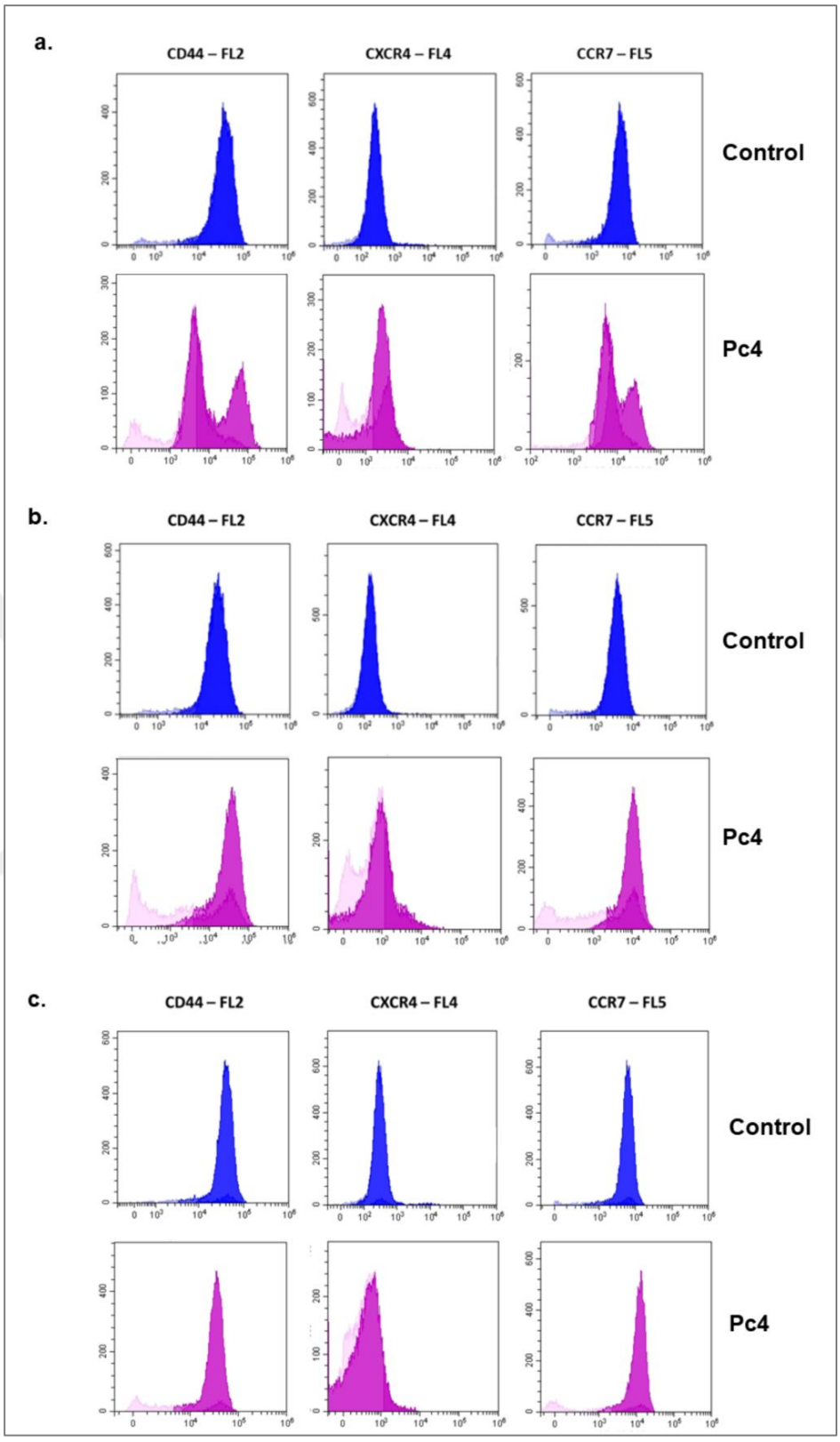


Figure B1.8: Representative flow cytometry histograms demonstrating CD44, CXCR4 and CCR7 protein levels of untreated and Pc4 treated a. HUVECs, b. MCF-7 cells, c. MDA-MB-231 cells.

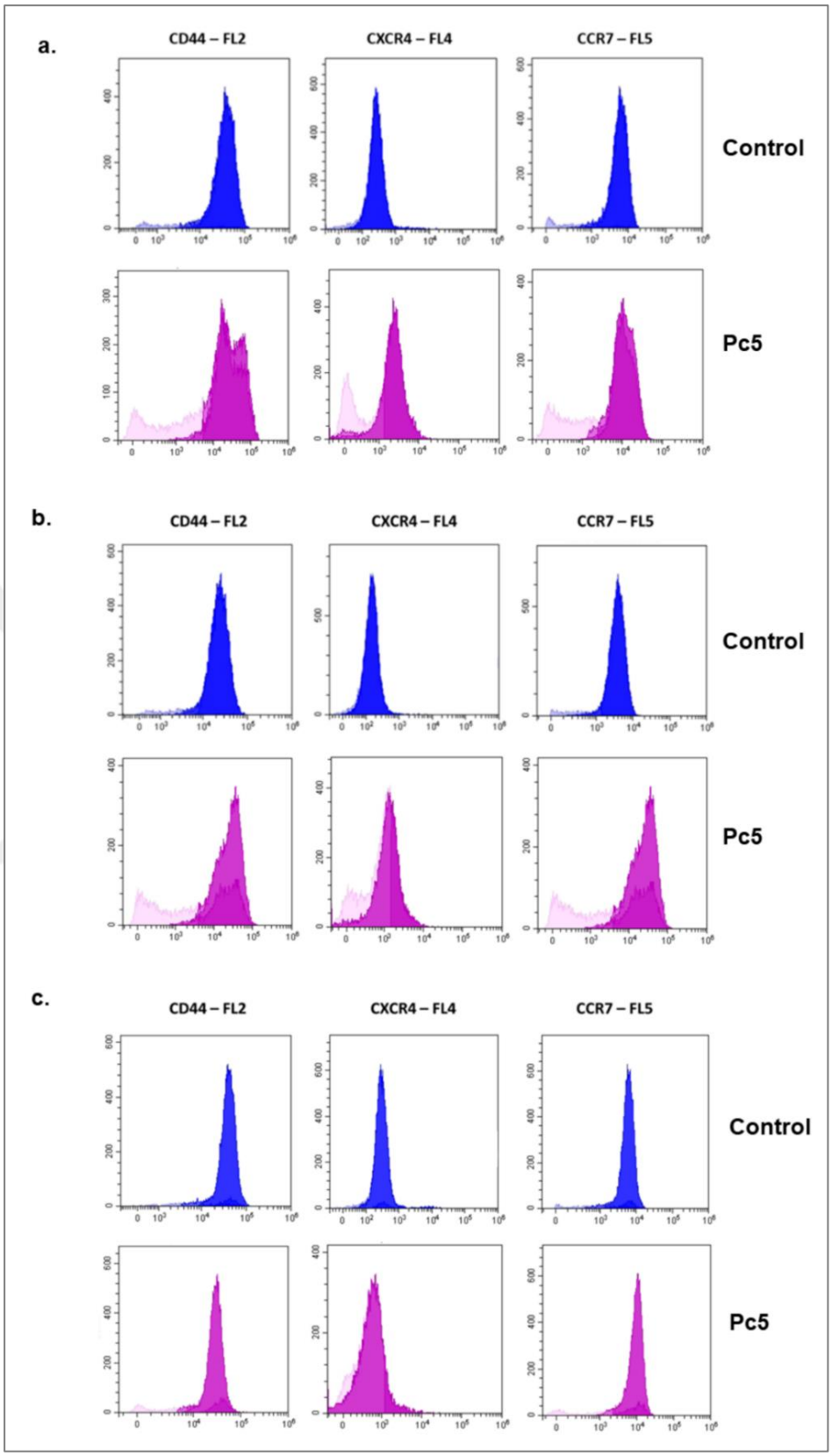


Figure B1.9: Representative flow cytometry histograms demonstrating CD44, CXCR4 and CCR7 protein levels of untreated and Pc5 treated a. HUVECs, b. MCF-7 cells, c. MDA-MB-231 cells.

# APPENDIX C: Copyright Permission

Table C1.1: Permissions for copyrighted materials.

| | License Date | License Number | Licensed Content Publisher |
|---|---|---|---|
| Figure 2.1 | Dec 18, 2020 | 4971821280895 | Elsevier |
| Figure 2.5 | Dec 18, 2020 | 4971820255310 | Springer Nature |